

---

# **Neutrino Interactions with Nucleons and Nuclei**

---

**Diplomarbeit**

**Tina J. Leitner**

**Institut für Theoretische Physik  
Justus-Liebig-Universität Gießen**

**September 2005**

## Cosmic Gall

Neutrinos, they are very small.  
They have no charge and have no mass  
And do not interact at all.

The earth is just a silly ball  
To them, through which they simply pass,  
Like dustmaids down a drafty hall  
Or photons through a sheet of glass.

They snub the most exquisite gas,  
Ignore the most substantial wall,  
Cold-shoulder steel and sounding brass,  
Insult the stallion in his stall.

And, scorning barriers of class,  
Infiltrate you and me! Like tall  
And painless guillotines, they fall  
Down through our heads into the grass.

At night, they enter at Nepal  
And pierce the lover and his lass  
From underneath the bed - you call  
It wonderful; I call it crass.

John Updike  
Telephone Poles and Other Poems  
1963

# Contents

<b>Introduction</b>	<b>1</b>
<b>I Preliminaries</b>	<b>3</b>
<b>1 Neutrino Physics</b>	<b>5</b>
1.1 Neutrino Properties . . . . .	5
1.2 Neutrino Oscillations . . . . .	8
1.3 Experiments and Uncertainties . . . . .	9
1.4 Existing Neutrino Scattering Data and Future Experiments . . . . .	10
<b>2 Weak and Electromagnetic Interactions</b>	<b>13</b>
2.1 Electroweak Theory . . . . .	13
2.1.1 Lagrangian of the Electroweak Interaction . . . . .	13
2.1.2 Leptonic Currents . . . . .	14
2.1.3 Quark Currents . . . . .	15
2.2 Properties of Quark Currents . . . . .	16
2.2.1 Vector Current . . . . .	16
2.2.2 Axial Current . . . . .	18
2.3 Hadronic Currents . . . . .	20
2.3.1 Hadronic Transition Currents . . . . .	20
2.3.2 Conserved Vector Current Hypothesis . . . . .	20
2.3.3 Partially Conserved Axial Current Hypothesis . . . . .	21
<b>II Neutrino Nucleon Scattering</b>	<b>23</b>
<b>3 Introduction to Neutrino Nucleon Scattering</b>	<b>25</b>
3.1 Inclusive Cross Section . . . . .	25
3.2 Decomposition of the Cross Section . . . . .	30
<b>4 (Quasi)Elastic Scattering</b>	<b>33</b>
4.1 Quasielastic Charged Current Interaction . . . . .	33
4.1.1 Formalism . . . . .	33

4.1.2	Form Factors . . . . .	38
4.1.3	Results . . . . .	41
4.2	Elastic Neutral Current Interaction . . . . .	44
4.2.1	Strangeness in the Nucleon . . . . .	44
4.2.2	Formalism . . . . .	47
4.2.3	Strange Form Factors . . . . .	50
4.2.4	Results . . . . .	53
<b>5</b>	<b>Production of the <math>\Delta</math> Resonance</b>	<b>63</b>
5.1	Formalism for Neutrino Induced $\Delta$ Production . . . . .	63
5.2	$N - \Delta$ Transition Form Factors . . . . .	65
5.3	Parametrization of the Width . . . . .	68
5.4	Results . . . . .	72
<b>6</b>	<b>Remaining Contributions to Neutrino Nucleon Scattering</b>	<b>77</b>
6.1	Higher-Mass Resonances . . . . .	77
6.2	Non-Resonant Background . . . . .	78
6.3	Deep Inelastic Scattering . . . . .	79
6.4	Strangeness Production . . . . .	80
<b>III</b>	<b>Neutrino Nucleus Scattering</b>	<b>81</b>
<b>7</b>	<b>Neutrino Nucleus Scattering within a BUU Transport Model</b>	<b>83</b>
7.1	BUU Transport Model . . . . .	83
7.1.1	Theoretical Background . . . . .	83
7.1.2	Numerical Implementation . . . . .	87
7.2	Numerical Implementation of Neutrino Cross Sections . . . . .	89
7.3	Other Models and Comparison . . . . .	93
<b>8</b>	<b>Results for Neutrino Nucleus Scattering</b>	<b>95</b>
8.1	Inclusive Cross Section . . . . .	95
8.1.1	Quasielastic Contribution . . . . .	95
8.1.2	$\Delta$ Resonance Contribution . . . . .	97
8.1.3	Inclusive Double Differential Cross Section . . . . .	99
8.2	Pion Production . . . . .	101
8.2.1	One Pion Production Cross Section . . . . .	101
8.2.2	Pion Momentum Distribution . . . . .	104
8.3	Nucleon Knockout . . . . .	108

<b>9 Simplified Model for Quasielastic Neutrino Nucleus Scattering</b>	<b>113</b>
9.1 Implementation . . . . .	113
9.2 Results . . . . .	114
<b>10 Summary and Outlook</b>	<b>119</b>
<b>Appendices</b>	<b>123</b>
<b>A Reference Formulæ</b>	<b>125</b>
A.1 Abbreviations . . . . .	125
A.2 Conventions . . . . .	125
A.3 Weak Interaction Constants . . . . .	127
<b>B Neutrino Kinematics</b>	<b>129</b>
B.1 Notation . . . . .	129
B.2 Energy Thresholds for Neutrino Production . . . . .	130
B.3 Integration Limits for $\nu N$ (Quasi)Elastic Scattering and $\Delta$ Production . .	130
B.3.1 (Quasi)Elastic Scattering . . . . .	130
B.3.2 $\Delta$ Production . . . . .	131
<b>C Cross Sections and Feynman Rules for Weak Interaction</b>	<b>133</b>
C.1 General Expression for the Cross Section . . . . .	133
C.2 Feynman Rules . . . . .	133
<b>Bibliography</b>	<b>135</b>
<b>Deutsche Zusammenfassung</b>	<b>145</b>



# Introduction

When Wolfgang Pauli postulated the neutrino in 1930 to retain the concept of energy and momentum conservation in  $\beta$  decay, he was afraid that this neutral and (almost) massless particle would never be detected. Seventy five years later and with not only one but three flavors confirmed, neutrino interactions offer unique opportunities for investigating fundamental questions in various domains of physics.

Neutrino experiments around the world now provide conclusive evidence that neutrino oscillations exist and, therefore, the neutrino is not massless. The absolute value of the mass, however, remains one of the greatest challenges in today's elementary particle physics. More specifically, some of the principal issues under debate are: What is the mass hierarchy? Is the neutrino a Dirac or a Majorana particle? Does the neutrino mixing matrix contain a CP-violating phase? Is there a sterile neutrino? Does the neutrino have a magnetic moment?

The interest in neutrinos goes beyond the study of their intrinsic properties and extends to a variety of topics in astro-, nuclear and hadronic physics. Neutrinos are an important tool for astrophysical issues like, for example, the understanding of the energy production in the sun or of supernova explosions. Neutrinos can probe the interior of objects that otherwise remain inaccessible. Even cosmological questions are influenced by neutrinos since they might play an important role in the matter-antimatter asymmetry of the universe.

Neutrinos are also a valuable tool in exploring nuclear and hadronic physics properties. An important challenge in nuclear research is to understand the hadronic structure within quantum chromodynamics (QCD). Therefore, the exploration of nucleons and their excited states by both electromagnetic and weak probes deserves special attention. Such information is important for testing current hadron models. The information obtained by weak interactions are often complementary to those from electromagnetic interactions. Especially, the unique  $(V - A)$  weak interaction structure probes properties of QCD, in particular the axial structure of the nucleon, that is difficult to unravel with electron or photon scattering. Charged current scattering is the only practical way towards an understanding of the axial form factors of the nucleon. Neutral current scattering, on the other hand, can probe the strange sea quark contribution to the nucleon spin.

Among the excited states of the nucleon, the  $\Delta$  resonance is the one studied best: by strong, electromagnetic and also weak interactions. Of particular interest are the  $N - \Delta$  transition form factors and the question whether the nucleon and the  $\Delta$  are deformed.

And if so, is it due to gluon interactions between quarks or due to the pion cloud which has resulted from spontaneously breaking of the chiral symmetry of QCD.

Even though neutrinos affect many domains of physics, they remain elusive particles, only weakly interacting and hard to detect. They can only be observed by detecting the secondary particles they create when interacting with matter. Often used targets in neutrino experiments are heavy nuclei, which provide relatively large cross sections. In turn, the detailed theoretical understanding of the weak nuclear response is a prerequisite for the analyses of current and future neutrino experiments and a precise knowledge of the neutrino nucleus cross section is therefore essential. So far, rather few attempts were made to study systematically nuclear effects and their influence on the weak pion production cross section, most existing investigations were focussing mainly on the quasielastic reaction. This situation motivates us to study neutrino scattering on nucleons and nuclei at low and intermediate energies up to about 2 GeV.

This thesis is organized as follows: Part I gives a general overview about the latest developments in neutrino physics and related experiments and further provides the theoretical background needed to calculate neutrino nucleon cross sections. The underlying theory, the Standard Model of Electroweak Interactions, and fundamental symmetries are presented.

In Part II we discuss neutrino nucleon interactions emphasizing the two most important processes in the energy range of interest, namely quasielastic scattering and  $\Delta$  production. We provide a fully-relativistic formalism to calculate those exclusive cross sections and study extensively the form factors for reasons outlined above.

In Part III of this thesis we investigate neutrino scattering off nuclei. In the framework of this work we extend the Giessen BUU model to describe neutrino nucleus interactions. After introducing our model and its numerical implementation we discuss in particular inclusive cross sections, one pion production and nucleon knockout.

We conclude with a summary of our main results. Some details of the calculation were deferred to the appendix, which also gives our conventions.



**Part I**  
**Preliminaries**



# 1 Neutrino Physics

In the course of the discovery of neutrino oscillation, new and better facilities are currently being built to address open questions in neutrino physics and to determine the oscillation parameters more precisely. They all have to face one issue: Going from the discovery to the precision phase requires better knowledge of the interaction with the detector, i. e. with nuclei. This knowledge will be crucial to reduce the systematic uncertainty of the next generation of high-precision measurements. Those problems are addressed in this chapter after presenting an overview about the history and the current status of neutrino physics and related experiments.

For detailed and complete reviews of neutrino physics and of recent experimental results the reader is referred to Refs. [Sch97, Gei03, Lip03, E<sup>+</sup>04, Kay05, LEP05] and to references therein as well as to the web sites [NUn, NOI, UNP].

## 1.1 Neutrino Properties

The history of neutrinos began 1930 with a proposal by Wolfgang Pauli at a conference he did not even attend. He "invented" the neutrino to retain energy-momentum conservation and Fermi statistics in nuclear  $\beta$  decay [vMWH85]:

Liebe radioaktive Damen und Herren,

wie der Überbringer dieser Zeilen, den ich huldvollst anzuhören bitte, Ihnen des näheren auseinandersetzen wird, bin ich angesichts [...] des kontinuierlichen beta-Spektrums auf einen verzweifelten Ausweg verfallen, um den "Wechselsatz" der Statistik und den Energiesatz zu retten. Nämlich die Möglichkeit, es könnten elektrisch neutrale Teilchen, die ich Neutronen nennen will, in den Kernen existieren, welche den Spin  $1/2$  haben und das Ausschliessungsprinzip befolgen und sich von Lichtquanten ausserdem noch dadurch unterscheiden, dass sie nicht mit Lichtgeschwindigkeit laufen. Die Masse der Neutronen müsste von derselben Grössenordnung wie die Elektronenmasse sein und jedenfalls nicht grösser als 0,01 Protonenmasse. - Das kontinuierliche beta-Spektrum wäre dann verständlich unter der Annahme, dass beim beta-Zerfall mit dem Elektron jeweils noch ein Neutron emittiert

wird, derart, dass die Summe der Energien von Neutron und Elektron konstant sind.

[...]

Ich traue mich vorläufig nicht, etwas über diese Idee zu publizieren, und wende mich vertrauensvoll an Euch, liebe Radioaktive, mit der Frage, wie es um den experimentellen Nachweis stände, wenn dieses Neutron ein ebensolches oder etwa 100 mal grösseres Durchdringungsvermögen besitzen würde wie ein Röntgenstrahl.

Ich gebe zu, dass mein Ausweg vielleicht von vornherein wenig wahrscheinlich erscheinen mag, weil man die Neutronen, wenn sie existieren, wohl längst gesehen hätte. Aber nur wer wagt, gewinnt, und der Ernst der Situation beim kontinuierlichen beta-Spektrum wird durch einen Ausspruch meines verehrten Vorgängers im Amte, Herrn Debye, beleuchtet, der mir kürzlich gesagt hat: "Oh, daran soll man am besten gar nicht denken, so wie an die neuen Steuern." Darum soll man jeden Weg zur Rettung ernstlich diskutieren. Also, liebe Radioaktive, prüfet und richtet. Leider kann ich nicht persönlich in Tübingen erscheinen, da ich infolge eines in der Nacht vom 6. zum 7. Dezember in Zürich stattfindenden Balles hier unabhkömmlich bin. - Mit vielen Grüßen an Euch, Euer untertänigster Diener

gez. W. Pauli

Pauli's neutron was later renamed to neutrino by Fermi because the "real" neutron was discovered in the meantime by Chadwick. 26 year after Pauli's letter the neutrino was experimentally detected by Reines and Cowan from a reactor source [RC53]. Since then the concept of neutrinos has undergone several developments and its status, as of today, is described briefly in the following. Their interactions will be covered in chapter 2.

### Neutrino flavors

The standard model of particle physics contains three neutrino flavors:  $\nu_e$ ,  $\nu_\mu$  and  $\nu_\tau$ . Each neutrino forms a doublet with the corresponding charged lepton. The  $\nu_\tau$  was discovered not even five years ago [DONUT01]. The number of neutrinos participating in the electroweak interaction can be determined by the  $Z^0$  decay width and it was beautifully confirmed at LEP, long before  $\nu_\tau$  was seen explicitly, that there are only three light neutrinos. In 1995 LSND claimed that three neutrinos were not enough to explain their results and introduced a "sterile" neutrino [LSND95]. This sterile neutrino does not undergo weak interactions or interacts in any other way (except gravity). However, the LSND experiment is still controversial and has not been confirmed by any other facility. MiniBooNE, presently taking data, aims to confirm or refute this result.

## Helicity

Wu showed in the late 1950s that parity is violated in weak interactions and Goldhaber observed that neutrinos have spin antiparallel to their momentum (left-handed) and antineutrinos have it parallel (right-handed). Therefore, in the Standard Model only left-handed neutrinos and right-handed antineutrinos exist (cf. chapter 2).

## Neutrino mass

Until recently, there was no compelling evidence that neutrinos have mass. Consequently, in the Standard Model neutrinos have been considered as massless and neutral stable particles and, reflecting parity violation, left-handed fields.

Today we know that this picture is outdated. There has been experimental evidence of neutrino oscillation in atmospheric [Super-K98], solar [SNO01], reactor [KamLAND03], and accelerator [K2K03] neutrino experiments (cf. chapter 1.2). Those experiments have obtained non-zero differences of squared neutrino masses and have therefore proven that neutrinos are massive. This fact requires at least a minimal extension of the Standard Model.

However, the absolute value of the neutrino mass has to be determined in a different way. Basically, there are two classes of experiments which have given upper limits for the neutrino mass so far. Direct mass experiments investigate the kinematics of the  $\beta$  decay. Numerous experiments have been studying the endpoint of the  $\beta$  spectrum from Tritium decay which yields  $m_{\bar{\nu}_e} < 3$  eV [E<sup>+</sup>04]. The second class of experiments observes the rates of nuclear double  $\beta$  decay which are sensitive to non-zero neutrino masses.

In order to have neutrinoless double  $\beta$  decay two conditions have to be fulfilled: The neutrino must be its own antiparticle, i. e. it is not a Dirac but a Majorana particle, and its mass is non-zero due to chirality arguments. A subgroup of the Heidelberg-Moscow collaboration claimed recently to have seen  $0\nu 2\beta$  [KKDHK01]. But their analysis was heavily criticized and this result has not yet been confirmed by any other experiment. If their claim is true, then this will establish that neutrinos are Majorana particles.

Currently, the absolute values of the neutrino masses are unknown - moreover it is still unknown whether the mass hierarchy is normal or inverted.

At present there are many alternative models to generate neutrino masses and to extend the Standard Model. The experiments are not yet able to exclude some of them (especially with the possible existence of Majorana and sterile neutrinos). The most important models are summarized in Ref. [AF03]. Basically, there are two groups of models: Some imply the existence of right-handed neutrinos (Dirac mass models), other imply lepton number non-conservation (Majorana mass models) and some even imply both, as the most popular

explanation of why neutrinos - although massive - are so light, the so-called see-saw mechanism [LEP05]. Implications of non-zero neutrino masses are discussed in detail in Ref. [MP04].

## 1.2 Neutrino Oscillations

The discovery of non-zero neutrino masses is closely related to the discovery of neutrino oscillations - neutrino oscillations are only possible with massive neutrinos due to a distinction between flavor and mass eigenstates. The idea was first introduced by Pontecorvo [Pon68]. The principle is analogous to the time evolution of a classical coupled oscillator starting with an excitation that is not a normal mode.

For simplicity we consider a system with only two neutrinos. Neutrinos produced in charged current interactions are flavor eigenstates denoted as  $\nu_e$  and  $\nu_\mu$ . Those eigenstates have no well defined mass and are linear superpositions of the mass eigenstates  $\nu_1$  and  $\nu_2$  with masses  $m_1$  and  $m_2$ , respectively:

$$|\nu_e\rangle = |\nu_1\rangle \cos \theta + |\nu_2\rangle \sin \theta, \quad (1.1)$$

$$|\nu_\mu\rangle = -|\nu_1\rangle \sin \theta + |\nu_2\rangle \cos \theta, \quad (1.2)$$

where  $\theta$  is the neutrino mixing angle. At time  $t = 0$  we have a pure weak eigenstate, say  $|\nu(0)\rangle = |\nu_\mu\rangle$ . But  $\nu_\mu$  is a superposition of the mass eigenstates each of which is propagating with the time dependence dictated by the free Hamiltonian. Therefore at a time  $t$  the state will be given by

$$|\nu(t)\rangle = -|\nu_1\rangle \sin \theta e^{-iE_1 t} + |\nu_2\rangle \cos \theta e^{-iE_2 t}, \quad (1.3)$$

with  $E_{1,2} = \sqrt{p^2 + m_{1,2}^2} \approx p + \frac{m_{1,2}^2}{2p}$ . The probability of finding a neutrino with electron flavor is then

$$\begin{aligned} P(\nu_\mu \rightarrow \nu_e; t) &= |\langle \nu_e | \nu(t) \rangle|^2 \\ &= \sin^2 \theta \cos^2 \theta \left| -e^{-iE_1 t} + e^{-iE_2 t} \right|^2 \\ &= \sin^2 2\theta \sin^2 \left( \frac{\Delta m^2 t}{4E} \right) \\ &= \sin^2 2\theta \sin^2 \left( \frac{\Delta m^2 L}{4E} \right). \end{aligned} \quad (1.4)$$

Here  $\Delta m^2 = m_2^2 - m_1^2$  is the squared mass difference and  $E = p$ . The last line is valid for highly relativistic particles ( $L = t$ ) with  $L$  being the travelled distance.

Note that only the mass difference squared appears, hence measuring oscillation probabilities will not give absolute values of the neutrino masses, it can only say definitely that at least one of the two neutrinos has a non-zero mass.

The two-flavor-oscillation scheme can be easily extended to three flavor mixing. The neutrino mixing matrix<sup>1</sup> then contains three angles  $\theta_{12}$ ,  $\theta_{13}$ ,  $\theta_{23}$ , one Dirac CP violating phase and possibly two Majorana phases. Further we have three squared mass differences:  $\Delta m_{12}^2$ ,  $\Delta m_{13}^2$ ,  $\Delta m_{23}^2$  (cf. Ref. [E<sup>+</sup>04] for up-to-date numbers). Since the off-diagonal matrix elements seem to be large, also CP violation might be larger than in the quark sector.

In the presence of matter this vacuum oscillation scheme becomes more complicated [Sch97]. Those matter effects can be crucial. Under certain conditions an almost complete flavor inversion is possible which is known as the Mikheyev-Smirnov-Wolfenstein effect (MSW effect).

## 1.3 Experiments and Uncertainties

After Super-Kamiokande found a deficit of atmospheric muon neutrinos [Super-K98] and after SNO discovered the appearance of a non-electron flavor component in the solar neutrino flux [SNO01] there is no doubt that neutrinos oscillate.

Future precision experiments will mostly be performed with artificial (i. e. reactor and accelerator) neutrinos providing better controllable conditions. In particular, long-baseline experiments will be used. In those experiments two ideal setups are possible. In long-baseline experiments which have no near detector, the accuracy of the results is determined by the uncertainties in the knowledge of the beam parameters and the cross sections. In principle, a setup with identical near and far detectors could be used to cancel these uncertainties since both detect the same spectrum - oscillation parameters are then fitted to the difference of both. However, this setup is difficult to realize in practice [Har, MINERvA04a, MINERvA04b].

Among these long-baseline experiments are the K2K experiment (KEK to Kamioka) [K2K], the NuMI/MINOS project [MIN] and the CNGS project [CNG]. K2K uses a low energy neutrino beam of about 1.5 GeV sent from KEK to Super-Kamiokande at a distance of about 250 km. A near detector is located on the KEK site. Data taking started already in 1999. A few month ago, also MINOS started data taking. It is placed at a distance of 730 km in the NuMI beamline, a higher-energy tunable neutrino beam ( $E_\nu \sim 3 - 12$  GeV) provided by Fermilab. Finally, CNGS is located in Gran Sasso,

---

<sup>1</sup>known also as Pontecorvo-Maki-Nakagawa-Sakata matrix

730 km away from the neutrino source at CERN. Since it is planned to investigate  $\nu_\tau$  appearance, a high-energy neutrino beam ( $E_\nu \sim 17$  GeV) has to be used.

Even though the physics programs are complementary (K2K plans to confirm atmospheric neutrino results, MINOS will yield more precision measurements of the oscillation parameters, CNGS wants to settle the question whether oscillation will involve  $\tau$  neutrinos), all experiments will face similar problems, namely uncertainties in the knowledge of neutrino scattering: Obviously, the measurement of the flavor composition of a beam and its energy spectrum in a detector far away from the source is achieved by neutrino interactions with that detector. Uncertainties in the knowledge of this interaction will directly result into uncertainties of oscillations parameters, in particular into errors in the neutrino energy reconstruction. Since there is no test beam for "neutrino energy calibration", the energy has to be reconstructed from the measured final state particles using theoretical models (new experiments therefore use high- $Z$  calorimeters instead of Cerenkov detectors). Since the energy is directly related to the oscillation parameters, this technique is a source of systematic errors in the analysis.

Most important are uncertainties due to neutrino cross sections and nuclear effects - they are estimated to be 20 % [Lip02] or even 50 % [Har] in oscillation experiments.<sup>2</sup> Such a large error makes a precise determination of oscillation parameters difficult and experiments aiming to detect CP violation even impossible. For detailed discussions the reader is referred to Refs. [NuI02, NuI, NuI05], which conclude that a more precise knowledge of the cross section and a quantitative understanding of the weak nuclear response is a prerequisite for the analyses of future neutrino experiments.

### 1.4 Existing Neutrino Scattering Data and Future Experiments

The excitement about the discovery of the non-zero neutrino mass has driven many experiments as outlined above. But as just discussed those experiments now are in a position where a better knowledge of the detector response is essential, in particular neutrino cross sections and nuclear effects need to be understood. Therefore, we shall close these preliminaries with a brief summary of existing and planned experiments aiming at those questions.

In the 1 - 10 GeV region relevant existing data come from bubble chamber measurements running from the 1960's to the 1980's. Among them are most important the 12-foot bubble chamber Gargamelle at Argonne (ANL), the 7-foot bubble chamber at Brookhaven (BNL), the Big European Bubble Chamber (BEBC) at CERN, the Serpukhov bubble

---

<sup>2</sup>It was shown in Ref. [Super-K02] that even within these errors the oscillation hypothesis holds.



chamber SKAT, and the FNAL 15-foot bubble chamber (cf. Ref. [Wha05] for a collection of references and Ref. [Sak02] for a review). They studied neutrino and antineutrino interactions off free nucleons and heavy liquid targets. Data for quasielastic and inelastic scattering were taken on both light (Hydrogen and Deuterium) and heavy (Neon, Propane and Freon) targets. In nearly all cases, in measurements of the three charged current single pion channels cuts were placed on the hadronic invariant mass to limit the analysis to the resonant region.

Despite limited statistics and large neutrino flux uncertainties, it is primarily these data which are still used to fit neutrino scattering parameters. The cross sections calculated in this thesis also use these data. However, the quality of those old measurements is limited as are the kinematical regions covered.

Some newer neutrino scattering data will be available from K2K: The near detector has collected data on neutrino interactions [K2K05], which is currently the largest existing sample in the 1 GeV region.

Recently, two important experiments were proposed, namely MINER $\nu$ A [MINER $\nu$ A04a] and FINeSSE [FINeSSE04]. Both aim to explore neutrino nucleus scattering physics systematically, FINeSSE additionally aims to measure the strange-quark content in the nucleon. For their precision measurement of both the quasielastic and the inelastic neutrino nucleus cross sections, they will be able to identify and measure the momenta of leptons and hadrons as well as the energy of electromagnetic and hadronic showers.

To conclude, even though there are many neutrino experiments looking for oscillation and non-zero mass, there is lack of extensive and high-quality neutrino scattering data which can be used to address hadronic and nuclear physics questions.



## 2 Weak and Electromagnetic Interactions

While the first chapter aimed at giving a motivation and an experimental overview we now proceed to the theoretical framework. The electroweak interaction as part of the Standard Model is covered in many textbooks on Quantum Field Theory or High Energy Physics (see e. g. Refs. [Bai77, MS93, Rol94, AH96, Mos99]). Nonetheless, since it is the basis for our discussion of interactions of neutrinos with nucleons and nuclei, we shall briefly review the electroweak sector of the Standard Model and summarize basic facts on currents and their relations.

In the Standard Model, used in the following, neutrinos are considered massless and purely left-handed. This is in contrast to the experimental evidence for non-zero neutrino masses as discussed in the previous chapter. However, even though the non-zero mass is necessary for neutrino oscillations, it is not at all important for neutrino nucleon scattering simply because it is so small. This tiny mass will not affect any of the calculations, thus, we can assume it to be zero in the following.

### 2.1 Electroweak Theory

#### 2.1.1 Lagrangian of the Electroweak Interaction

The electroweak interaction is part of the Standard Model and based on a local  $SU(2) \times U(1)$  gauge symmetry. After spontaneous symmetry breaking via the Higgs mechanism we get for the interaction part of the Lagrangian [TW01]:

$$\mathcal{L}_{int} = -\frac{g}{2\sqrt{2}} (\mathcal{J}_\alpha^{CC} W^{\alpha\dagger} + \text{h. c.}) - \frac{g}{2 \cos \theta_W} \mathcal{J}_\alpha^{NC} Z^\alpha - e \mathcal{J}_\alpha^{EM} A^\alpha. \quad (2.1)$$

The weak charged current (CC)  $\mathcal{J}_\alpha^{CC}$ , the weak neutral current (NC)  $\mathcal{J}_\alpha^{NC}$  and the electromagnetic current (EM)  $\mathcal{J}_\alpha^{EM}$  couple to the charged  $W$ -boson field  $W^\alpha$ , the neutral  $Z$ -boson field  $Z^\alpha$  and the photon field  $A^\alpha$ , respectively. Relations between the coupling constants are outlined in Appendix A.3. The currents can be separated into a leptonic part, denoted by  $j_\alpha$ , and a hadronic part  $J_\alpha$ :

$$\mathcal{J}_\alpha = j_\alpha + J_\alpha. \quad (2.2)$$

$$\mathcal{L}_{int}^{leptonic} = \underbrace{\begin{array}{c} l \\ \diagdown \\ \text{---} W \\ \diagup \\ \nu_l \end{array}}_{\text{CC}} + \underbrace{\left( \begin{array}{c} l \\ \diagdown \\ \text{---} Z \\ \diagup \\ l \end{array} + \begin{array}{c} \nu_l \\ \diagdown \\ \text{---} Z \\ \diagup \\ \nu_l \end{array} \right)}_{\text{NC}} + \underbrace{\begin{array}{c} l \\ \diagdown \\ \text{---} \gamma \\ \diagup \\ l \end{array}}_{\text{EM}}$$

Figure 2.1: Leptonic part of the interaction Lagrangian ( $l = e, \mu$  or  $\tau$ ).

Since parity is maximal violated in weak interactions, the weak currents have to have a vector-axialvector ( $V - A$ ) structure.

The leptonic part of  $\mathcal{L}_{int}$  is schematically shown in Fig. 2.1. We shall now give explicit expressions for the leptonic and quark currents. For the Feynman rules we refer to Appendix C.

### 2.1.2 Leptonic Currents

We start the discussion of the currents with the leptonic part. The charged current couples to a charged  $W^\pm$  boson. It does not change the flavor but turns a charged lepton into a neutrino or vice versa. The coupling involves only left-handed fields leading to a vector-axialvector structure in the current, which is given by

$$j_\alpha^{CC} = \bar{\nu}_l \gamma_\alpha (1 - \gamma_5) l. \quad (2.3)$$

Neutral currents are mediated by neutral  $Z^0$  bosons. Those interactions also cannot change the flavor and even keep the identity of the lepton (cf. Fig. 2.1). For neutrinos only coupling to left handed fields is possible, for charged leptons both left and right-handed fields are involved but with different couplings:

$$j_\alpha^{NC} = \frac{1}{2} \bar{\nu}_l \gamma_\alpha (1 - \gamma_5) \nu_l - \frac{1}{2} (1 - 2 \sin^2 \theta_W) \bar{l} \gamma_\alpha (1 - \gamma_5) l + \sin^2 \theta_W \bar{l} \gamma_\alpha (1 + \gamma_5) l, \quad (2.4)$$

with the weak mixing angle (Weinberg angle)  $\sin \theta_W$ .

Finally, the electromagnetic current couples to photons and is given by

$$j_\alpha^{EM} = \bar{l} \gamma_\alpha l. \quad (2.5)$$

The interaction Lagrangian of course includes all lepton flavors, therefore a sum over all flavors is understood implicitly in these expressions.

### 2.1.3 Quark Currents

Omitting the heavy quark sector, in  $SU(3)_f$   $u$ ,  $d$  and  $s$  quarks are the building blocks of matter. Under the assumption that quarks are pointlike Dirac particles, their electromagnetic current is<sup>1</sup>

$$J_\alpha^{EM} = \bar{q}Q\gamma_\alpha q, \quad (2.6)$$

with

$$q = \begin{pmatrix} u \\ d \\ s \end{pmatrix} \quad \text{and} \quad Q = \text{diag} \left( \frac{2}{3}, -\frac{1}{3}, -\frac{1}{3} \right). \quad (2.7)$$

This yields more explicitly

$$J_\alpha^{EM} = \frac{2}{3}\bar{u}\gamma_\alpha u - \frac{1}{3}(\bar{d}\gamma_\alpha d + \bar{s}\gamma_\alpha s). \quad (2.8)$$

For the leptonic neutral current we showed that the coupling depends on the helicity of the fields and the current is diagonal in flavor. This is also valid for the hadronic neutral current which couples to the quark fields in the following way

$$J_\alpha^{NC} = \sum_q \bar{q}\gamma_\alpha [(t_3 - e_q \sin^2 \theta_W)(1 - \gamma_5) - e_q \sin^2 \theta_W(1 + \gamma_5)] q, \quad (2.9)$$

where  $e_q$  is the electric charge and  $t_3$  is the third component of the weak isospin. For up quarks we have  $t_3 = 1/2$ , for down and strange quarks it is  $t_3 = -1/2$ . The neutral current can be rewritten as

$$\begin{aligned} J_\alpha^{NC} &= \bar{u}\gamma_\alpha \left[ \frac{1}{2} - \frac{2}{3}2\sin^2 \theta_W - \frac{1}{2}\gamma_5 \right] u \\ &+ \bar{d}\gamma_\alpha \left[ -\frac{1}{2} - \left( -\frac{1}{3} \right) 2\sin^2 \theta_W + \frac{1}{2}\gamma_5 \right] d \\ &+ \bar{s}\gamma_\alpha \left[ -\frac{1}{2} - \left( -\frac{1}{3} \right) 2\sin^2 \theta_W + \frac{1}{2}\gamma_5 \right] s. \end{aligned} \quad (2.10)$$

Finally, we consider the charged current for quarks. The mass eigenstates with weak isospin of  $-1/2$  (the  $d$  and  $s$  quark) are not the weak eigenstates. However, both sets of

<sup>1</sup>Color plays no role here, since electroweak interactions are colorblind; note, however, that the currents here include an implicit sum over color.

eigenstates are connected through a unitary transformation. In the case of  $SU(3)_f$ , we get with the Cabbibo mixing matrix

$$\begin{pmatrix} d' \\ s' \end{pmatrix} = \begin{pmatrix} \cos \theta_C & \sin \theta_C \\ -\sin \theta_C & \cos \theta_C \end{pmatrix} \begin{pmatrix} d \\ s \end{pmatrix}, \quad (2.11)$$

where  $\theta_C$  is the Cabbibo mixing angle with  $\cos \theta_C = 0.974$ . The charged current is then given by

$$\begin{aligned} J_\alpha^{CC} &= \bar{q} \gamma_\alpha (1 - \gamma_5) q' \\ &= \bar{u} \gamma_\alpha (1 - \gamma_5) (\cos \theta_C d + \sin \theta_C s), \end{aligned} \quad (2.12)$$

which again reflects the  $(V - A)$  structure. In the following we neglect the part suppressed by the Cabbibo mixing, i. e. the one proportional to  $\sin \theta_C$  and we obtain

$$\begin{aligned} J_\alpha^{CC} &= \bar{u} \gamma_\alpha (1 - \gamma_5) \cos \theta_C d \\ &= \cos \theta_C (V_\alpha^{CC} - A_\alpha^{CC}). \end{aligned} \quad (2.13)$$

## 2.2 Properties of Quark Currents

### 2.2.1 Vector Current

We now study general properties and symmetries of the introduced currents. We shall show that the electromagnetic and the weak currents can be expressed as linear combinations of the conserved  $SU(3)_f$  vector current.

The quarks are described within QCD, the theory of strong interactions, by the Lagrangian [Wei]

$$\mathcal{L} = \bar{q} [\gamma_\alpha D^\alpha - m] q - \frac{1}{4} G_{\alpha\beta} G^{\alpha\beta} \quad (2.14)$$

with the non-Abelian gluon field tensor  $G_{\alpha\beta}$  and the mass matrix

$$m = \text{diag} (m_u, m_d, m_s). \quad (2.15)$$

The couplings of the quarks and gluons are encoded in the gauge covariant derivative  $D_\alpha$ . Apart from its local  $SU(3)_{color}$  gauge symmetry, QCD has global unitary symmetries. They imply conserved currents, which impose constraints on the dynamics of strongly interacting systems, irrespective whether those are quarks, gluons or composite hadrons.

Assuming isospin symmetry, i. e.  $m_u = m_d = m_s$ , the Lagrangian has a global  $SU(3)_f$  symmetry and is invariant under

$$q \rightarrow \exp\left(i\theta^a \frac{\lambda_a}{2}\right) q, \quad (2.16)$$

with  $\lambda_a$  being the Gell-Mann matrices which are listed in Appendix A.2. The corresponding conserved Noether currents are

$$V_\alpha^a = \bar{q}\gamma_\alpha \frac{\lambda_a}{2} q. \quad (2.17)$$

Note that this symmetry is broken by the quark mass differences:

$$\partial^\alpha V_\alpha^a = i\bar{q} \left[ m, \frac{\lambda_a}{2} \right] q. \quad (2.18)$$

Combinations of those flavor currents appear in the quark electromagnetic current. Rewriting Eq. (2.6) by using the charge operator

$$Q = \frac{Y}{2} + I_3, \quad (2.19)$$

the hypercharge

$$Y = B + S = \frac{\lambda_8}{\sqrt{3}} = \text{diag} \left( \frac{1}{3}, \frac{1}{3}, -\frac{2}{3} \right), \quad (2.20)$$

where  $B$  is the baryon number and  $S$  is the strangeness, and the third component of the strong isospin

$$I_3 = \frac{\lambda_3}{2} \quad (2.21)$$

yields for the electromagnetic current

$$J_\alpha^{EM} = \frac{1}{2} J_\alpha^Y + V_\alpha^3. \quad (2.22)$$

Here

$$V_\alpha^3 = \bar{q}\gamma_\alpha \frac{\lambda_3}{2} q \quad (2.23)$$

is the isovector (isospin) current and

$$J_\alpha^Y = \bar{q}\gamma_\alpha \frac{\lambda_8}{\sqrt{3}} q \quad (2.24)$$

the isoscalar (hypercharge) current.

Also the vector part of the charged current can be expressed as a linear combination of the flavor currents by

$$\begin{aligned}
 V_\alpha^{CC} &= \bar{u}\gamma_\alpha d \\
 &= \bar{q}\gamma_\alpha \frac{\lambda_1 + i\lambda_2}{2} q \\
 &= \bar{q}\gamma_\alpha \frac{\lambda_+}{2} q \\
 &= V_\alpha^1 + iV_\alpha^2.
 \end{aligned} \tag{2.25}$$

Finally, we rewrite the vector part of the neutral current in terms of the flavor currents and obtain

$$V_\alpha^{NC} = (1 - 2\sin^2\theta_W)V_\alpha^3 - 2\sin^2\theta_W \frac{1}{2}J_\alpha^Y - \frac{1}{2}J_\alpha^S, \tag{2.26}$$

with  $V_\alpha^3$  and  $J_\alpha^Y$  as above and  $J_\alpha^S$  given by

$$J_\alpha^S = \bar{s}\gamma_\alpha s. \tag{2.27}$$

We conclude that the isovector part of the electromagnetic current and the vector part of the weak currents are components of the same conserved  $SU(3)_f$  vector current.

## 2.2.2 Axial Current

In the limit of massless quarks, QCD has an additional symmetry, the so-called chiral symmetry. The QCD Lagrangian is invariant under independent transformations

$$q_L \rightarrow \exp\left(i\theta_L^a \frac{\lambda_a}{2}\right) q_L \quad \text{and} \quad q_R \rightarrow \exp\left(i\theta_R^a \frac{\lambda_a}{2}\right) q_R, \tag{2.28}$$

where  $q_L$  and  $q_R$  are the left and right-handed quark fields, respectively, and are defined as

$$q_{L,R} = \frac{1}{2}(1 \mp \gamma_5) q. \tag{2.29}$$

The corresponding conserved Noether currents are

$$J_\alpha^{a,L} = \bar{q}_L \gamma_\alpha \frac{\lambda_a}{2} q_L \quad \text{and} \quad J_\alpha^{a,R} = \bar{q}_R \gamma_\alpha \frac{\lambda_a}{2} q_R, \tag{2.30}$$



which yield the already introduced vector current

$$V_\alpha^a = J_\alpha^{a,L} + J_\alpha^{a,R} = \bar{q}\gamma_\alpha \frac{\lambda_a}{2} q \quad (2.31)$$

and the axial current

$$A_\alpha^a = J_\alpha^{a,R} - J_\alpha^{a,L} = \bar{q}\gamma_\alpha \gamma_5 \frac{\lambda_a}{2} q. \quad (2.32)$$

The chiral symmetry is explicitly broken by the non-zero quark masses, and the divergence of the axial current becomes

$$\partial^\alpha A_\alpha^a = i\bar{q} \left\{ m, \frac{\lambda_a}{2} \right\} \gamma_5 q. \quad (2.33)$$

The weak axial charged current is given by

$$\begin{aligned} A_\alpha^{CC} &= \bar{u}\gamma_\alpha \gamma_5 d \\ &= \bar{q}\gamma_\alpha \gamma_5 \frac{\lambda_+}{2} q \\ &= A_\alpha^1 + iA_\alpha^2, \end{aligned} \quad (2.34)$$

with the divergence

$$\partial^\alpha A_\alpha^{CC} = \frac{1}{2}i(m_u + m_d)\bar{u}\gamma_5 d. \quad (2.35)$$

Therefore, the weak axial current is conserved in the chiral limit  $m_u \rightarrow 0$  and  $m_d \rightarrow 0$ .

Finally, for the axial part of the neutral current, we obtain

$$A_\alpha^{NC} = A_\alpha^3 + \frac{1}{2}A_\alpha^S, \quad (2.36)$$

with

$$A_\alpha^a = \bar{q}\gamma_\alpha \gamma_5 \frac{\lambda_3}{2} q \quad (2.37)$$

and

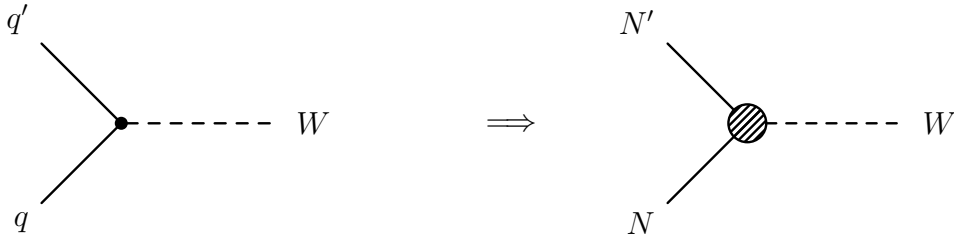
$$A_\alpha^S = \bar{s}\gamma_\alpha \gamma_5 s. \quad (2.38)$$

As the for the vector current, we conclude that the axial parts of both the neutral current ( $A_\alpha^3$ ) and the charged current ( $A_\alpha^1$  and  $A_\alpha^2$ ) belong to the same conserved  $SU(3)_f$  axial current. Note that there is no electromagnetic analogue in this case.

## 2.3 Hadronic Currents

### 2.3.1 Hadronic Transition Currents

At the low energies under consideration here quarks form baryons. While the elementary quark vertex is well-known as shown before, this is not the case for composite particles. For hadrons and nucleons, effective interactions can be introduced to parametrize our ignorance of low-energy QCD:



Even though the quark picture does not apply any more, its symmetries and Lorentz structures are reflected in the effective vertices. For example, the charged current will always have a  $(V - A)$  structure. Based on this symmetry argument we are then able to calculate cross sections in terms of *a priori* unknown form factors. We now extend the discussions on current algebra from quarks to composite systems. Those general theorems will be applied later to calculate explicit neutrino cross sections.

### 2.3.2 Conserved Vector Current Hypothesis

We showed that the electromagnetic current and the weak vector currents are related through the conserved flavor current. We only assumed isospin symmetry of the strong interaction. Thus, one expects the obtained relations to be independent of the details of the hadronic structure if isospin symmetry is a good symmetry of the particular hadronic system.

Assuming the hadronic currents to have the same structure as the quark currents discussed in chapter 2.2.1, we obtain for the electromagnetic current

$$J_{\alpha}^{EM} = \frac{1}{2}J_{\alpha}^Y + V_{\alpha}^3. \quad (2.39)$$

The vector part of the charged current is given by

$$V_{\alpha}^{CC} = V_{\alpha}^1 + iV_{\alpha}^2, \quad (2.40)$$

and the vector part of the neutral current by

$$V_\alpha^{NC} = (1 - 2 \sin^2 \theta_W) V_\alpha^3 - 2 \sin^2 \theta_W \frac{1}{2} J_\alpha^Y - \frac{1}{2} J_\alpha^S. \quad (2.41)$$

We further assume that the matrix elements of the hadronic currents  $V_\alpha^{CC}$  and  $V_\alpha^3$  are the same, being related by isospin rotation.

Before the advent of QCD this presumption was postulated by Feynman and Gell-Mann [FGM58] as the so-called conserved vector current hypothesis (CVC), a name we adopt in the following. We stress that on the quark level this hypothesis holds exactly as a consequence of QCD.

An implication of this hypothesis is that, because the electromagnetic current is conserved, also the weak vector current is conserved. Ref. [TH95] reviews further predictions of CVC and their experimental checks.

CVC will be used in the next chapters to express explicit neutrino cross sections in terms of electromagnetic form factors. In practice one usually assumes CVC and substitutes the weak vector charged current matrix elements with the isovector matrix elements from the electromagnetic interaction - in the words of Walecka [Wal95]: *CVC implies that the vector part of the single nucleon matrix element of the charge changing weak current whatever the detailed dynamic structure of the nucleon, can be obtained from electron scattering through the electromagnetic interaction!*

### 2.3.3 Partially Conserved Axial Current Hypothesis

Having discussed the vector part we now turn to the axial part. Again, we assume the hadronic currents to have the same structure as the quark currents discussed in chapter 2.2.2, which yields

$$A_\alpha^{CC} = A_\alpha^1 + i A_\alpha^2, \quad (2.42)$$

$$A_\alpha^{NC} = A_\alpha^3 + \frac{1}{2} A_\alpha^S. \quad (2.43)$$

Also for the axial current we assume that the matrix elements of the hadronic currents  $A_\alpha^{CC}$  and  $A_\alpha^3$  are the same - which holds exactly on the quark level.

We showed that in the limit of massless quarks, the axial current is conserved. When going from quark currents to hadronic currents one can show that (cf. Refs. [BD67, Bai77, IZ80, TH95, Wei])

$$\partial^\alpha A_\alpha^{CC} = \frac{1}{2} i (m_u + m_d) \bar{u} \gamma_5 d \rightarrow m_\pi^2 f_\pi \pi, \quad (2.44)$$

with the pion mass  $m_\pi$ , the pion decay constant  $f_\pi$  and the pion field operator  $\pi$ . The divergence of the axial current is therefore proportional to the square of the pion mass and vanishes in the chiral limit  $m_\pi \rightarrow 0$ . This is known as the partially conserved axial current hypothesis (PCAC) (for experimental validation see Ref. [TH95] (Goldberger-Treiman relation)). In practice, as for CVC, we assume PCAC and, as will be shown later, this can only be fulfilled if the axial current is dominated by a pion pole graph.

Being equipped with these powerful tools we shall close the preliminaries and proceed with the calculation of neutrino nucleon cross sections.

## **Part II**

# **Neutrino Nucleon Scattering**



## 3 Introduction to Neutrino Nucleon Scattering

Before we consider neutrino scattering off nuclei, we first need to develop the formalism of neutrino nucleon scattering to be used in our transport model (cf. chapter 7). Therefore in this and the following three chapters we shall provide a general discussion of neutrino nucleon reactions. This first chapter in the series starts with a general derivation of the inclusive inelastic cross section to point out relevant symmetries. It will become clear that inclusive cross sections are not suited for our requisites since they contain not enough information. More exclusive quantities need to be considered and thus, are calculated in the next two chapters applying those general symmetries. The relative importance of the various contributions to the cross section will be discussed in the second part of this chapter.

### 3.1 Inclusive Cross Section

We start our general discussion with reactions of the type

$$\nu N \rightarrow l^- X \quad \text{and} \quad \nu N \rightarrow \nu X \quad (3.1)$$

$$\bar{\nu} N \rightarrow l^+ X \quad \text{and} \quad \bar{\nu} N \rightarrow \bar{\nu} X \quad (3.2)$$

where  $l^\pm$  is an arbitrary lepton and  $X$  stands for the hadronic debris produced in the inelastic collision (Fig. 3.1). In these inclusive reactions only the energy and the scattering angle of the outgoing lepton are measured.

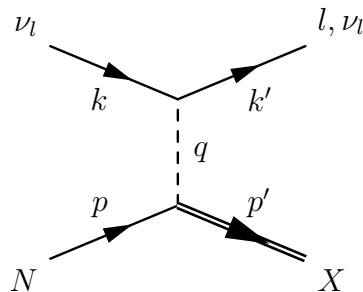


Figure 3.1: Inelastic neutrino-nucleon scattering (analogous for antineutrinos).

These reactions are similar to inelastic electron-nucleon (or photo-nucleon) scattering. The nucleon is not probed by a (virtual) photon but by a gauge vector boson and the coupling now contains both vector and axial vector parts as discussed in the previous chapter.

In the Born approximation, the invariant matrix element for charged current reactions of neutrinos can be written as

$$\mathcal{M} = \left( \frac{g}{2\sqrt{2}} \right)^2 \bar{u}_l(k') \gamma_\alpha (1 - \gamma_5) u_\nu(k) \frac{i}{q^2 - M_W^2} \left( -g^{\alpha\beta} + \frac{q^\alpha q^\beta}{M_W^2} \right) \langle X(p') | J_\beta(0) | N(p) \rangle. \quad (3.3)$$

For scattering with low momentum transfer ( $|q^2| \ll M_W^2$ ) we can replace the propagator

$$\frac{i}{q^2 - M_W^2} \left( -g^{\alpha\beta} + \frac{q^\alpha q^\beta}{M_W^2} \right) \longrightarrow \frac{i g^{\alpha\beta}}{M_W^2} \quad (3.4)$$

and obtain

$$\mathcal{M} = i \frac{g^2}{8M_W^2} \bar{u}_l(k') \gamma_\alpha (1 - \gamma_5) u_\nu(k) \langle X(p') | J^\alpha(0) | N(p) \rangle. \quad (3.5)$$

The spin averaged matrix element squared is then given by

$$|\bar{\mathcal{M}}|^2 = \frac{G_F^2}{2} L_{\alpha\beta} W^{\alpha\beta}, \quad (3.6)$$

where we used

$$\frac{g^2}{8M_W^2} = \frac{G_F}{\sqrt{2}}. \quad (3.7)$$

The lepton tensor  $L_{\alpha\beta}$  is easily calculated to

$$\begin{aligned} L_{\alpha\beta} &= \sum_{\substack{\text{initial} \\ \text{spins}}} \sum_{\substack{\text{final} \\ \text{spins}}} [\bar{u}_l(k') \gamma_\alpha (1 - \gamma_5) u_\nu(k)]^\dagger [\bar{u}_l(k') \gamma_\beta (1 - \gamma_5) u_\nu(k)] \\ &= \text{Tr} [(\not{k}' + m_l) \gamma_\alpha (1 - \gamma_5) (\not{k}' + m_l) \gamma_\beta (1 - \gamma_5)] \\ &= 8 [k'_\alpha k_\beta + k_\alpha k'_\beta - g_{\alpha\beta} k \cdot k' + i \epsilon_{\alpha\beta\rho\sigma} k^\rho k'^\sigma] \\ &= L_{\alpha\beta}^S + i L_{\alpha\beta}^A. \end{aligned} \quad (3.8)$$

The superscripts  $S$  and  $A$  refer to the symmetry under interchange of the Lorentz indices  $\alpha$  and  $\beta$ . For antineutrinos the antisymmetric piece proportional to the totally antisymmetric



tensor  $\epsilon_{\alpha\beta\rho\sigma}$  gets a minus sign and we end up with the following expression for the lepton tensor:

$$L_{\alpha\beta}^{\nu,\bar{\nu}} = L_{\alpha\beta}^S \pm iL_{\alpha\beta}^A. \quad (3.9)$$

We emphasize that this antisymmetric piece is not contained in the electromagnetic lepton tensor.

The hadronic tensor  $W^{\alpha\beta}$  is more complicated for weak interactions than in the electromagnetic case because parity and current conservation are no constraints any more. The hadronic tensor must have the same Lorentz structure as the leptonic tensor, hence we obtain

$$W^{\alpha\beta} = W_S^{\alpha\beta} + iW_A^{\alpha\beta}, \quad (3.10)$$

with  $W_{S(A)}^{\alpha\beta}$  being real symmetric (antisymmetric) tensor. The most general tensor, representing the structure of the nucleon, is completely determined by six independent structure functions [TW01]:

$$\begin{aligned} W^{\alpha\beta} = & -g^{\alpha\beta}W_1 + \frac{p^\alpha p^\beta}{M^2}W_2 + \frac{i\epsilon^{\alpha\beta\rho\sigma}p_\rho q_\sigma}{2M^2}W_3 + \frac{q^\alpha q^\beta}{M^2}W_4 \\ & + \frac{p^\alpha q^\beta + q^\alpha p^\beta}{2M^2}W_5 + \frac{i(p^\alpha q^\beta - q^\alpha p^\beta)}{2M^2}W_6. \end{aligned} \quad (3.11)$$

The functions  $W_i$  are real and Lorentz scalar functions of  $\nu = p \cdot q$  and  $q^2$ . Contrary to the electromagnetic case,  $W_3$  and  $W_6$  appear here because of parity violation, and  $W_4$  and  $W_5$  because they cannot be related to  $W_1$  and  $W_2$  by current conservation.

The calculation of the cross section requires the contraction of both tensors in Eq. (3.6). The only non-zero contributions involve the contractions of the symmetric part of  $W^{\alpha\beta}$ ,  $W_{1,2,4,5}$ , with  $L_{\alpha\beta}^S$  and the antisymmetric parts  $W_{3,6}$  with  $L_{\alpha\beta}^A$ . Doing the algebra, one finds that the terms proportional to  $W_6$  do not survive the contraction. The terms involving  $W_4$  and  $W_5$  are proportional to the lepton mass.

At this point, it is again worthwhile to mention a major difference between neutrino and electron scattering. While for electron scattering one must prepare a polarized beam to probe the antisymmetric part of the hadronic tensor, for neutrinos this comes for free.

The cross section follows from Eq. (C.1) in the appendix:

$$\frac{d^2\sigma}{d\Omega dE_l} = \frac{G_F^2}{4\pi^2} \frac{|\vec{k}|}{|\vec{k}'|} L_{\alpha\beta} W^{\alpha\beta} \quad (3.12)$$

with  $d\Omega = d\cos\theta d\phi$ , and  $\theta$  being the angle between incoming neutrino and outgoing lepton.  $E_l$  is the energy of the outgoing lepton.

For charged current neutrino scattering, one obtains the expression

$$\begin{aligned} \frac{d^2\sigma}{d\Omega dE_l} = & \frac{|\vec{k}'| E_l M G_F^2}{\pi^2} \left\{ 2W_1 \sin^2 \frac{\theta}{2} + W_2 \cos^2 \frac{\theta}{2} - W_3 \frac{E_\nu + E_l}{M} \sin^2 \frac{\theta}{2} \right. \\ & + \frac{m_l^2}{E_l(E_l + |\vec{k}'|)} \left[ W_1 \cos \theta - \frac{W_2}{2} \cos \theta \right. \\ & + \frac{W_3}{2} \left( \frac{E_l + |\vec{k}'|}{M} - \frac{E_\nu + E_l}{M} \cos \theta \right) \\ & \left. \left. + \frac{W_4}{2} \left( \frac{m_l^2}{M^2} \cos \theta + \frac{2E_l(E_l + |\vec{k}'|)}{M^2} \sin^2 \theta \right) - W_5 \frac{E_l + |\vec{k}'|}{2M} \right] \right\}, \quad (3.13) \end{aligned}$$

where  $M$  is the nucleon mass. For antineutrinos, the sign in front of  $W_3$  changes.

For neutral currents the matrix element of Eq. (3.3) is modified due to the different coupling:

$$\mathcal{M} = \left( \frac{e}{2 \sin \theta_W \cos \theta_W} \right)^2 \bar{u}_l(k') \gamma_\alpha \frac{1 - \gamma_5}{2} u_\nu(k) \frac{i \left( -g^{\alpha\beta} + \frac{q^\alpha q^\beta}{M_Z^2} \right)}{q^2 - M_Z^2} \langle X(p') | J_\beta(0) | N(p) \rangle. \quad (3.14)$$

The index  $l$  refers to the outgoing neutrino. For scattering with low momentum transfer ( $|q^2| \ll M_Z^2$ ) the propagator reads

$$\frac{i}{q^2 - M_Z^2} \left( -g^{\alpha\beta} + \frac{q^\alpha q^\beta}{M_Z^2} \right) \longrightarrow \frac{i g^{\alpha\beta}}{M_Z^2} \quad (3.15)$$

and one obtains

$$\mathcal{M} = \left( \frac{e}{2M_Z \sin \theta_W \cos \theta_W} \right)^2 \bar{u}_l(k') \gamma_\alpha \frac{1 - \gamma_5}{2} u_\nu(k) \langle X(p') | J^\alpha(0) | N(p) \rangle. \quad (3.16)$$

The coupling can be rewritten as

$$\frac{e^2}{8M_Z^2 \sin^2 \theta_W \cos^2 \theta_W} = \frac{G_F}{\sqrt{2}}, \quad (3.17)$$

where we used

$$e = g \sin \theta_W, \quad (3.18)$$

$$\cos \theta_W = \frac{M_W}{M_Z}, \quad (3.19)$$

$$\frac{G_F}{\sqrt{2}} = \frac{g^2}{8M_W^2}. \quad (3.20)$$

Therefore, for the spin averaged matrix element squared we obtain the same as for the charged current interactions in Eq. (3.6):

$$|\bar{\mathcal{M}}|^2 = \frac{G_F^2}{2} L_{\alpha\beta} W^{\alpha\beta}. \quad (3.21)$$

$L_{\alpha\beta}$  and  $W^{\alpha\beta}$  are as in Eq. (3.8) and in Eq. (3.11), respectively, but with  $m_l = 0$  due to the vanishing neutrino mass. The neutral current cross section is then given in analogy to Eq. (3.13)

$$\frac{d^2\sigma}{d\Omega dE_l} = \frac{|\vec{k}'| E_l M G_F^2}{\pi^2} \left\{ 2W_1 \sin^2 \frac{\theta}{2} + W_2 \cos^2 \frac{\theta}{2} - W_3 \frac{E_\nu + E_l}{M} \sin^2 \frac{\theta}{2} \right\}. \quad (3.22)$$

For antineutrinos, the  $W_3$  term has a different sign.

To deal with the available data, we also need the differential cross section in terms of the invariant mass  $W$  of the hadronic final state and the squared momentum transfer  $Q^2 = -q^2$ , which equals the Mandelstam variable  $t$ , instead of the lepton energy  $E_l$  and the scattering angle  $\theta$ . The relations between them are

$$Q^2 = 2E_\nu E_l - 2|\vec{k}||\vec{k}'| \cos \theta - m_l^2 \quad (3.23)$$

and

$$W^2 = M^2 + 2M(E_\nu - E_l) - Q^2. \quad (3.24)$$

By using these relations we obtain

$$\frac{d^2\sigma}{dQ^2 dW} = \frac{\pi W}{M |\vec{k}||\vec{k}'|} \frac{d^2\sigma}{d\Omega dE_l}. \quad (3.25)$$

The total cross section for a given incident neutrino energy is then given by

$$\sigma(E_\nu) = \int_{W_{min}}^{W_{max}} dW \int_{Q_{min}^2}^{Q_{max}^2} dQ^2 \frac{d^2\sigma}{dQ^2 dW} \quad (3.26)$$

with the integration bounds

$$W_{min} = M, \quad (3.27)$$

$$W_{max} = \sqrt{s} - m_l. \quad (3.28)$$

Here  $\sqrt{s}$  is the invariant mass of the initial  $\nu - N$  system. For a fixed  $W$ ,  $Q^2$  runs in the range of

$$Q_{min}^2 = -m_l^2 + 2E_\nu(E_l - |\vec{k}'|), \quad (3.29)$$

$$Q_{max}^2 = -m_l^2 + 2E_\nu(E_l + |\vec{k}'|). \quad (3.30)$$

Eq. (3.13) is the most general expression for charged current neutrino-nucleon scattering at energies small compared to the vector boson mass. Thus, the differential cross section is completely defined by a set of five structure functions which parametrize our ignorance about QCD. In principle, these functions could be measured. In practice, however, this is beyond realistic expectations and it is not possible to proceed further without an explicit model of the hadronic vertex. Therefore, we will disentangle different processes and discuss the individual terms in the following chapters.

## 3.2 Decomposition of the Cross Section

We shall now decompose the neutrino nucleon scattering into its pieces. In the next chapters we shall present models of those parts and calculate exclusive cross sections instead of the inclusive one just presented.

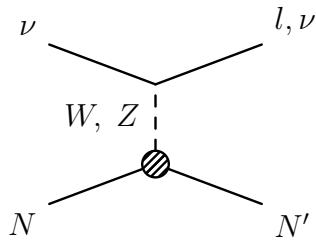
For neutrinos, as well as for antineutrinos, we can distinguish neutral and charged current interactions:

$$\sigma = \sigma^{CC} + \sigma^{NC}. \quad (3.31)$$

For each part there are basically three processes which add up to the total cross section

$$\sigma^{CC,NC} = \sigma(\text{QE}) + \sigma(\text{RES}) + \sigma(\text{Non-RES/DIS}). \quad (3.32)$$

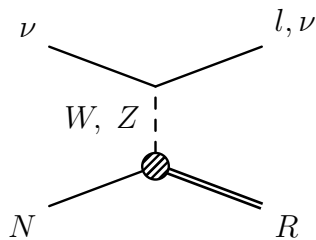
- **(Quasi)Elastic (QE):**



$$\text{CC: } \nu N \rightarrow l N' \quad (3.33)$$

$$\text{NC: } \nu N \rightarrow \nu N \quad (3.34)$$

- **Resonance production (RES):**



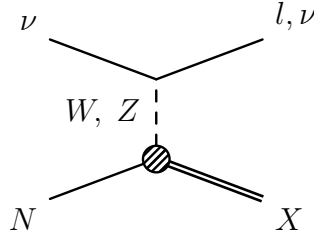
$$\text{CC: } \nu N \rightarrow l R \quad (3.35)$$

$$\text{NC: } \nu N \rightarrow \nu R \quad (3.36)$$

• **Non-resonant background / Deep inelastic scattering (DIS):**



$$\text{CC: } \nu N \rightarrow lX \quad (3.37)$$



$$\text{NC: } \nu N \rightarrow \nu X \quad (3.38)$$

$\nu$  stands here for every kind of neutrino flavor as well as for its antiparticle. The term "quasielastic" refers to the fact that the neutrino changes its identity to a charged lepton. If the outgoing lepton is still a neutrino, the reaction is denoted as "elastic". The term "deep inelastic" refers to the kinematical regime where both  $Q^2$  and the mass of the hadronic final state are large compared to typical hadron masses.

Having those three basic processes at hand we can describe all relevant physical reactions. The cross section is then a sum of all single contribution, namely the production of nucleons, of pions, etas and kaons, etc:

$$\sigma^{CC,NC} = \underbrace{\sigma(N)}_{\text{mainly from QE}} + \underbrace{\sigma(\pi)}_{\text{mainly from RES}} + \underbrace{\sigma(\eta) + \sigma(K)}_{\text{from RES, DIS}} + \dots \quad (3.39)$$

In this thesis we are mostly interested in energies in the resonance region, i. e. neutrino energies up to about 2 GeV. This will mainly probe the first two parts of the above equation. The most important processes at these energies are quasielastic scattering and resonance production (see Fig. 3.2). The resonance production, however, is dominated by the  $\Delta(1232)$  (cf. chapter 6) which subsequently decays into a pion nucleon pair (cf. Eq. (3.39)). Therefore, the next two chapters will be devoted to the calculation of quasielastic scattering and of  $\Delta$  production. In chapter 6 we shall discuss the remaining contributions needed for a full description of neutrino nucleon scattering.

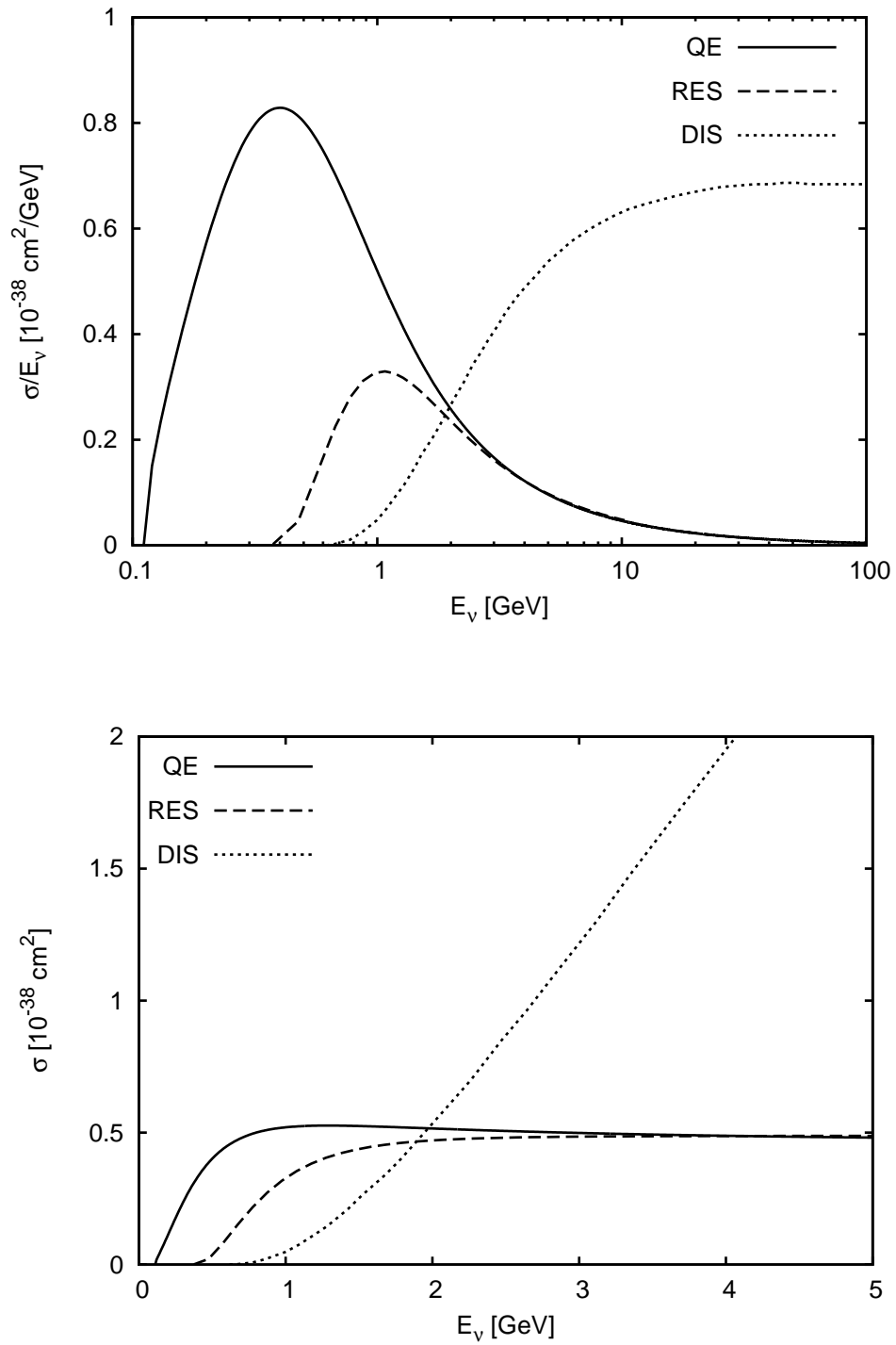


Figure 3.2: Total cross sections as a function of the neutrino energy for  $\nu_\mu N \rightarrow \mu^- X$  decomposed in QE, RES and DIS. The upper plot is scaled by the neutrino energy. The DIS curve is taken from Ref. [Super-K05].

## 4 (Quasi)Elastic Scattering

We start our discussion of the various processes with quasielastic scattering (QE). As shown in Fig. 3.2, this is the most important reaction for neutrino energies up to about 1 GeV. This chapter is organized in the following way: First charged current (CC) interactions are calculated and discussed in detail, followed by the neutral current (NC) reactions. This discrimination is necessary due to the effects of the strange sea in the nucleon which is important for NC scattering.

### 4.1 Quasielastic Charged Current Interaction

#### 4.1.1 Formalism

Here we consider the charged current quasielastic reactions. For antineutrinos a negatively charged vector boson is exchanged,

$$\bar{\nu}p \rightarrow l^+n, \quad (4.1)$$

while for neutrinos the vector boson is positively charged,

$$\nu n \rightarrow l^-p. \quad (4.2)$$

The derivation of the cross section will be given explicitly for neutrinos, the final result is then straightforward to extend to antineutrinos. The calculations are not restricted to a particular neutrino flavor. We use the notation as defined in Appendix B.1.

The spin averaged matrix element squared is given by Eq. (3.6):

$$|\bar{\mathcal{M}}|^2 = \frac{G_F^2}{2} L_{\alpha\beta} W^{\alpha\beta}. \quad (4.3)$$

The leptonic tensor was already calculated in Eq. (3.8). For the hadronic tensor we found a general expression (cf. Eq. (3.11)) with so far unspecified structure functions. To introduce our model of the hadronic vertex we go back to Eq. (3.5) and to the hadronic current:

$$J_\alpha^{CC} = \langle p(p') | J_\alpha^{CC}(0) | n(p) \rangle, \quad (4.4)$$

where  $|n(p)\rangle$  denotes a neutron of momentum  $p$  and  $|p(p')\rangle$  is a proton of momentum  $p'$ . The transformation of a neutron into a proton means, in the valence quark model, the transformation of a down quark into an up quark. It then follows from Eq. (2.12) that we must include Cabbibo mixing - this gives a factor of  $\cos\theta_C$ . From Lorentz invariance arguments we know that  $J_\alpha$  is consisting of vector and axial vector currents, thus we obtain

$$J_\alpha^{CC} = \cos\theta_C(V_\alpha^{CC} - A_\alpha^{CC}). \quad (4.5)$$

Following the arguments of Ref. [NPR05] we construct the most general form out of the four-vectors at our disposal:  $p_\alpha, p'_\alpha$  and  $q_\alpha = p'_\alpha - p_\alpha$ . Gordon identities (cf. e. g. Appendix A.2 in Ref. [IZ80]) limit the number of terms and we get the following expression for the vector part:

$$V_\alpha^{CC} = \bar{u}_p(p') \left[ \gamma_\alpha F_1^V(Q^2) + \frac{i}{2M} \sigma_{\alpha\beta} q^\beta F_2^V(Q^2) + \frac{q_\alpha}{M} F^S(Q^2) \right] u_n(p), \quad (4.6)$$

with  $Q^2 = -q^2$  and the nucleon mass  $M$ .<sup>1</sup>  $F_{1,2}^V$  are the vector form factors and  $F^S$  is the scalar form factor. The same procedure yields for the axial part:

$$-A_\alpha^{CC} = \bar{u}_p(p') \left[ \gamma_\alpha \gamma_5 F_A(Q^2) + \frac{i}{2M} \sigma_{\alpha\beta} q^\beta \gamma_5 F_T(Q^2) + \frac{q_\alpha}{M} \gamma_5 F_P(Q^2) \right] u_n(p). \quad (4.7)$$

Here  $F_A$  is the axial form factor,  $F_T$  the tensor and  $F_P$  the pseudoscalar form factor.

Thus, the one-nucleon matrix element is described by six form factors which are functions of  $Q^2$ . When invariance under time inversions holds, the form factors, defined through the matrix element above, are real. This is explicitly derived in Appendix G of Ref. [Bil94]. Furthermore, we shall show, that

$$F^S = 0 \quad \text{and} \quad F_T = 0. \quad (4.8)$$

Those two terms have the opposite behavior under charge symmetry from the other terms. Protons are turned into neutrons (and vice versa) through a rotation by  $\pi$  about the  $y$ -axis in isospace [Bil94, TW01]:

$$\mathcal{C} = \exp(i\pi I_2), \quad (4.9)$$

with  $I_2$  being the isospin generator. Thus  $\mathcal{C}J_\alpha^{CC}\mathcal{C}^{-1}$  describes the same transition as  $J_\alpha^{CC\dagger}$ . It is shown in detail in Ref. [Bil94] that

$$\mathcal{C}J_\alpha^{CC}\mathcal{C}^{-1} = -J_\alpha^{CC\dagger} \quad (4.10)$$

---

<sup>1</sup>We do not distinguish proton and neutron masses here as well as anywhere else in this work - it was shown in Ref. [SV03] that this approximation affects only the lowest energies close to threshold (cf. Appendix B.2). Therefore, a more complicated formalism is not required here.



holds only if  $F_T = F^S = 0$  because the terms involving  $F_T$  and  $F^S$  transform with the opposite sign. Such a transformation defines so-called second-class currents [Wei58] which, motivated by the experiments placing accurate limits on those currents [Wil00], shall be ignored from now on.

With the hadronic current

$$J_\alpha^{CC} = \cos \theta_C \bar{u}_p(p') \left[ \gamma_\alpha F_1^V + \frac{i}{2M} \sigma_{\alpha\beta} q^\beta F_2^V + \gamma_\alpha \gamma_5 F_A + \frac{q_\alpha}{M} \gamma_5 F_P \right] u_n(p), \quad (4.11)$$

the cross section is given by ( $Q^2 = -q^2$ ) [LS72]

$$\frac{d\sigma^{\nu,\bar{\nu}}}{dQ^2} = \frac{M^2 G_F^2 \cos^2 \theta_C}{8\pi E_\nu^2} \left[ A \mp \frac{s-u}{M^2} B + \frac{(s-u)^2}{M^4} C \right], \quad (4.12)$$

with

$$s - u = 4ME_\nu - Q^2 - m_l^2, \quad (4.13)$$

$$\tau = \frac{Q^2}{4M^2}, \quad (4.14)$$

and

$$A = \frac{(m_l^2 + Q^2)}{M^2} \left[ (1 + \tau) F_A^2 - (1 - \tau) (F_1^V)^2 + \tau (1 - \tau) (F_2^V)^2 + 4\tau F_1^V F_2^V - \frac{m_l^2}{4M^2} \left( (F_1^V + F_2^V)^2 + (F_A + 2F_P)^2 - \left( \frac{Q^2}{M^2} + 4 \right) F_P^2 \right) \right], \quad (4.15)$$

$$B = \frac{Q^2}{M^2} F_A (F_1^V + F_2^V), \quad (4.16)$$

$$C = \frac{1}{4} (F_A^2 + (F_1^V)^2 + \tau (F_2^V)^2). \quad (4.17)$$

Neutrino and antineutrino scattering differ by the sign in front of the  $B$  term. The form factors for neutrino and antineutrino scattering are the same because of charge symmetry of the matrix element. With the given dependence on the lepton mass  $m_l$ , the cross section is valid for all flavors. Note that  $F_P$  is multiplied by  $m_l^2/M^2$  so its contribution is negligible for  $\nu_\mu$  and  $\nu_e$ , but becomes important for  $\nu_\tau$ .

At this point, the cross section is given in terms of four unknown form factors  $F_1^V$ ,  $F_2^V$ ,  $F_A$  and  $F_P$ . The vector form factors can now be related to electron scattering form factors by assuming CVC (cf. chapter 2.3.2). We start with an isospin doublet of proton and neutron:

$$u = \begin{pmatrix} u_p \\ u_n \end{pmatrix}. \quad (4.18)$$

The electromagnetic matrix element reads:

$$J_\alpha^{EM} = \bar{u}_p(p') \left[ \gamma_\alpha F_1^p + \frac{i}{2M} \sigma_{\alpha\beta} q^\beta F_2^p \right] u_p(p) + \bar{u}_n(p') \left[ \gamma_\alpha F_1^n + \frac{i}{2M} \sigma_{\alpha\beta} q^\beta F_2^n \right] u_n(p), \quad (4.19)$$

where  $F_1^{p,n}$  and  $F_2^{p,n}$  are the well-known Dirac and Pauli form factors of the nucleon. As shown in chapter 2.3.2, the electromagnetic current can be split into an isovector and an isoscalar part,

$$J_\alpha^{EM} = V_\alpha^3 + \frac{1}{2} J_\alpha^Y, \quad (4.20)$$

where

$$V_\alpha^3 = \bar{u} \left[ \gamma_\alpha F_1^v + \frac{i}{2M} \sigma_{\alpha\beta} q^\beta F_2^v \right] \frac{\tau_3}{2} u, \quad (4.21)$$

$$\frac{1}{2} J_\alpha^Y = \bar{u} \left[ \gamma_\alpha F_1^s + \frac{i}{2M} \sigma_{\alpha\beta} q^\beta F_2^s \right] \frac{\mathbb{1}}{2} u, \quad (4.22)$$

and hence

$$F_{1,2}^{v,s} = F_{1,2}^p \mp F_{1,2}^n. \quad (4.23)$$

Rewriting the vector part of the charged current of Eq. (4.11) in terms of the nucleon isospin doublet yields

$$V_\alpha^{CC} = \bar{u} \left[ \gamma_\alpha F_1^V + \frac{i}{2M} \sigma_{\alpha\beta} q^\beta F_2^V \right] \frac{\tau_+}{2} u. \quad (4.24)$$

CVC now implies that the currents of Eq. (4.21) and Eq. (4.24) are components of the same isospin multiplet of conserved currents, and therefore their form factors are equal:

$$F_{1,2}^v = F_{1,2}^V. \quad (4.25)$$

The implications are remarkable: With the electromagnetic current also the weak vector current is conserved, and for the form factors CVC finally yields

$$F_{1,2}^V = F_{1,2}^p - F_{1,2}^n, \quad (4.26)$$

where  $F_1^{p,n}$  and  $F_2^{p,n}$  are the Dirac and Pauli form factors of the nucleon. Rewriting them in terms of Sachs form factors (cf. e. g. Ref. [Sto93]),

$$G_M^{p,n} = F_1^{p,n} + F_2^{p,n}, \quad (4.27)$$

$$G_E^{p,n} = F_1^{p,n} - \frac{Q^2}{4M^2} F_2^{p,n}, \quad (4.28)$$

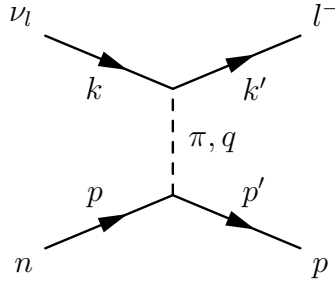


Figure 4.1: Pion pole dominance of the pseudoscalar form factor.

one gets

$$F_1^V(Q^2) = \frac{(G_E^p(Q^2) - G_E^n(Q^2)) + \frac{Q^2}{4M^2}(G_M^p(Q^2) - G_M^n(Q^2))}{1 + \frac{Q^2}{4M^2}}, \quad (4.29)$$

$$F_2^V(Q^2) = \frac{(G_M^p(Q^2) - G_M^n(Q^2)) - (G_E^p(Q^2) - G_E^n(Q^2))}{1 + \frac{Q^2}{4M^2}}. \quad (4.30)$$

$G_M$  and  $G_E$  are the magnetic and the electric form factors of the nucleon, respectively.

Having related the vector form factors to electron scattering, we shall now discuss the axial and the pseudoscalar form factors. The axial part of Eq. (4.11) can be rewritten using the nucleon isospin doublet as

$$A_\alpha^{CC} = \bar{u} \left[ \gamma_\alpha \gamma_5 F_A + \frac{q_\alpha}{M} \gamma_5 F_P \right] \frac{\tau_+}{2} u. \quad (4.31)$$

Assuming PCAC (cf. chapter 2.3.3), the divergence of Eq. (4.31) must be proportional to the pion mass squared. Thus, in the chiral limit the axial current is conserved. However, this is not the case for the  $F_A$  term alone. But if we additionally assume that the pseudoscalar term is dominated by a pion pole graph then PCAC can indeed be satisfied [TH95, Wal95].

There is a one-pion exchange process with contributes to the matrix element - a pion is created at the proton-neutron vertex and then couples to the lepton pair (see Fig. 4.1). The axial current is then given by

$$\begin{aligned} A_\alpha^\pi &= (n \rightarrow p\pi^- \text{ vertex}) \times (\pi^- \text{ propagator}) \times (\pi^- \rightarrow \bar{\nu}l \text{ vertex}) \\ &= (-ig_{\pi NN} F_{\pi NN}(Q^2) \bar{u} \gamma_5 \tau_+ u) \times \left( \frac{1}{Q^2 + m_\pi^2} \right) \times (if_\pi q_\alpha), \end{aligned} \quad (4.32)$$

where  $g_{\pi NN} = 13.1$  is the pion-nucleon coupling constant and  $f_\pi = 92.4$  MeV is the pion-decay constant.  $F_{\pi NN}(Q^2)$  is a vertex form factor, taken to be a smooth function of  $Q^2$  with  $F_{\pi NN}(Q^2 = m_\pi^2) = 1$ , so that  $g_{\pi NN}$  becomes the physically measured coupling constant.

Comparing Eq. (4.31) with Eq. (4.32) motivates the assumption of identifying the pseudoscalar form factor term with the pion pole contribution:

$$\frac{F_P(Q^2)}{M} = \frac{2g_{\pi NN}F_{\pi NN}(Q^2)f_\pi}{Q^2 + m_\pi^2}. \quad (4.33)$$

The divergence of the axial current then gives

$$\partial^\alpha A_\alpha^{CC} = \bar{u}_p \left[ 2MF_A(Q^2) - Q^2 \frac{2g_{\pi NN}F_{\pi NN}(Q^2)f_\pi}{Q^2 + m_\pi^2} \right] \gamma_5 u_n. \quad (4.34)$$

As required by PCAC, the divergence is proportional to  $m_\pi^2$  if the following relation holds:

$$MF_A(Q^2) = g_{\pi NN}F_{\pi NN}(Q^2)f_\pi. \quad (4.35)$$

At  $Q^2 = 0$  and  $F_{\pi NN}(Q^2 = 0) \approx F_{\pi NN}(Q^2 = m_\pi^2) = 1$  this is known as the Goldberger-Treiman relation. Its prediction for the axial vector constant  $F_A(0)$  is reasonably close (as good as 2 % [TH95]) to the experimental value obtained from neutron  $\beta$  decay. This accuracy shows the excellent prediction of PCAC.<sup>2</sup>

Now the pseudoscalar form factor  $F_P$  and the axial form factors  $F_A$  can be related:

$$F_P(Q^2) = \frac{2M^2}{Q^2 + m_\pi^2} F_A(Q^2). \quad (4.36)$$

For a detailed discussion of the axial structure of the nucleon the reader is referred to Ref. [BEM02].

Before proceeding we shall briefly summarize. Starting with four unknown form factors  $F_1^V$ ,  $F_2^V$ ,  $F_A$  and  $F_P$  we are now left with the Sachs form factors  $G_E^{p,n}$  and  $G_M^{p,n}$  which are known from electron scattering and with the axial form factor  $F_A$  which can only be accessed through weak interaction processes.

### 4.1.2 Form Factors

The simplest parametrization of the form factors used in the literature is the dipole form. For the Sachs form factors we have

$$G_E^p(Q^2) = G_D(Q^2), \quad (4.37)$$

$$G_E^n(Q^2) = 0, \quad (4.38)$$

$$G_M^p(Q^2) = \mu_p G_D(Q^2), \quad (4.39)$$

$$G_M^n(Q^2) = \mu_n G_D(Q^2), \quad (4.40)$$

---

<sup>2</sup>The pseudoscalar form factor was also measured directly and the PCAC prediction was confirmed (cf. Ref. [BEM02] and Ref. [TW01]).

with the magnetic moments of the proton  $\mu_p = 2.793$  and of the neutron  $\mu_n = -1.913$ .  $G_D$  is given by

$$G_D(Q^2) = \frac{1}{\left(1 + \frac{Q^2}{M_V^2}\right)^2}, \quad (4.41)$$

with the vector mass  $M_V = 0.843$  GeV. At zero momentum transfer the form factors are fixed by the electric charge and the magnetic moments of the nucleon.

Also for the axial form factor we apply a dipole form:

$$F_A(Q^2) = \frac{g_A}{\left(1 + \frac{Q^2}{M_A^2}\right)^2}, \quad (4.42)$$

where we have for the axial vector constant  $g_A = -1.267$  and for the axial mass  $M_A = 1.026$  GeV [BEM02].

However, the best analysis as of today is from Bodek et al. [BBA03] which takes into account recent electron scattering data from JLAB [A00, A02] to obtain updated values for the Sachs form factors. With those new vector form factors, they fitted again the old neutrino data and updated also the axial mass which is the largest uncertainty in neutrino nucleon scattering. We will use their set of form factors (BBA-2003 form factors) in this thesis. The BBA-2003 form factors are given by

$$G_{E,M}^N(Q^2) = \frac{G_{E,M}^N(0)}{1 + a_2 Q^2 + a_4 Q^4 + a_6 Q^6 + a_8 Q^8 + a_{10} Q^{10} + a_{12} Q^{12}}. \quad (4.43)$$

The fit parameters  $a_2 \dots a_{12}$  are listed in Table 4.1.  $G_{E,M}^N(0)$  equals those of the dipole

	$a_2$	$a_4$	$a_6$	$a_8$	$a_{10}$	$a_{12}$
$G_E^p$	3.253	1.422	0.08582	0.3318	-0.09371	0.01076
$G_M^p$	3.104	1.428	0.1112	-0.006981	0.0003705	$-0.7063 \cdot 10^{-5}$
$G_M^n$	3.043	0.8548	0.6806	-0.1287	0.008912	

Table 4.1: Coefficients of the BBA-2003 form factor fit, cf. Eq. (4.43); the dimension of  $a_i$  is  $\text{GeV}^{-i}$ .

form factors at  $Q^2 = 0$  because the values at zero momentum transfer are directly related to the electric and magnetic properties of the nucleon. For the electric form factor of the neutron we take the following parametrization [KT03]:

$$G_E^n(Q^2) = -\mu_n \frac{a\tau}{1 + b\tau} G_D(Q^2) \quad (4.44)$$

with  $a = 0.942$  and  $b = 4.61$ , and  $\tau = Q^2/(4M^2)$ . For the axial form factor the dipole form of Eq. (4.42) is still used, however, the BBA-2003 analysis gave a slightly reduced axial mass of  $M_A = 1.00$  GeV.

In Fig. 4.2 the BBA-2003 form factors are plotted versus  $Q^2$ . From Eq. (4.29) and

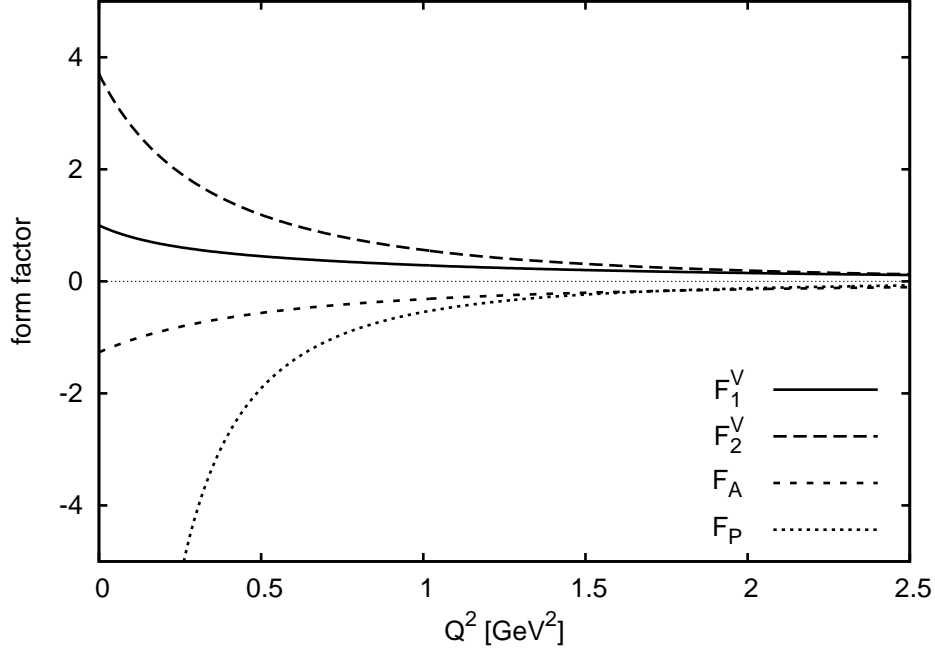


Figure 4.2: Nuclear charged current form factors, which are related to the Sachs form factors by Eq. (4.29) and Eq. (4.30), in the BBA-2003 form factor parametrization.

Eq. (4.30) one obtains

$$F_1^V(0) = G_E^p(0) - G_E^n(0) \approx 1, \quad (4.45)$$

$$F_2^V(0) = G_M^p(0) - G_M^n(0) - G_E^p(0) + G_E^n(0) \approx 3.7. \quad (4.46)$$

For the axial form factors we have (cf. Eq. (4.42) and Eq. (4.36))

$$F_A(0) = g_A \approx -1.26, \quad (4.47)$$

$$F_P(0) = \frac{2M^2}{m_\pi^2} g_A \approx -115.6. \quad (4.48)$$

A comparison of the BBA-2003 form factors and dipole form factors is shown in Fig. 4.3. Since the form factors are fixed at  $Q^2 = 0$ , both parametrizations coincide at this point. The ratio plotted shows clearly the deviation from the dipole form of the  $Q^2$  dependence as measured recently at JLAB.

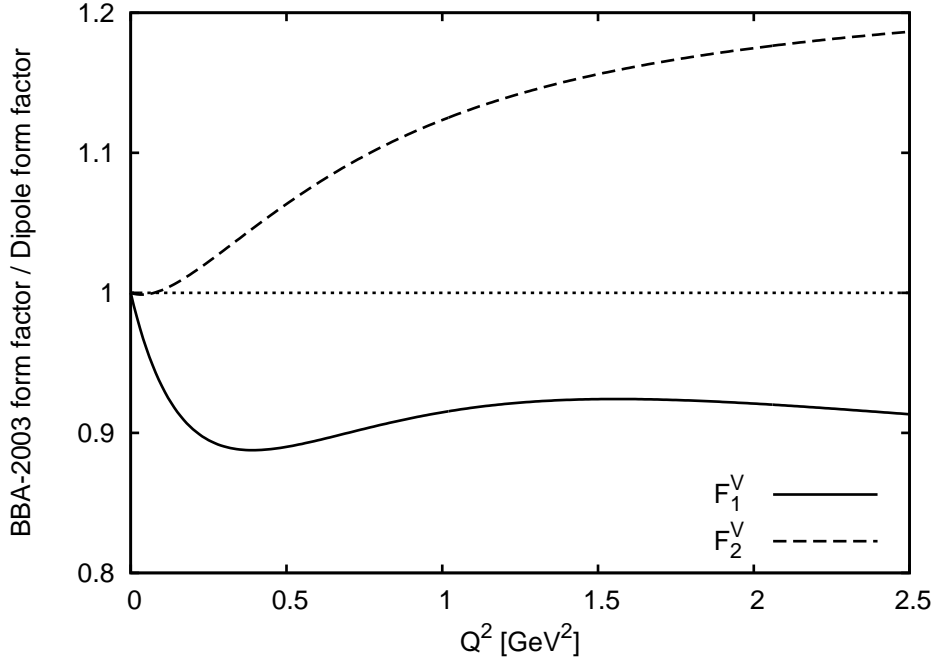


Figure 4.3: Ratio of BBA-2003 and Dipole form factors for  $F_1^V$  and  $F_2^V$ .

### 4.1.3 Results

Having now a complete formalism and a state-of-the-art parametrization of the form factors we can study the charged current cross sections.

Fig. 4.4 shows the differential cross section for various values of the neutrino energy for the reaction  $\nu_\mu n \rightarrow \mu^- p$ . For a given neutrino energy  $E_\nu$ , the kinematically allowed values of  $Q^2$  are constrained to the interval  $[Q_{min}^2, Q_{max}^2]$ . Detailed expressions for  $Q_{min}^2$  and  $Q_{max}^2$  as a function of  $E_\nu$  are given in Appendix B.3. Also the shape of the cross section depends on the neutrino energy and at higher energies the curves converge.

For an interpretation of the shape of the cross section we show in Fig. 4.5 the differential cross section for  $E_\nu = 0.5$  GeV and  $E_\nu = 2$  GeV and indicate the contribution of the form factors. The figures (a) and (b) were obtained by setting all form factors to zero except one. The most important contribution comes from the axial form factor, the pseudoscalar form factor does not contribute. Most sensitive to the energy is the contribution coming from  $F_1^V$ . Figures (c) and (d) show the contributions from the interference terms in the cross section. These plots were obtained by "switching off" all terms except the ones indicated. We see that the term  $B$  in Eq. (4.12), which includes  $F_A F_1^V$  and  $F_A F_2^V$ , is important for the shape of the differential cross section at low energies. The contribution

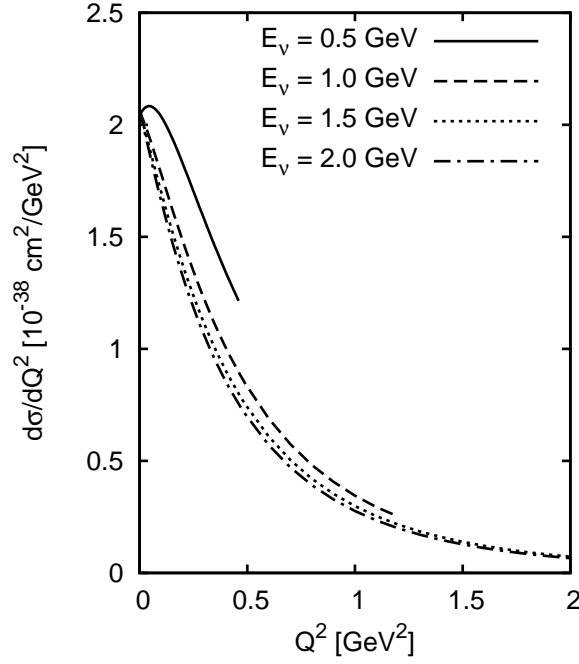


Figure 4.4: Differential cross section for  $\nu_\mu n \rightarrow \mu^- p$ .

coming from  $F_A F_2^V$  explains the "dip" at low  $Q^2$ . For higher energies the term  $B$  becomes less important.

Integration of  $d\sigma/dQ^2$  over  $Q^2$  yields the total cross section (solid line in Fig. 4.6). The strong increase at small energies is due to the opening phase space. For higher energies, the tail of  $d\sigma/dQ^2$  does not contribute much and therefore the total cross section saturates. This can also be seen from the cross section formula (Eq. (4.12)): With increasing energy the integral over the  $A$  and  $B$  terms tends to zero,<sup>3</sup> while the integral over the  $C$  term tends to a constant.

Also shown in Fig. 4.6 (a) is the contribution from the various form factors to the total cross section. The curves were obtained by setting all form factors to zero except for  $F_A$ ,  $F_1^V$  or  $F_2^V$ , respectively. The full result is displayed by the solid line.  $F_P$  does not contribute to the cross section because it is multiplied by  $(m_l/M)^2$ . Clearly dominant are the axial form factor and  $F_1^V$ ;  $F_2^V$  is kinematically suppressed. But neither one of the form factors itself nor the sum of the single form factor terms reproduces the full cross section. This indicates that the interference terms  $F_1^V F_2^V$ ,  $F_A F_1^V$  and  $F_A F_2^V$  are important for the charged current process. Those are plotted in Fig. 4.6 (b). Most important is  $F_A F_2^V$  as

<sup>3</sup>The vanishing integral over the  $B$  term for high  $E_\nu$  implies that the cross section for neutrino and antineutrino are equal in the high energy limit. This is consistent with the Pomernichuk theorem [Wei61].



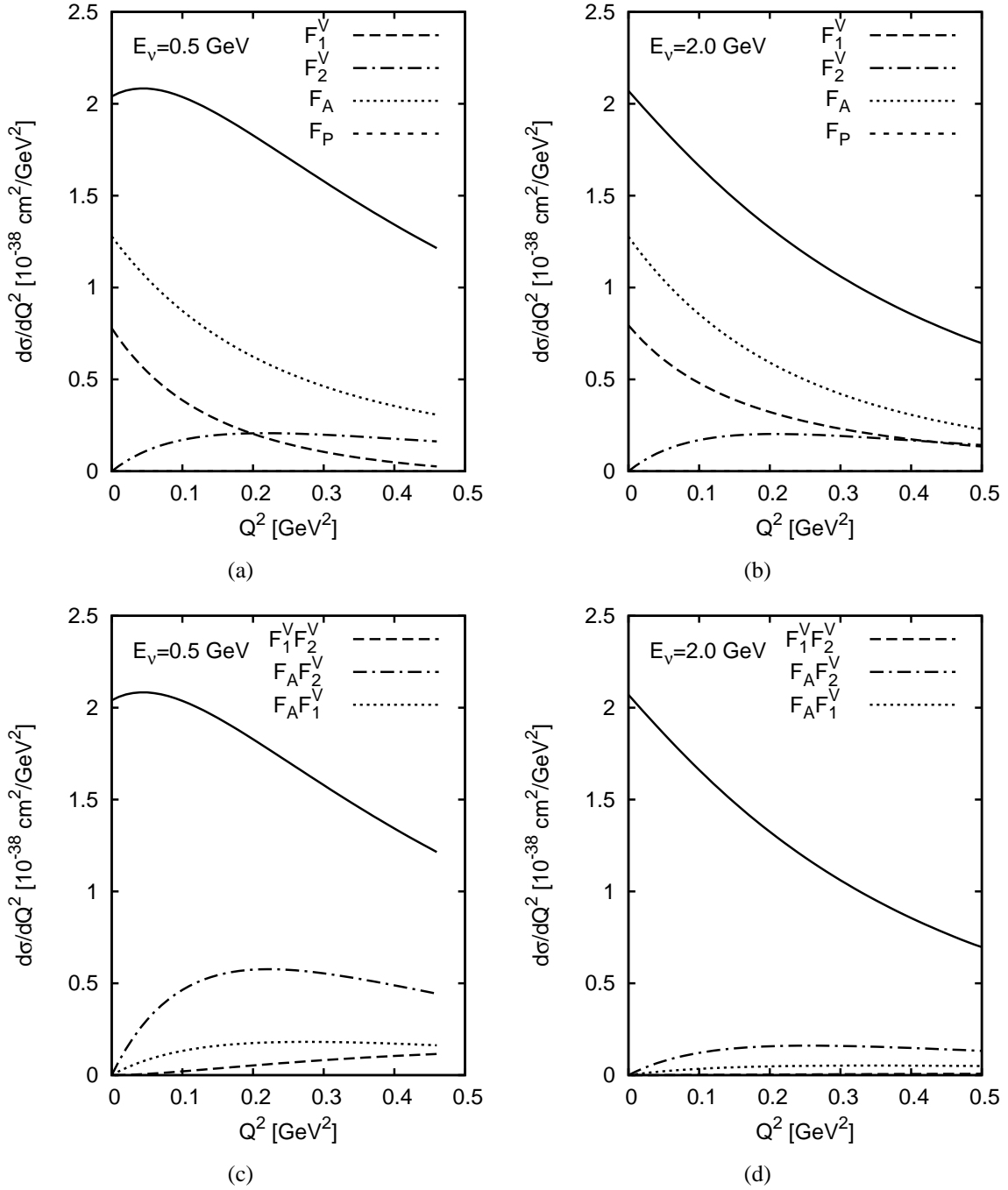


Figure 4.5: Differential cross section for  $\nu_\mu n \rightarrow \mu^- p$  showing the form factor contributions. The  $F_P$  contribution is very small and not visible; the solid line represents the full calculation including all form factors.

it was the case for the differential cross section. The interference terms tend to zero at higher energies.

A comparison with experimental data is shown in Fig. 4.7. The references are given in the plot. The data are obtained with scattering from Deuterium in bubble chamber experiments. The experimental data and the calculation nicely agree.

Next we study the dependence on the neutrino flavor. The total cross section for the three flavors is plotted in Fig. 4.8. Producing a lepton of a specific flavor requires a certain threshold energy (cf. Appendix B.2). If the mass difference between electron and muon is small compared to the neutrino energy, their cross sections are very similar. For the very heavy tau lepton, the shape of the cross section changes significantly. Here also  $F_P$  becomes important. However, as soon as the neutrino energy is an order of magnitude higher than the lepton masses all three curves converge and are equal in the high-energy limit.

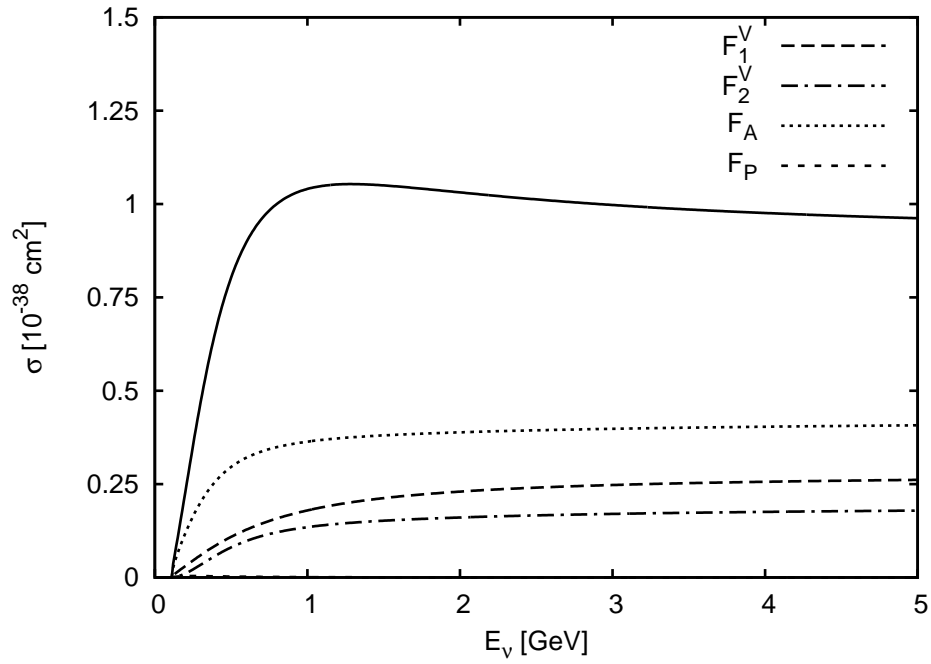
## 4.2 Elastic Neutral Current Interaction

### 4.2.1 Strangeness in the Nucleon

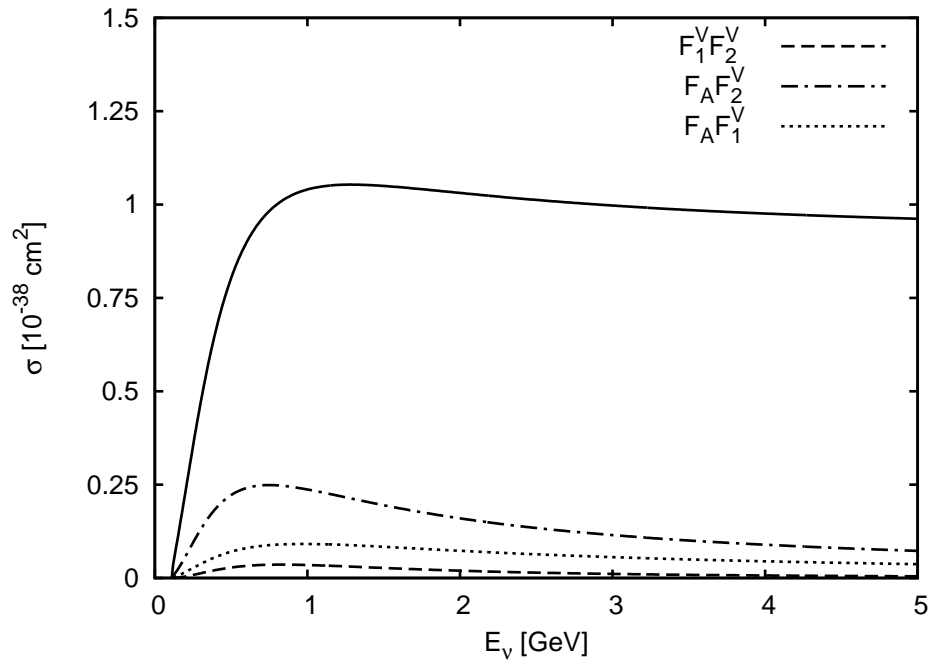
A fundamental question for our understanding of the hadronic structure is how the non-valence quarks contribute to the observed properties of the nucleon, in particular, how do the strange sea quarks contribute to the spin of the nucleon. It is not the aim of this thesis to review all aspects of this topic - we only want to point out those that are relevant for our argumentation. For an extensive review the reader is referred e. g. to Ref. [ABM02] (see also references therein).

One of the first hints that sea quarks are important for the nucleon spin came from measurements of deep-inelastic scattering of polarized muons on polarized protons [EMC89]. They revealed a disagreement with the Ellis-Jaffe sum rule [EJ74], which assumes that only up and down quarks make up the proton spin.

The spin structure can be experimentally accessed in different ways [ABM02, FINeSSE04, ERM05]. Some of them are: (i) deep-inelastic scattering of polarized leptons (e. g. [HERMES04, SMC97]), (ii) parity-violating electron scattering (e. g. [A404, SAMPLE05, HAPPEX05]) and (iii) neutral current scattering of neutrinos [A<sup>+</sup>87, FINeSSE04]. The results, however, are controversial: (i) sees a non-zero strangeness contribution to the nucleon spin (even though the experiments do not agree with each other) but (ii) indicates a strange quark contribution to the charge and the magnetic moment consistent with zero. The great advantage of (iii) in contrast to the other two possibilities is that it does not suffer from some of the theoretical uncertainties used in their analyses [KM88].



(a)



(b)

Figure 4.6: Contributions of the various form factors to the total cross section for  $\nu_\mu n \rightarrow \mu^- p$ . The  $F_P$  contribution is very small and almost not visible; the solid line represents the total cross section.

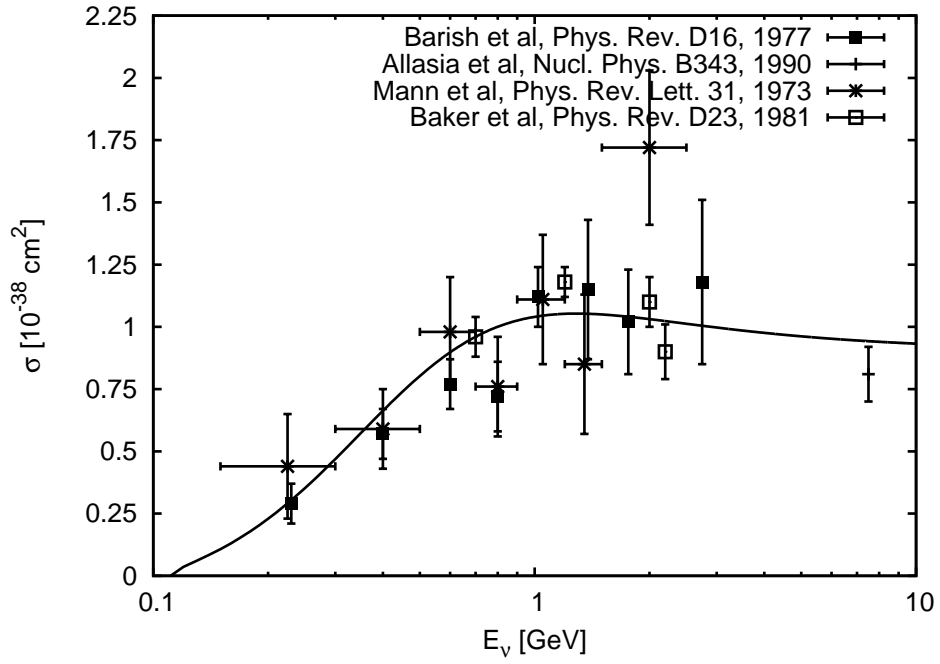


Figure 4.7: Total cross section for  $\nu_\mu n \rightarrow \mu^- p$ .

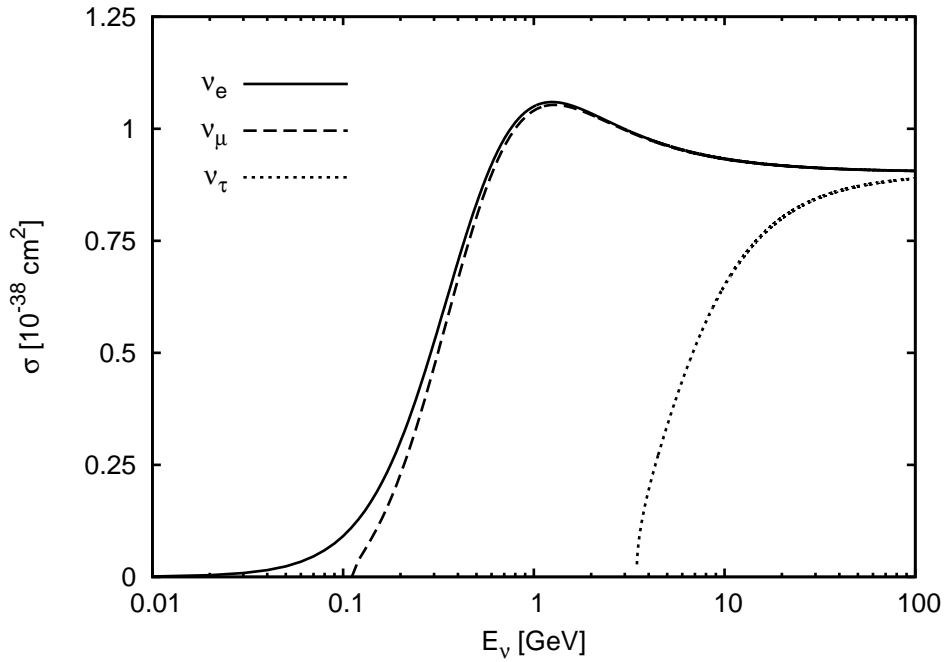


Figure 4.8: Total cross section for  $\nu_l n \rightarrow l^- p$  for different neutrino flavors.

A powerful approach to a full measurement of the strange form factors would be a combined study of parity-violating electron scattering and neutral current neutrino scattering [FINeSSE04, vdVP05]. Parity-violating electron scattering is very sensitive to the strange electric and magnetic form factors and much less to the strange axial vector form factor (cf. e. g. Ref. [TW01]). The opposite holds for neutrino scattering. In the previous chapter we saw that the charge changing interaction is only sensitive to the isovector quark current of the nucleon. However, neutral current scattering can probe the isoscalar strange quark contribution to the nucleon spin as will be shown in the next section.

Data on neutral current scattering are scarce. The best measurement to date is the E734 experiment at BNL [A<sup>+</sup>87]. It measured neutrino-proton and antineutrino-proton elastic scattering albeit with large systematical errors and only small statistics. This gap will hopefully be filled when the proposed FINeSSE experiment will start data taking - it plans to focus on strangeness in the nucleon [FINeSSE04].

## 4.2.2 Formalism

In neutral current interactions,

$$\nu N \rightarrow \nu N, \quad (4.49)$$

$$\bar{\nu} N \rightarrow \bar{\nu} N, \quad (4.50)$$

neutrinos as well as antineutrinos exchange a neutral vector boson,  $Z^0$ , which does not change the quark flavor of the hadron. We calculate now explicitly the cross section for neutrinos, the extension to antineutrinos will be given.

The spin averaged matrix element squared is given in Eq. (3.21)

$$|\bar{\mathcal{M}}|^2 = \frac{G_F^2}{2} L_{\alpha\beta} W^{\alpha\beta}. \quad (4.51)$$

The leptonic tensor was already calculated in Eq. (3.8) where, due to the zero neutrino mass, we take  $m_l = 0$ . For the hadronic tensor we do not use Eq. (3.11) but an explicit model of the hadronic vertex as was done for the charged current quasielastic scattering. We start with the hadronic matrix element

$$J_\alpha^{NC} = \langle N(p') | J_\alpha^{NC}(0) | N(p) \rangle, \quad (4.52)$$

where  $|N(p)\rangle$  denotes a nucleon of momentum  $p$  and  $|N(p')\rangle$  one of momentum  $p'$ .  $N$  can be either a neutron  $n$  or a proton  $p$ . Lorentz invariance arguments require

$$J_\alpha^{NC} = V_\alpha^{NC} - A_\alpha^{NC}, \quad (4.53)$$

where  $V_\alpha^{NC}$  is a Lorentz vector and  $A_\alpha^{NC}$  an axial vector.

The most general expression for the vector part is obtained analogous to Eq. (4.6) and, ignoring second-class currents (cf. page 35), is given by ( $N = p, n$ )

$$V_\alpha^{NC} = \bar{u}_N \left[ \gamma_\alpha \tilde{F}_1^N(Q^2) + \frac{i}{2M} \sigma_{\alpha\beta} q^\beta \tilde{F}_2^N(Q^2) \right] u_N, \quad (4.54)$$

where  $\tilde{F}_{1,2}^N$  are the neutral current vector form factors. For the axial part, we find in analogy to Eq. (4.7)

$$A_\alpha^{NC} = \bar{u}_N \left[ \gamma_\alpha \gamma_5 \tilde{F}_A^N(Q^2) + \frac{q_\alpha}{M} \gamma_5 \tilde{F}_P^N(Q^2) \right] u_N, \quad (4.55)$$

with the axial form factor  $\tilde{F}_A^N$  and the pseudoscalar form factor  $\tilde{F}_P^N$ . Due to time invariance, the form factors are real functions of  $Q^2$ . Note that the neutral current form factors  $\tilde{F}$  are different from the charged current form factors  $F$ .

The neutral current cross section is then calculated to ( $N = p, n$ )

$$\frac{d\sigma_N^{\nu,\bar{\nu}}}{dQ^2} = \frac{M^2 G_F^2}{8\pi E_\nu^2} \left[ A \mp \frac{s-u}{M^2} B + \frac{(s-u)^2}{M^4} C \right], \quad (4.56)$$

with

$$s - u = 4ME_\nu - Q^2, \quad (4.57)$$

$$\tau = \frac{Q^2}{4M^2}, \quad (4.58)$$

and

$$A = \frac{Q^2}{M^2} \left[ (1 + \tau) (\tilde{F}_A^N)^2 - (1 - \tau) (\tilde{F}_1^N)^2 + \tau (1 - \tau) (\tilde{F}_2^N)^2 + 4\tau \tilde{F}_1^N \tilde{F}_2^N \right], \quad (4.59)$$

$$B = \frac{Q^2}{M^2} \tilde{F}_A^N (\tilde{F}_1^N + \tilde{F}_2^N), \quad (4.60)$$

$$C = \frac{1}{4} \left( (\tilde{F}_A^N)^2 + (\tilde{F}_1^N)^2 + \tau (\tilde{F}_2^N)^2 \right). \quad (4.61)$$

The cross section is not sensitive to the neutrino flavor. Note that the pseudoscalar form factor does not appear in the cross section as a consequence of the zero neutrino mass. Neutrino and antineutrino cross sections differ by the sign in front of the  $B$  term. The cross section is thus determined at this point by three unknown form factors.

The vector form factors can be related to electron scattering form factors via CVC. We have shown in chapter 2.3.2 that  $V_\alpha^{NC}$  has the structure

$$V_\alpha^{NC} = (1 - 2 \sin^2 \theta_W) V_\alpha^3 - 2 \sin^2 \theta_W \frac{1}{2} J_\alpha^Y - \frac{1}{2} J_\alpha^S, \quad (4.62)$$

with the isovector  $V_\alpha^3$ , the isoscalar  $J_\alpha^Y$  and the strange part  $J_\alpha^S$ . The first two were already used for relating the charged current form factors to the ones from electron scattering. They were given in Eq. (4.21) and Eq. (4.22) as

$$V_\alpha^3 = \bar{u} \left[ \gamma_\alpha F_1^v + \frac{i}{2M} \sigma_{\alpha\beta} q^\beta F_2^v \right] \frac{\tau_3}{2} u, \quad (4.63)$$

$$\frac{1}{2} J_\alpha^Y = \bar{u} \left[ \gamma_\alpha F_1^s + \frac{i}{2M} \sigma_{\alpha\beta} q^\beta F_2^s \right] \frac{\mathbb{1}}{2} u, \quad (4.64)$$

where

$$F_{1,2}^{v,s} = F_{1,2}^p \mp F_{1,2}^n. \quad (4.65)$$

$F_1^{p,n}$  and  $F_2^{p,n}$  are the Dirac and Pauli form factors of the nucleon. For the strange part  $J_\alpha^S$  one can write a similar expression:

$$\frac{1}{2} J_\alpha^S = \bar{u} \left[ \gamma_\alpha F_1^S + \frac{i}{2M} \sigma_{\alpha\beta} q^\beta F_2^S \right] \frac{\mathbb{1}}{2} u, \quad (4.66)$$

with the two strange vector form factors  $F_{1,2}^S$ .

Combining Eqs. (4.63), (4.64) and (4.66) with Eq. (4.54) via Eq. (4.62) under the assumption of CVC gives

$$\tilde{F}_{1,2}^N = (1 - 2 \sin^2 \theta_W) F_{1,2}^v \tau_3 - \sin^2 \theta_W F_{1,2}^s - \frac{1}{2} F_{1,2}^S, \quad (4.67)$$

where  $\tau_3 = 1(-1)$  for proton (neutron). Using Eq. (4.65), we can write this expression explicitly for neutrons and protons

$$2\tilde{F}_{1,2}^p = (1 - 4 \sin^2 \theta_W) F_{1,2}^p - F_{1,2}^n - F_{1,2}^S, \quad (4.68)$$

$$2\tilde{F}_{1,2}^n = (1 - 4 \sin^2 \theta_W) F_{1,2}^n - F_{1,2}^p - F_{1,2}^S. \quad (4.69)$$

The Dirac and Pauli form factors  $F_1^{p,n}$  and  $F_2^{p,n}$  are related to the Sachs form factors (cf. Eq. (4.27) and Eq. (4.28)) - their parametrizations were given in chapter 4.1.2. For parametrizations of the strange vector formfactors  $F_{1,2}^S$  we refer to the next section.

We shall now turn to the axial form factor  $\tilde{F}_A^N$  and use PCAC to relate them to the ones from charged current scattering. We have shown in chapter 2.3.3 that the axial current consists of an isovector and a strangeness part

$$A_\alpha^{NC} = A_\alpha^3 + \frac{1}{2} A_\alpha^S, \quad (4.70)$$

where  $A_\alpha^3$  belongs to the same isovector of axial currents as  $A_\alpha^{CC}$ . This implies, that their form factors are equal and we can use the charged current axial form factors for neutral current scattering. Therefore, we obtain

$$A_\alpha^3 = \bar{u} \left[ \gamma_\alpha \gamma_5 F_A + \frac{q_\alpha}{M} \gamma_5 F_P \right] \frac{\tau_3}{2} u, \quad (4.71)$$

with  $F_A$  and  $F_P$  as defined in Eq. (4.7). For the strange part we can write a similar expression:

$$\frac{1}{2}A_\alpha^S = \bar{u} \left[ \gamma_\alpha \gamma_5 F_A^S + \frac{q_\alpha}{M} \gamma_5 F_P^S \right] \frac{1}{2}u, \quad (4.72)$$

with the strange axial form factors  $F_A^S$  and  $F_P^S$ .

Combining now Eqs. (4.71) and (4.72) with Eq. (4.55) via Eq. (4.70) gives

$$2\tilde{F}_{A,P}^{p,n} = \pm F_{A,P} + F_{A,P}^S. \quad (4.73)$$

Note the different sign in front of the charged current axial form factor for protons and neutrons. The parametrization of  $F_A$  is given in chapter 4.1.2. We shall give an explicit parametrization for the strange axial form factor  $F_A^S$  in the next section, while we do not need to parametrize  $F_P^S$  since  $\tilde{F}_P^{p,n}$  does not contribute to the cross section due to the zero neutrino mass.

### 4.2.3 Strange Form Factors

In chapter 4.2.1 we briefly reviewed the experimental status of the question of strangeness contributions and related problems and uncertainties. For the parametrization of the strange form factors we use a reanalysis of the BNL E734 experiment [GLW93]. The form factors are parametrized by:

$$F_1^S(Q^2) = \frac{F_1^S(0)Q^2}{(1 + \tau) \left(1 + \frac{Q^2}{M_V^2}\right)^2}, \quad (4.74)$$

$$F_2^S(Q^2) = \frac{F_2^S(0)}{(1 + \tau) \left(1 + \frac{Q^2}{M_V^2}\right)^2}, \quad (4.75)$$

$$F_A^S(Q^2) = \frac{\Delta s}{\left(1 + \frac{Q^2}{M_A^2}\right)^2}, \quad (4.76)$$

where  $F_1^S(0) = -\frac{1}{6}\langle r_S^2 \rangle$  and  $F_2^S(0) = \mu_S$  with  $\langle r_S^2 \rangle$  being the strange radius and  $\mu_S$  the strange magnetic moment of the nucleon.  $\Delta s$  is the strange contribution to the nucleon spin. We compare three different fits, each with  $M_V = 0.843$  GeV, which are representative parametrizations as discussed below:

- **Fit I:** [GLW93]

$$\Delta s = -0.21 \pm 0.10 \quad (4.77)$$

$$F_1^S(0) = 0.53 \pm 0.70 \quad (4.78)$$

$$F_2^S(0) = -0.40 \pm 0.72 \quad (4.79)$$

$$M_A = 1.012 \pm 0.032 \text{ GeV} \quad (4.80)$$



• **Fit II:** [GLW93]

$$\Delta s = -0.15 \pm 0.07 \quad (4.81)$$

$$F_1^S(0) = 0 \quad (4.82)$$

$$F_2^S(0) = 0 \quad (4.83)$$

$$M_A = 1.049 \pm 0.019 \text{ GeV} \quad (4.84)$$

• **Fit III:**

$$\Delta s = 0 \quad (4.85)$$

$$F_1^S(0) = 0 \quad (4.86)$$

$$F_2^S(0) = 0 \quad (4.87)$$

$$M_A = 1.00 \text{ GeV} \quad (4.88)$$

This set of fits allows us to study the influence of the strangeness on the cross section and to estimate the order of theoretical uncertainties. Note that a dipole parametrization of the non-strange form factors was assumed in extracting the parameters. Therefore we use the dipole parametrization given in chapter 4.1.2 for the Dirac and Pauli form factor and not the BBA-2003 parametrization.

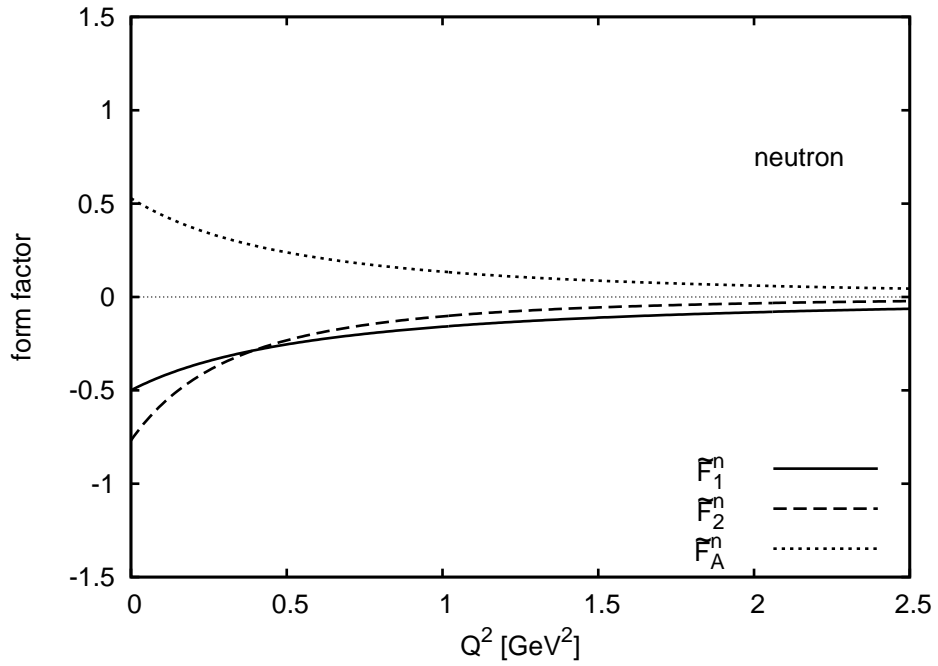
In Fig. 4.9 (a) we show the form factors  $\tilde{F}_A^p$ ,  $\tilde{F}_1^p$  and  $\tilde{F}_2^p$  obtained from Fit I for neutrons, and in Fig. 4.9 (b) for protons, respectively. The comparison reveals a significant difference between neutron and proton as expected from the calculation. At zero momentum transfer, as for the charged currents, the form factors are fixed by the electric, magnetic and also by the strange properties of the nucleons. Especially interesting is the behavior of  $\tilde{F}_1^{p,n}$ . In order to calculate those values from Eq. (4.68) and Eq. (4.69) we need expression for the Dirac and the Pauli form factor in terms of the Sachs form factors. Those follow from Eq. (4.27) and Eq. (4.28):

$$F_1^{n,p} = \frac{G_E^{n,p} + \frac{Q^2}{4M^2} G_M^{n,p}}{1 + \frac{Q^2}{4M^2}}, \quad (4.89)$$

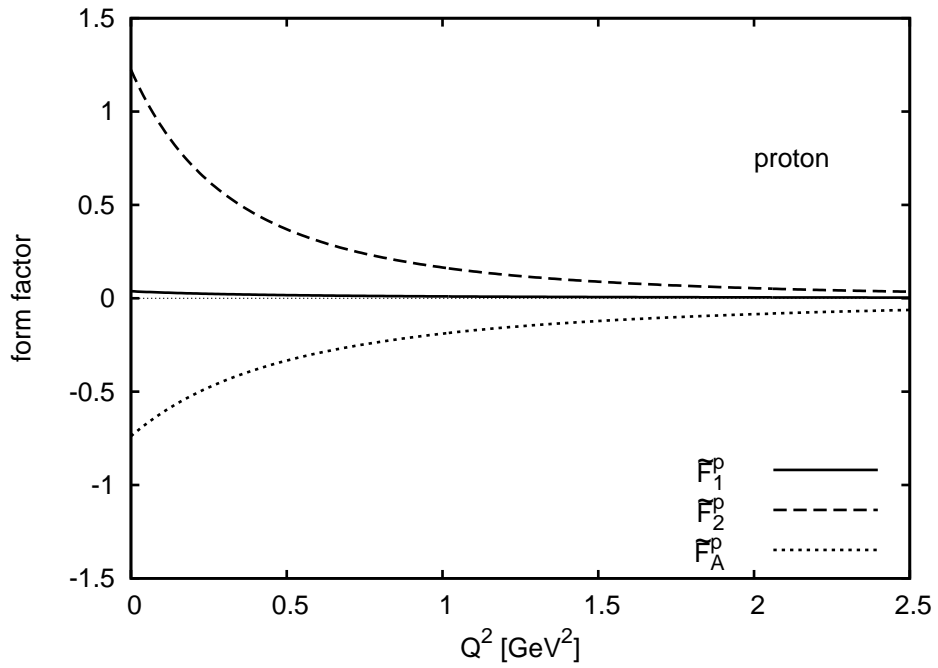
$$F_2^{n,p} = \frac{G_M^{n,p} - G_E^{n,p}}{1 + \frac{Q^2}{4M^2}}. \quad (4.90)$$

This yields for  $\tilde{F}_1^p$  with Eq. (4.68)

$$\begin{aligned} 2\tilde{F}_1^p(0) &= (1 - 4 \sin^2 \theta_W) G_E^p(0) - G_E^n(0) - F_1^S(0) \\ &\approx 0.075. \end{aligned} \quad (4.91)$$



(a)



(b)

Figure 4.9: Neutral current form factors  $\tilde{F}_A$ ,  $\tilde{F}_1$  and  $\tilde{F}_2$  of Eq. (4.68) or Eq. (4.69), respectively, and Eq. (4.73) for (a) neutron and (b) proton (Fit I).

For  $\tilde{F}_1^n$  we obtain with Eq. (4.69)

$$\begin{aligned} 2\tilde{F}_1^n(0) &= (1 - 4 \sin^2 \theta_W) G_E^n(0) - G_E^p(0) - F_1^S(0) \\ &\approx -1. \end{aligned} \quad (4.92)$$

Hence,  $\tilde{F}_1^p$  is strongly suppressed due to the weak mixing angle.

For  $\tilde{F}_2^p$  we obtain

$$\begin{aligned} 2\tilde{F}_2^p(0) &= (1 - 4 \sin^2 \theta_W) (G_M^p(0) - G_E^p(0)) - (G_M^n(0) - G_E^n(0)) - F_2^S(0) \\ &\approx 2.4, \end{aligned} \quad (4.93)$$

and for  $\tilde{F}_2^n$

$$\begin{aligned} 2\tilde{F}_2^n(0) &= (1 - 4 \sin^2 \theta_W) (G_M^n(0) - G_E^n(0)) - (G_M^p(0) - G_E^p(0)) - F_2^S(0) \\ &\approx -1.5. \end{aligned} \quad (4.94)$$

Using Eq. (4.73) gives for  $\tilde{F}_A^N$

$$\begin{aligned} 2\tilde{F}_A^p(0) &= F_A(0) + F_A^S(0) \\ &= g_A + \Delta s \\ &\approx -1.47, \end{aligned} \quad (4.95)$$

and

$$\begin{aligned} 2\tilde{F}_A^n(0) &= -F_A(0) + F_A^S(0) \\ &= -g_A + \Delta s \\ &\approx 1.06, \end{aligned} \quad (4.96)$$

We stress, that the three fits described above have to be taken with some care [A<sup>+</sup>99]: *The experimental uncertainty is still too large to be conclusive about specific values of the strange form factors of the nucleon. A rather wide range of values for the strange parameters is compatible with the BNL E734 data and more precise measurements are thus needed in order to determine simultaneously the electric, magnetic and axial strange form factors of the nucleon.* A summary of recent fits also including non-neutrino experiments can be found in Refs. [ERM05, ABM02].

## 4.2.4 Results

We start our discussion of the neutral current scattering with the differential cross section for the reaction  $\nu N \rightarrow \nu N$ . It is plotted in Fig. 4.10 as a function of  $Q^2$  using Fit I. Plot

(a) shows scattering on neutrons, (b) scattering on protons. Only a certain range of  $Q^2$  is kinematically allowed for a given neutrino energy  $E_\nu$ . Explicit expression for  $Q_{min}^2$  and  $Q_{max}^2$  can be found in Appendix B.3. The energy dependence is also reflected in the shape of the cross sections; analogously to the CC case, the curves converge at higher energy.

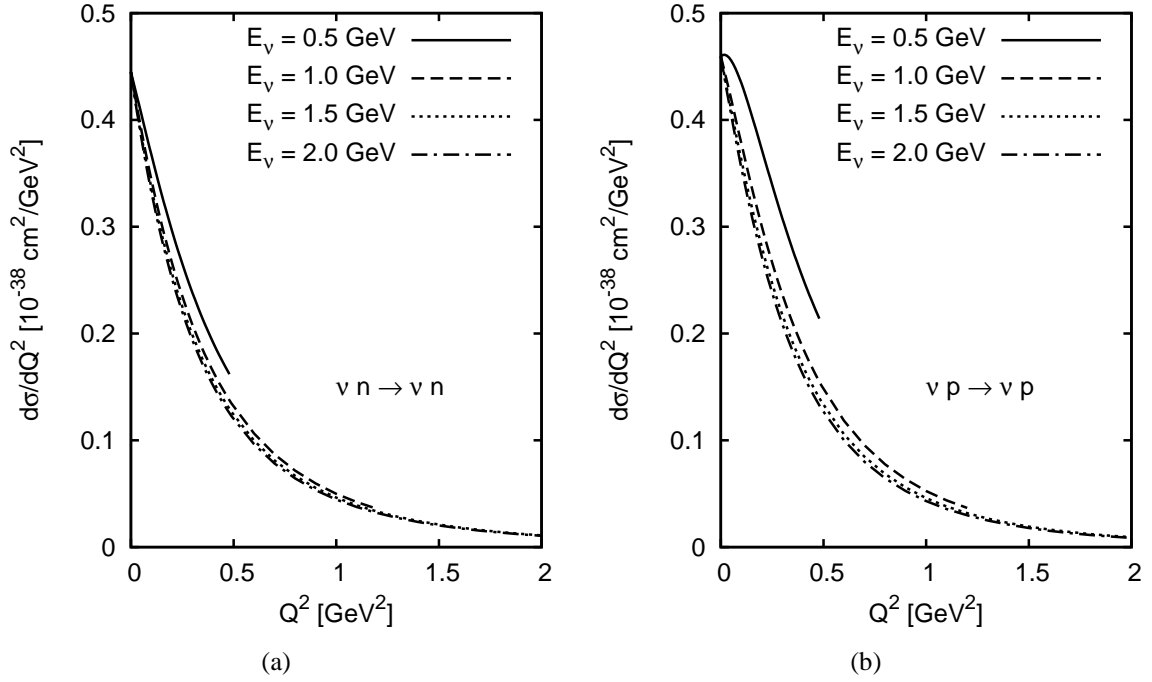


Figure 4.10: Differential cross section for (a)  $\nu n \rightarrow \nu n$  and (b)  $\nu p \rightarrow \nu p$  using the parametrization set Fit I of the form factors.

For a discussion of the shape of the differential cross section we study the form factor contribution. In Fig. 4.11 the differential cross section for  $\nu n \rightarrow \nu n$  is plotted. Fig. 4.12 shows it for  $\nu p \rightarrow \nu p$ . Both figures include the calculation for  $E_\nu = 0.5 \text{ GeV}$  and  $E_\nu = 2 \text{ GeV}$  and indicate the contribution of the form factors. In both figures the panels (a) and (b) were obtained by setting all form factors to zero except the ones indicated. Panels (c) and (d) show the contributions from the interference terms in the cross section. These plots were obtained by "switching off" all terms except the ones indicated.

For scattering on neutrons (Fig. 4.11) the axial form factor  $\tilde{F}_A^n$  and the vector form factor  $\tilde{F}_2^n$  contribute almost equally to the cross section, whereas the energy dependence of the  $\tilde{F}_2^n$  term is more significant. The contribution of  $\tilde{F}_1^n$  is negligible. The interference terms also contribute notably to the cross section. In particular the term  $B$  of Eq. (4.56) including  $\tilde{F}_A^n \tilde{F}_1^n$  and  $\tilde{F}_A^n \tilde{F}_2^n$  is important at low energies for the shape of the differential cross section. Its importance becomes less with increasing energies.

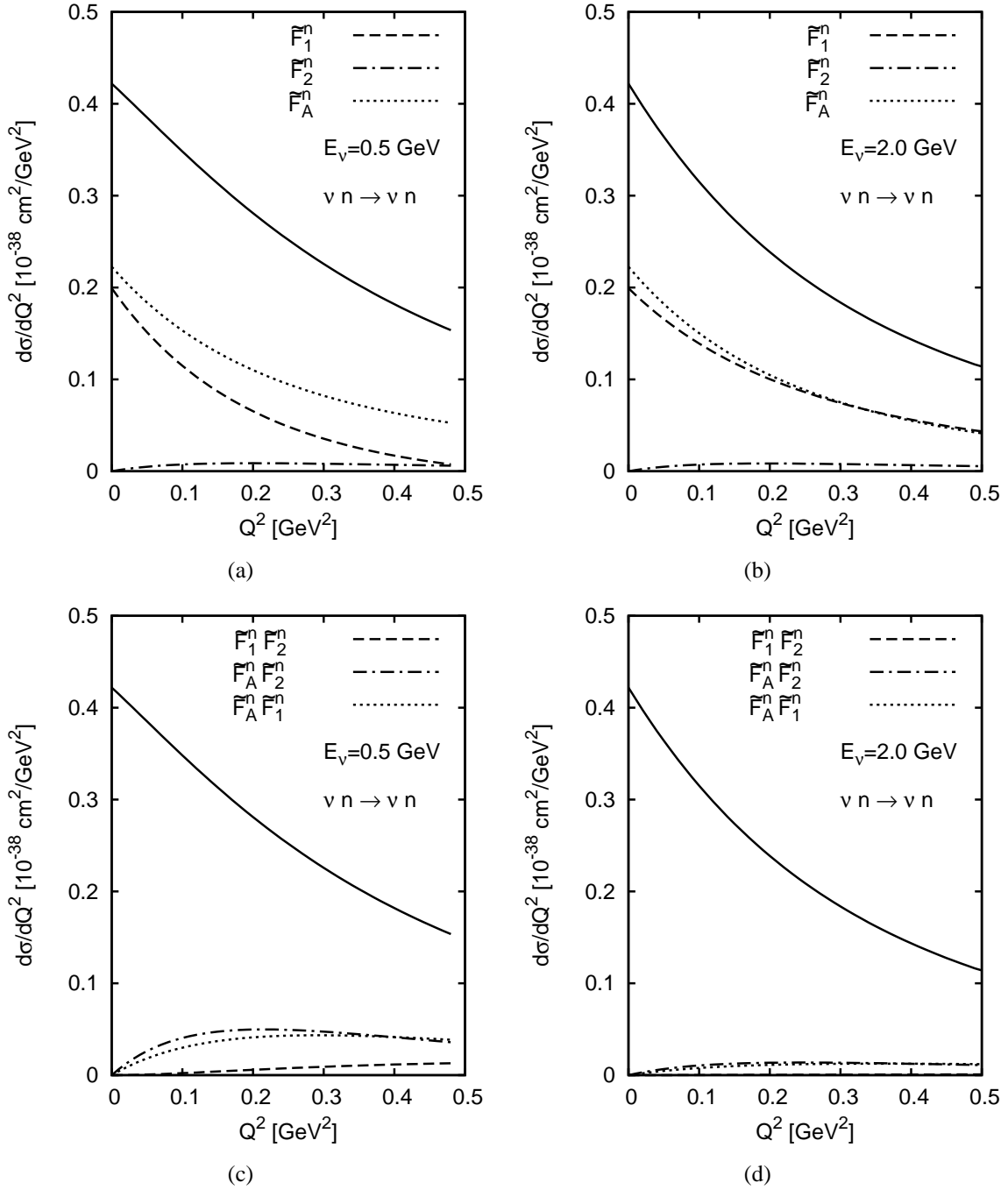


Figure 4.11: Differential cross section for  $\nu n \rightarrow \nu n$  showing the form factor contributions using the parametrization set Fit I of the form factors; the solid line represents the full calculation including all form factors.

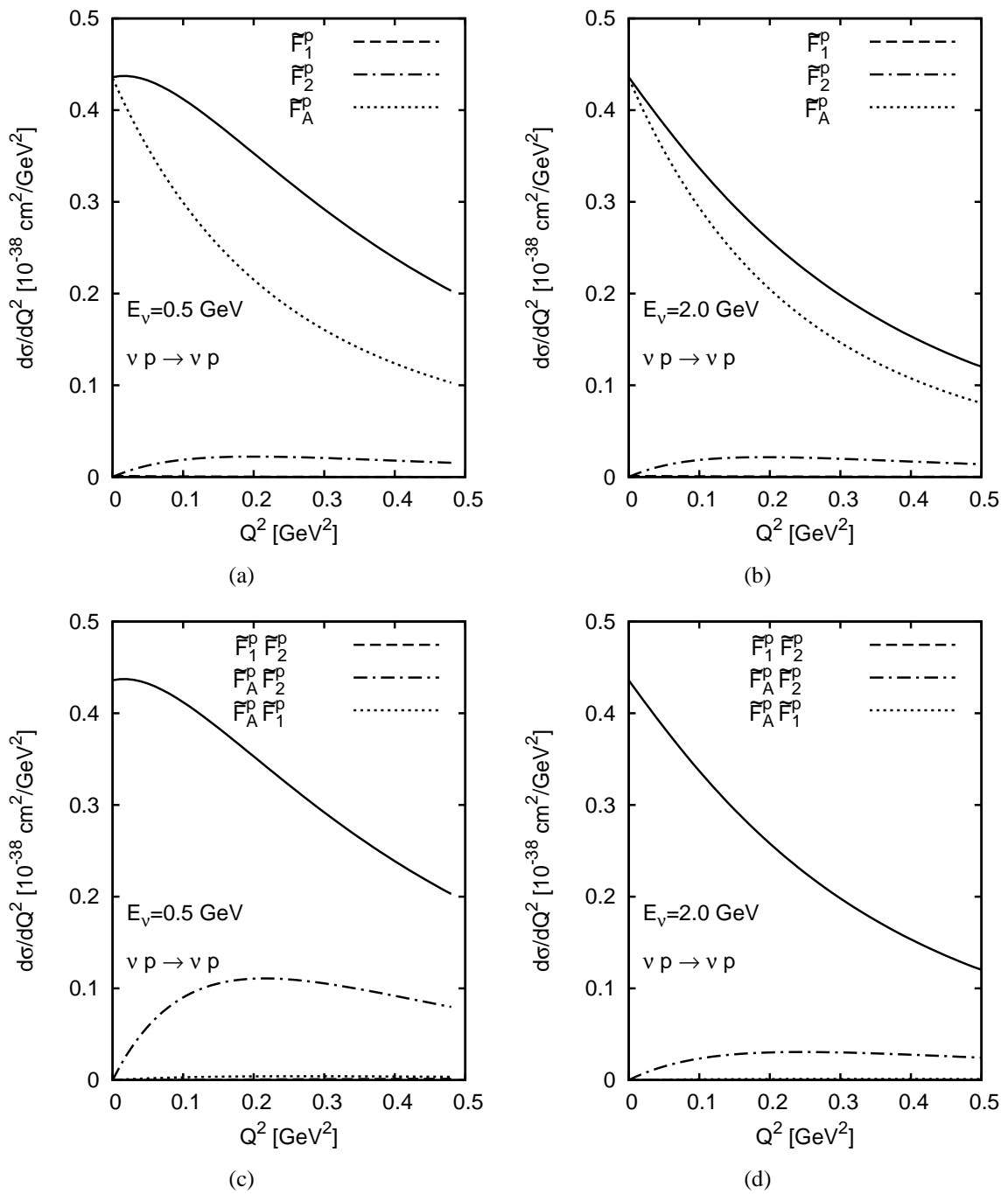


Figure 4.12: Differential cross section for  $\nu p \rightarrow \nu p$  showing the form factor contributions using the parametrization set Fit I of the form factors; the solid line represents the full calculation including all form factors. The  $\tilde{F}_1^p$  contribution is strongly suppressed and therefore not visible.

Neutral current interactions with protons (Fig. 4.12) are clearly dominated by the axial form factor  $\tilde{F}_A^p$ . Minor contributions come also from terms involving  $\tilde{F}_2^p$ . The strong suppression of  $\tilde{F}_1^p$ , discussed in chapter 4.2.3, is reflected in the cross section:  $\tilde{F}_1^p$  does not influence the cross section for protons, neither directly nor through the interference term  $\tilde{F}_A^p \tilde{F}_1^p$ . All those terms are almost energy independent. Therefore, the difference in the shape for  $E_\nu = 0.5$  GeV and  $E_\nu = 2$  GeV is due to the interference term  $\tilde{F}_A^p \tilde{F}_2^p$ . This term again appears only in the term  $B$  of Eq. (4.56) which is strongly energy dependent. Thus, this is only important at low energies, and its influence becomes less important for higher energies.

Integration of the differential cross section over  $Q^2$  yields the total cross section. Since the shapes of the differential cross sections for charged current and neutral current scattering are similar, we expect the same for the total cross section. Both, charged current and neutral current reactions, are plotted in Fig. 4.13 for comparison. The strong increase

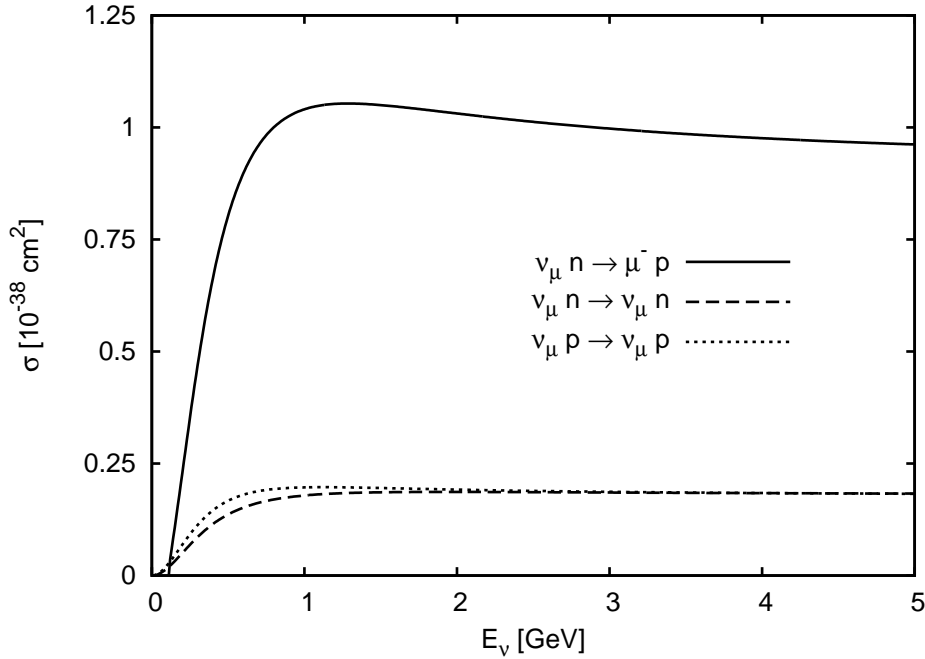


Figure 4.13: Total (quasi)elastic cross section for neutral and charged currents with the BBA-2003 form factors for the charged current and Fit I for parametrization of the neutral current form factors.

is again an effect due to the opening phasespace. The cross section saturates at higher energies since the tail of  $d\sigma/dQ^2$  does not contribute much with increasing  $Q_{max}^2$ . Note the different thresholds which can be seen in Fig. 4.13. The neutral current reaction does not require a minimal neutrino energy, since the outgoing neutrino is massless. The

charged current reaction, however, has to "produce" the lepton mass, here the muon mass, and thus, a minimal energy is required (cf. chapter B.2).

We continue with the investigation of the contribution of the various form factors. The upper plot in Fig. 4.14 and in Fig. 4.15 shows the contributions for  $\nu n \rightarrow \nu n$ , the lower one for  $\nu p \rightarrow \nu p$ . Fig. 4.14 shows the contributions coming from the single form factors, in Fig. 4.15 the interference terms are plotted. A comparison displays significant differences.

For the neutron cross section,  $\tilde{F}_1^n$  and  $\tilde{F}_A^n$  contribute equally and also the interference terms  $\tilde{F}_A^n \tilde{F}_2^n$  and  $\tilde{F}_A^n \tilde{F}_1^n$  play a role (Fig. 4.14 (a) and Fig. 4.15 (a)). However, contribution from  $\tilde{F}_2^n$  and  $\tilde{F}_1^n \tilde{F}_2^n$  are negligible.

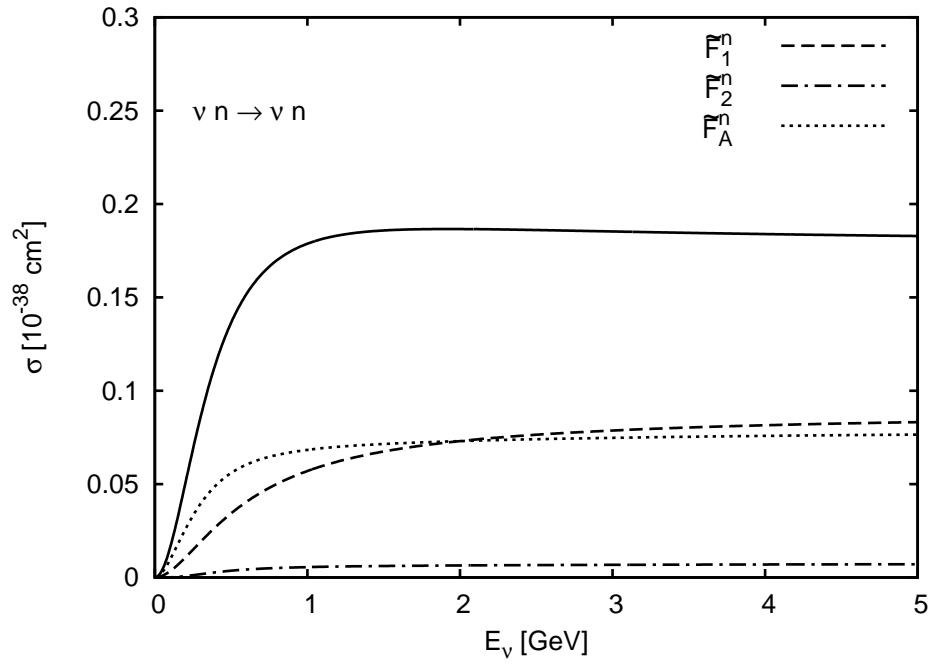
The proton cross section however is clearly dominated by the axial form factor  $\tilde{F}_A^p$  with minor contribution from  $\tilde{F}_2^p$ . The only interference term important here is  $\tilde{F}_A^p \tilde{F}_2^p$ . This is due to the strong suppression of  $\tilde{F}_1^p$  (cf. chapter 4.2.3).

The sensitivity of the total cross section to the parametrization of the strange form factors is shown in Fig. 4.16. Panel (a) shows scattering on neutrons and panel (b) on protons. The cross section for each fit in chapter 4.2.3 is plotted. For both neutrons and protons the cross sections obtained with Fit I and II are almost equal. The main difference between Fit I and II is the inclusion of  $F_1^S$  and  $F_2^S$  - in contrast to Fit I they are "switched off" in Fit II. Thus, the cross section is not very sensitive to the strange vector form factors. The sensitivity to the strange axial form factor can be seen by comparing the cross section obtained with Fit III to the one with Fit II - in Fit III,  $F_A^S$  is set to zero. For the neutron cross section, this leads to a slight enhancement. The effect becomes more significant for scattering on protons. Here the cross section is reduced when  $F_A^S$  is "switched off". The dominance of the axial vector in  $\nu p \rightarrow \nu p$  (cf. Fig. 4.14 and Fig. 4.15) makes this reaction more sensitive to the strange axial form factor than the reaction  $\nu n \rightarrow \nu n$ . The size of this reduction on protons can be easily estimated assuming axial vector dominance. This yields for the ratio of the cross sections for the different fits:

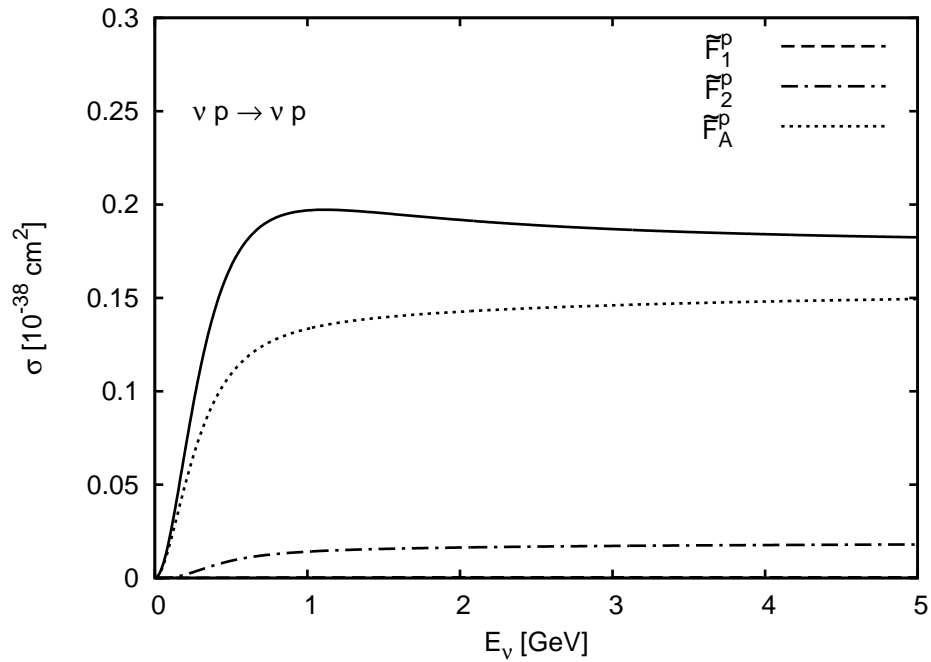
$$\frac{\sigma(\Delta s = -0.21 \Leftrightarrow \text{Fit I})}{\sigma(\Delta s = 0 \Leftrightarrow \text{Fit III})} \approx \left(1 + \frac{\Delta s}{g_A}\right)^2 \approx 1.36. \quad (4.97)$$

This factor matches very well the exact result shown in the lower plot of Fig. 4.16. Switching  $\Delta s$  off and on gives the expected deviation of about 30 %. Besides the difficulty of measuring neutrons, for unraveling the strange quark content of the nucleon the better choice is definitely the reaction on protons.





(a)



(b)

Figure 4.14: Contribution of the form factors to the neutral current total cross section, (a)  $\nu n \rightarrow \nu n$ , (b)  $\nu p \rightarrow \nu p$  with the form factor parametrization of Fit I; the solid line represents the total cross section.

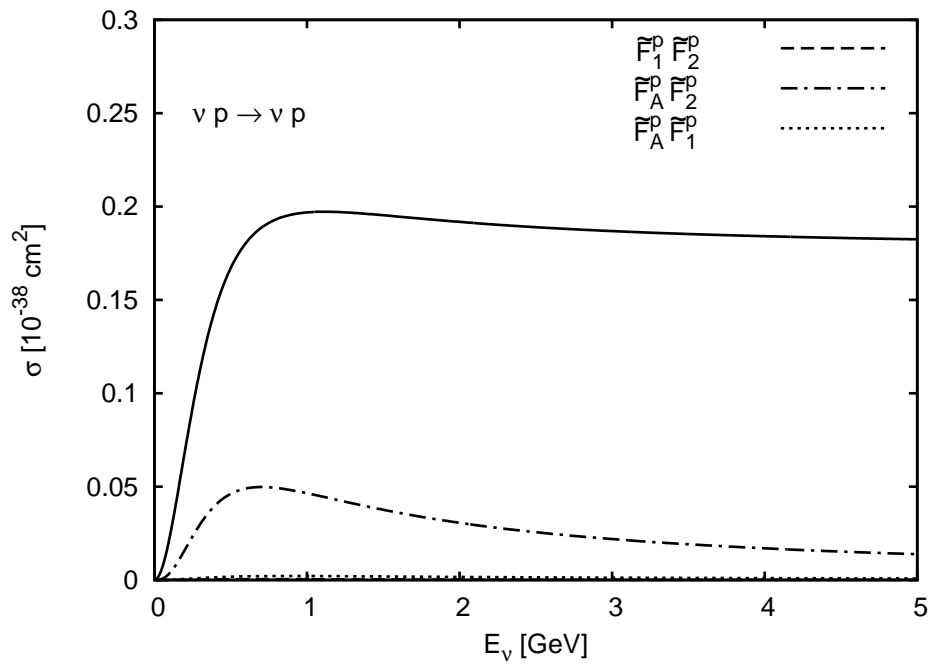
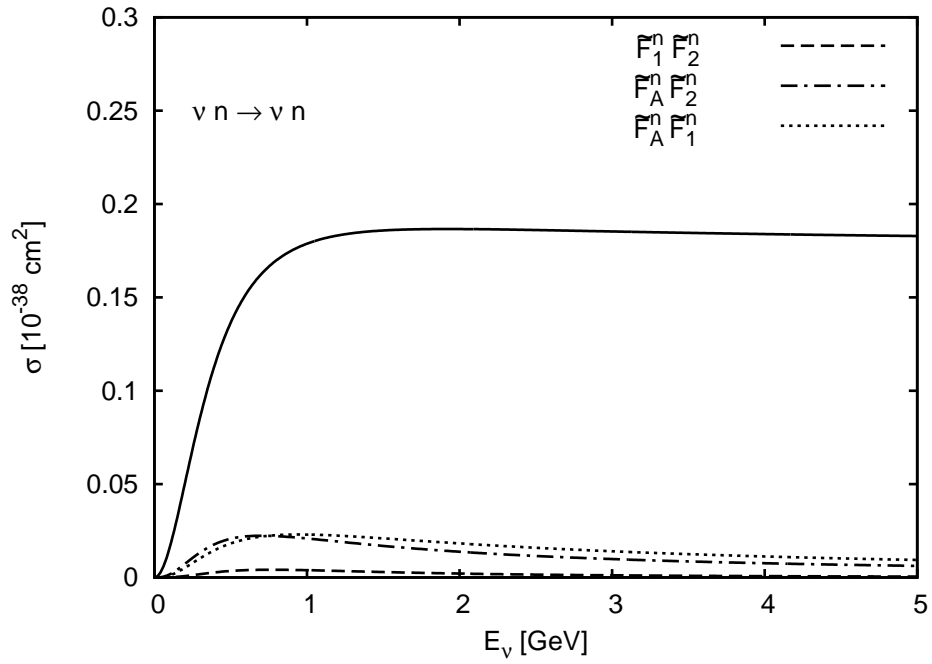


Figure 4.15: Contribution of the form factors to the neutral current total cross section, (a)  $\nu n \rightarrow \nu n$ , (b)  $\nu p \rightarrow \nu p$  with the form factor parametrization of Fit I; the solid line represents the total cross section.

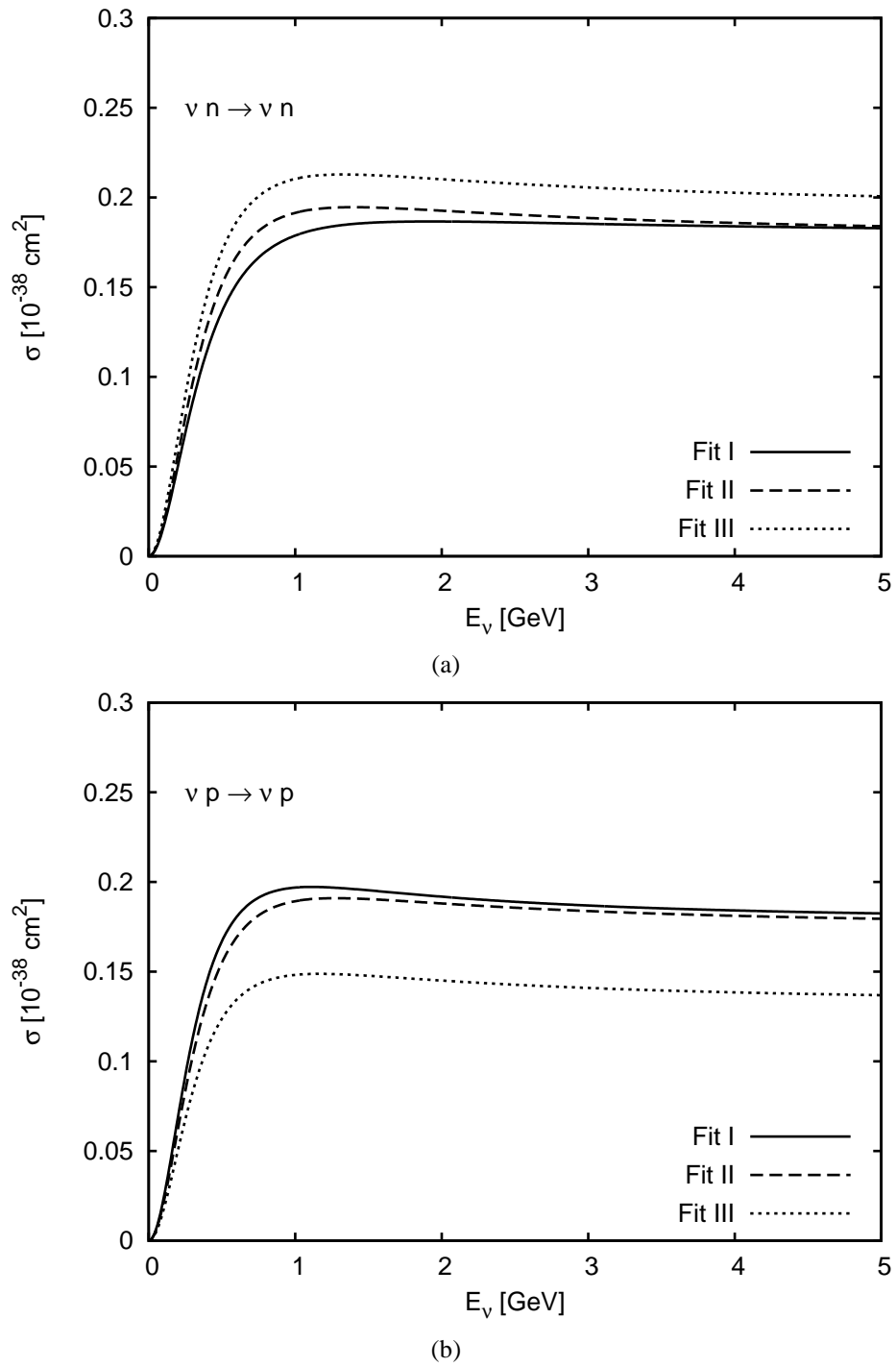


Figure 4.16: Comparison of NC form factor fits and their influence on the cross section. (a)  $\nu n \rightarrow \nu n$ , (b)  $\nu p \rightarrow \nu p$ .



## 5 Production of the $\Delta$ Resonance

Recalling chapter 3.2, the most important process for neutrino scattering in the energy range of interest besides quasielastic scattering is the neutrino induced production of the  $\Delta$  resonance. In the first part of this chapter we present a general formalism applicable to all spin 3/2 resonances. We shall then discuss the form factors used for  $\Delta$  production and also the parametrization of the  $\Delta$  width. Finally, results are presented.

### 5.1 Formalism for Neutrino Induced $\Delta$ Production

The charged current processes under investigation are, for neutrinos

$$\nu p \rightarrow l^- \Delta^{++} \quad (5.1)$$

$$\nu n \rightarrow l^- \Delta^+ \quad (5.2)$$

and for antineutrinos

$$\bar{\nu} p \rightarrow l^+ \Delta^0 \quad (5.3)$$

$$\bar{\nu} n \rightarrow l^+ \Delta^- . \quad (5.4)$$

For the neutral currents we consider the reactions

$$\nu p \rightarrow \nu \Delta^+ \quad (5.5)$$

$$\nu n \rightarrow \nu \Delta^0, \quad (5.6)$$

and

$$\bar{\nu} p \rightarrow \bar{\nu} \Delta^+ \quad (5.7)$$

$$\bar{\nu} n \rightarrow \bar{\nu} \Delta^0. \quad (5.8)$$

Our calculation will be presented for the charged current neutrino interaction. A straightforward extension for the others will be given. Since the calculation techniques, i. e. using the underlying symmetries, CVC and PCAC, are similar to the quasielastic case and were discussed in detail in the previous chapter, we shall not repeat them here.

The standard method in a theoretical treatment of the neutrino induced charged current  $\Delta$  production follows the Rarita-Schwinger formalism (cf. Refs. [SvH73, FN79] or more

## 5 Production of the $\Delta$ Resonance

---

recently [ARSVV98, SVVO98, LP05]). The notation of the  $N - \Delta$  transition form factors is based on Ref. [LS72]. Thus, the hadronic current for the reaction (5.2) is given by:

$$\begin{aligned} J_\alpha &= \langle \Delta^+ | J_\alpha(0) | n \rangle \\ &= \cos \theta_C \bar{\psi}^\beta(p') D_{\beta\alpha} u(p) \end{aligned} \quad (5.9)$$

with

$$\begin{aligned} D_{\beta\alpha} &= \left[ \frac{C_3^V}{M} (g_{\alpha\beta} \not{q} - q_\beta \gamma_\alpha) + \frac{C_4^V}{M^2} (g_{\alpha\beta} q \cdot p' - q_\beta p'_\alpha) \right. \\ &\quad \left. + \frac{C_5^V}{M^2} (g_{\alpha\beta} q \cdot p - q_\beta p_\alpha) + g_{\alpha\beta} C_6^V \right] \gamma_5 \\ &\quad + \frac{C_3^A}{M} (g_{\alpha\beta} \not{q} - q_\beta \gamma_\alpha) + \frac{C_4^A}{M^2} (g_{\alpha\beta} q \cdot p' - q_\beta p'_\alpha) + C_5^A g_{\alpha\beta} + \frac{C_6^A}{M^2} q_\beta q_\alpha, \end{aligned} \quad (5.10)$$

where  $\bar{\psi}^\beta(p')$  is the Rarita-Schwinger spinor for the  $\Delta$  and  $u(p)$  is the Dirac spinor for the nucleon. This yields the hadronic tensor

$$W_{\alpha\beta} = \frac{1}{2} Tr \left[ (\not{p} + M) \gamma_0 D_{\alpha\rho}^\dagger \gamma_0 P^{\rho\sigma} D_{\sigma\beta} \right] \quad (5.11)$$

with the Rarita-Schwinger spin 3/2 projection operator [AR99, AR05]

$$P_{\rho\sigma} = -(\not{p}' + W) \left( g_{\rho\sigma} - \frac{2 p'_\rho p'_\sigma}{3 W^2} + \frac{1 p'_\rho \gamma_\sigma - p'_\sigma \gamma_\rho}{3 W} - \frac{1}{3} \gamma_\rho \gamma_\sigma \right). \quad (5.12)$$

$W$  is the invariant mass of the  $\Delta$  with  $W = \sqrt{p'^2}$ . The leptonic tensor is unchanged and given by Eq. (3.8).

With those preliminaries and Eq. (C.1) the differential cross section for the process (5.2) is calculated to be

$$\frac{d^2 \sigma^{\nu n}}{dQ^2 dW} = \frac{G_F^2 \cos^2 \theta_C}{16\pi} \frac{W}{(s - M^2)^2} \delta(W^2 - M_\Delta^2) L^{\alpha\beta} W_{\alpha\beta}, \quad (5.13)$$

where  $M_\Delta$  is the pole mass of the  $\Delta$ . The width is accounted for in the cross section by replacing  $\delta(W^2 - M_\Delta^2)$  with the spectral function  $\mathcal{A}$ :

$$\delta(W^2 - M_\Delta^2) \rightarrow \left( -\frac{1}{\pi} \right) \mathcal{A}, \quad (5.14)$$

with

$$\mathcal{A} = \mathcal{I}m \left( \frac{1}{W^2 - M_\Delta^2 + iWT} \right), \quad (5.15)$$

and hence

$$\delta(W^2 - M_\Delta^2) \rightarrow \frac{1}{\pi} W \frac{\Gamma}{(W^2 - M_\Delta^2)^2 + W^2 \Gamma^2}. \quad (5.16)$$

The lepton mass is contained in the contraction of the tensors - we do not neglect it like many other authors (e. g. [PYS04]). In particular at low momentum transfer the lepton mass becomes important [ARSVV99, LP05].

Applying isospin relations, the cross section for the reaction (5.1) is simply Eq. (5.13) multiplied by a factor of three [LS72]. This results from

$$\langle \Delta^{++} | J_\alpha(0) | p \rangle = \sqrt{3} \langle \Delta^+ | J_\alpha(0) | n \rangle. \quad (5.17)$$

For antineutrinos we obtain similar results - the hadronic tensor remains unchanged but a different sign appears in the leptonic tensor (cf. Eq. (3.8)). The transition amplitudes are again related:

$$\langle \Delta^- | J_\alpha(0) | n \rangle = \sqrt{3} \langle \Delta^0 | J_\alpha(0) | p \rangle. \quad (5.18)$$

Finally, we discuss the neutral current processes. We saw that for quasielastic scattering, the neutral current is sensitive to the isoscalar quark content of the nucleon. However, the  $N - \Delta$  transition is purely isovector. Therefore, the neutral current of Eq. (2.41) and Eq. (2.43) reduces to

$$J_\alpha^{NC} = (1 - 2 \sin^2 \theta_W) V_\alpha^3 - A_\alpha^3. \quad (5.19)$$

These currents are members of the same isospin multiplet as the charged current and with that, their form factors are equal up to the scaling factor of  $(1 - 2 \sin^2 \theta_W)$  for the vector form factors. In the expression for the cross section, the lepton mass has to be replaced by zero and  $\cos \theta_C$  by one.

## 5.2 $N - \Delta$ Transition Form Factors

The vector and axial vector transition form factors  $C_i^{V,A}$  with  $i = 3, \dots, 6$ , which are the subject of our interest now, have been discussed for more than 30 years without general consensus. Up to the present day different authors use different form factors. Basically two approaches are discussed in the literature, first the parametrization of the neutrino scattering data with phenomenological form factors and second, the calculation of those form factors within quark models. Early attempts for the latter are reviewed in Ref. [SvH73] (see also references therein); more recent ones are summarized

in Ref. [LMZ95]. Rein and Sehgal [RS81] adopted, for their model of resonance production, the quark model of Feynman, Kislinger and Ravndal [FKR71]. This Rein-Sehgal model is still used today in many Monte Carlo generators for oscillation experiments. A more recent calculation was done by the authors of Ref. [LMZ95] who apply the Isgur-Karl quark model. Finally, Sato, Uno and Lee [SUL03] developed a dynamical model which includes pion cloud effects. This was recommended as a model of first choice in the NuINT conference summary [NuI] (see there for a comparison of the Sato-Lee and the Rein-Sehgal model).

In this thesis, however, we choose the first approach, namely the phenomenological form factors, as most of the authors aiming at neutrino nucleus reactions (e. g. [SVVO98, PYS04, SAA05]).

We start with the four vector form factors  $C_i^V$ . For quasielastic scattering the implications of CVC were discussed in detail. But also here we can assume CVC for the  $\Delta$  production, and this imposes for  $C_6^V(Q^2)$ :

$$q^\alpha V_\alpha^{CC} = 0 \Rightarrow C_6^V(Q^2) = 0. \quad (5.20)$$

CVC further implies that members of the same isopin multiplet have the same form factors. We obtain for the neutrino induced charged current channels:

$$\langle \Delta^+ | V_\alpha^{CC} | n \rangle = \langle \Delta^0 | V_\alpha^3 | n \rangle, \quad (5.21)$$

$$\langle \Delta^{++} | V_\alpha^{CC} | p \rangle = \sqrt{3} \langle \Delta^+ | V_\alpha^3 | p \rangle. \quad (5.22)$$

Therefore the vector form factors can again be extracted from electroproduction experiments. Assuming  $M_{1+}$  dominance of the electroproduction amplitude, as favored in experiments (cf. e. g. Refs. [BL04, Dre99]), one finds for the form factors [FN79]:

$$C_5^V(Q^2) = 0 \quad \text{and} \quad C_4^V(Q^2) = -\frac{M}{W} C_3^V(Q^2). \quad (5.23)$$

This leaves only one independent vector form factor,  $C_3^V$ , which can be parametrized in various forms to describe electroproduction data. We adopt the parametrization of Refs. [PYS04, OOM78]:

$$C_3^V(Q^2) = \frac{C_3^V(0)}{\left[1 + \frac{Q^2}{M_V^2}\right]^2} \frac{1}{1 + \frac{Q^2}{4M_V^2}} \quad (5.24)$$

with  $C_3^V(0) = 1.95$  and  $M_V = 0.84$  GeV.

Considering the axial form factors  $C_i^A$ , we apply similar techniques as in the quasielastic case. Pion pole dominance yields for  $C_6^A$  [AR99, SvH73]:

$$C_6^A(Q^2) = \frac{g_{\Delta N \pi} f_\pi}{\sqrt{6} M} \frac{M^2}{Q^2 + m_\pi^2} F_\pi(Q^2) \quad (5.25)$$



with  $g_\Delta$  being the  $\Delta^{++} \rightarrow p\pi^+$  coupling constant and  $f_\pi$  the pion decay constant.  $F_\pi(Q^2)$  is the vertex form factor with  $F_\pi(Q^2 = m_\pi^2) = 1$ . This relation together with the assumption of PCAC connects  $C_6^A$  and  $C_5^A$  in the axial current:

$$C_6^A(Q^2) = C_5^A(Q^2) \frac{M^2}{Q^2 + m_\pi^2}. \quad (5.26)$$

In the limit  $Q^2 = 0$  and with the assumption that  $F_\pi(Q^2)$  is a slowly varying function with  $F_\pi(Q^2 = m_\pi^2) \approx F_\pi(Q^2 = 0) = 1$ , we obtain the off-diagonal Goldberger-Treiman relation:

$$C_5^A(0) = \frac{g_{\Delta N\pi} f_\pi}{\sqrt{6}M} \simeq 1.2. \quad (5.27)$$

This coupling was extracted from the BNL data by Alvarez-Ruso et al. [ARSVV99] and found to be consistent with the PCAC prediction.

Since there are no other theoretical constraints for  $C_3^A(Q^2)$ ,  $C_4^A(Q^2)$  and  $C_5^A(Q^2)/C_5^A(0)$  they have to be fitted to neutrino scattering experiments. The existing data come mainly from two bubble chamber experiments, ANL [B<sup>+</sup>79, R<sup>+</sup>82] and BNL [K<sup>+</sup>90], which measured 0.5 – 6 GeV  $\nu_\mu$  induced events. We use the parametrization of Ref. [PYS04]:

$$C_5^A(Q^2) = \frac{C_5^A(0)}{\left[1 + \frac{Q^2}{M_A^2}\right]^2} \frac{1}{1 + \frac{Q^2}{3M_A^2}} \quad (5.28)$$

with  $M_A = 1.05$  GeV and

$$C_4^A(Q^2) = -\frac{C_5^A(Q^2)}{4}, \quad (5.29)$$

$$C_3^A(Q^2) = 0. \quad (5.30)$$

Once more we point out that this set of form factors is only one out of many which are equally good (cf. Ref. [ARSVV98] for a comparison of two sets of phenomenological form factors and one set obtained from quark model calculation). Electroproduction as well as neutrino production data used for the fits are rather old and with poor statistics. In the meantime electroproduction was measured with better accuracy and several sophisticated theoretical calculations exist [BL04]; for better neutrino scattering data one still has to wait. But refitting the vector form factors with the new and better electron input will also affect the quality of the axial parameters, i. e. the axial form factor parameters and the axial mass, even without new neutrino data. Thus, a better overall fit can be obtained. This surely has to be the next step towards a better description of neutrino nucleon and nucleus scattering.

### 5.3 Parametrization of the Width

While there exist several discussions in the literature about the influence of different form factor parametrizations on the cross section, the parametrization of the width is not covered extensively. But, as Alvarez-Ruso et al. [ARSVV99] have pointed out, this is of equal importance as the form factors and both influence each other.

Resonances are labeled by a set of quantum numbers of the partial wave in which it appears in  $\pi N$  scattering. This set consists of spin  $J$ , isospin  $I$ , relative angular momentum of the  $\pi N$  pair  $l$  and parity  $P$ . The common notation reads  $l_{ij}$  where  $J = \frac{j}{2}$  and  $I = \frac{i}{2}$ . The parity follows from  $P = (-1)^{l+1}$ . Around the decay threshold  $W_{min}$  the energy dependence of the width is determined by the orbital angular momentum [Pos04]:

$$\Gamma(W \approx W_{min}) \sim q_{CM}^{2l+1}, \quad (5.31)$$

where  $q_{CM}$  is the pion momentum in the rest frame of the resonance:

$$q_{CM}(W) = \frac{\sqrt{(W^2 - m_\pi^2 - M^2)^2 - 4m_\pi^2 M^2}}{2W}. \quad (5.32)$$

Away from the threshold, the width is modified by higher orders of  $p$ .

The  $\Delta$  resonance has the quantum numbers  $P_{33}$ , therefore,  $\Gamma(W \approx W_{min}) \sim q_{CM}^3$  is required, i. e. a  $P$ -wave width. But the extraction of the form factors from the ANL and BNL data was done assuming an  $S$ -wave width ( $l = 0$ ) for the  $\Delta$  [SvH73, K<sup>+</sup>90, R<sup>+</sup>82, B<sup>+</sup>79]. An  $S$ -wave width, even though this clearly violates angular momentum conservation, was still used in recent works of Paschos et al. [PYS04]. But most new calculations use the correct  $P$ -wave width [ARSVV98, LP05, SAA05].

The influence of the width on the cross section shall now be studied. Furthermore, we investigate the effect of applying a cut on the invariant mass as done in experiments as well as in some theoretical calculations.

For  $\Gamma$  in Eq. (5.16) we use the following representative parametrizations with  $M_\Delta = 1.232$  GeV and  $\Gamma_0 = 0.120$  GeV [E<sup>+</sup>04]:

- **W1:**  $S$ -wave [SvH73]:

$$\Gamma = \Gamma_0 \frac{q_{CM}(W)}{q_{CM}(M_\Delta)}. \quad (5.33)$$

- **W2:**  $P$ -wave [LP05]:

$$\Gamma = \Gamma_0 \left( \frac{q_{CM}(W)}{q_{CM}(M_\Delta)} \right)^3. \quad (5.34)$$

- **W3:** Blatt-Weisskopf parametrization [Leu01]:

$$\Gamma = \Gamma_0 \frac{\beta(W)}{\beta(M_\Delta)} \quad (5.35)$$

with

$$\beta(W) = \frac{q_{CM}(W)}{W^2} \frac{(q_{CM}(W)R)^2}{1 + (q_{CM}(W)R)^2}, \quad R = 1 \text{ fm}. \quad (5.36)$$

- **W4:** form factor parametrization [Pos04, AR05]:

$$\Gamma = \Gamma_0 \frac{q_{CM}(W)^3}{W} F_S^2 \quad (5.37)$$

with

$$F_S = \frac{\Lambda^2}{\Lambda^4 + (W^2 - M_\Delta^2)^2}, \quad \Lambda = 1.0 \text{ GeV}. \quad (5.38)$$

Fig. 5.1 shows a comparison of the widths. All parametrizations are constructed such, that  $\Gamma(M_\Delta) = \Gamma_0$ . Except W1, all possibilities fulfill the required  $q_{CM}^3$  dependence which follows from Eq. (5.31). W3 and W4 decrease for higher invariant masses which is required for the normalization of the spectral function.

A comparison of the different spectral functions is plotted in Fig. 5.2. Even though the widths differ significantly with increasing invariant mass, the effects in the spectral functions are rather small since the peak around the pole mass is narrow.

The influence on the total cross section can be seen in Fig. 5.3. Part (a) shows the calculation obtained by integrating over the whole range of  $W$  without any cut on the invariant mass. In (b) we applied an invariance mass cut at 1.6 GeV. This cut truncates the spectral function tail, i. e. for  $W > 1.6$  GeV, the spectral function is set to zero. This reduces all cross sections. Except for the  $S$ -wave parametrization W1, the deviations are within a few per cent.

Note that different authors use different parametrizations with different cuts: For comparison we mention Paschos et al. [PPY00] using a cut at the  $S$ -wave width at 1.6 GeV, and Alvarez-Ruso et al. [ARSVV98] cutting the  $P$ -wave width at 1.4 GeV. Also experimental data are available with and without cuts.

The following results were obtained with the parametrization W4 without any cuts.

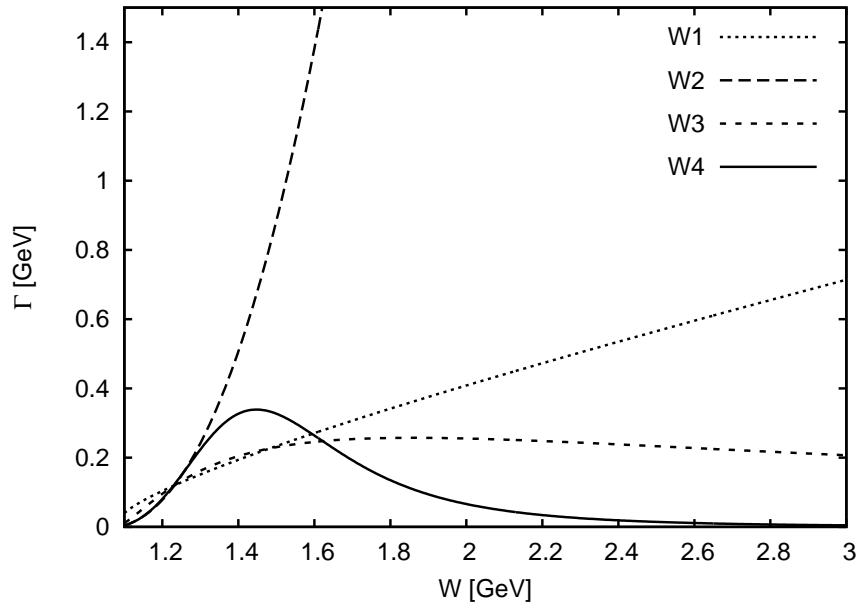


Figure 5.1: Comparison of the various parametrizations of the  $\Delta$  width. The single lines are explained in the text.

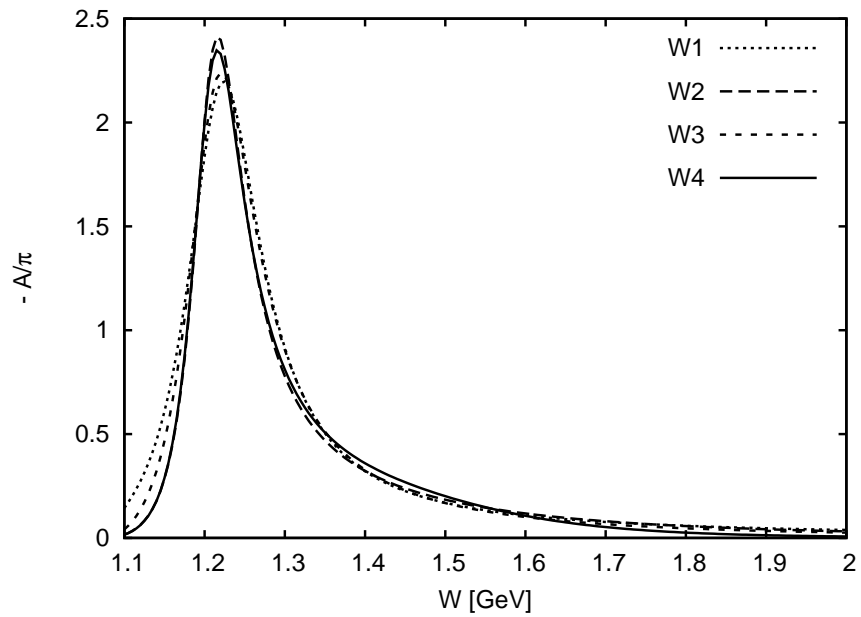
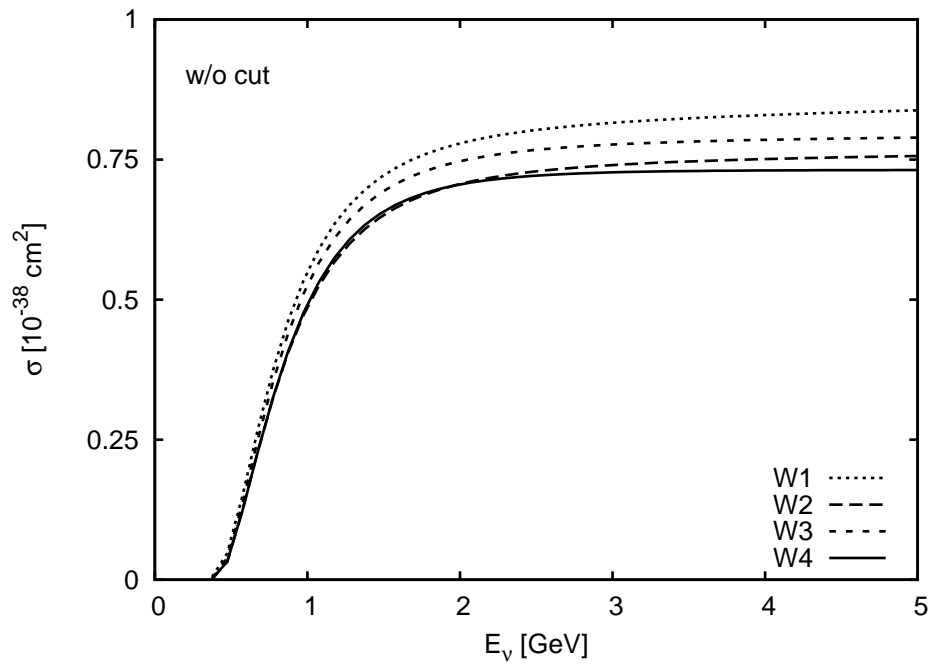
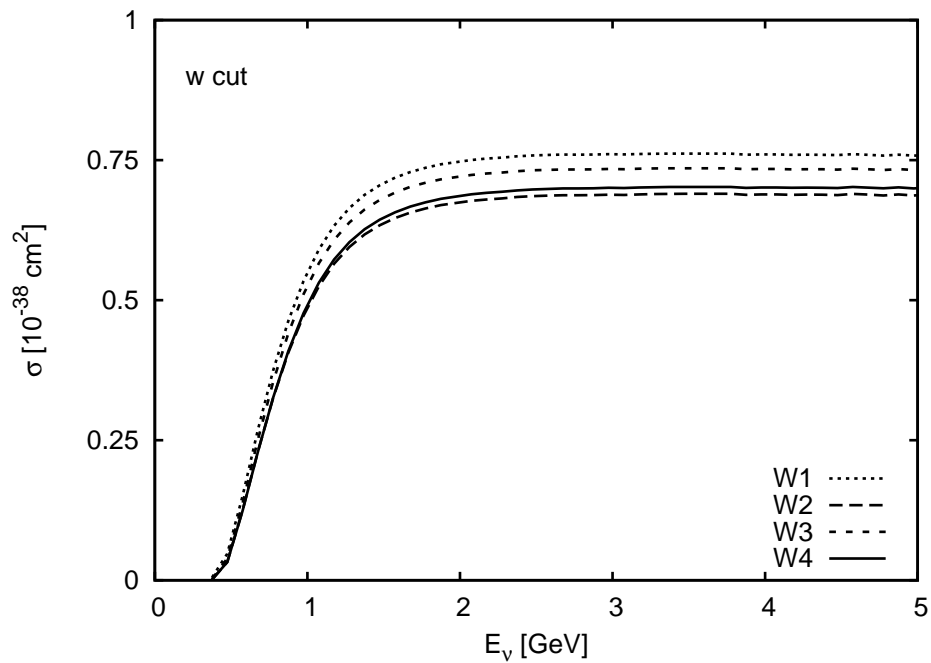


Figure 5.2: The spectral function  $\mathcal{A}$  of the  $\Delta$  resonance (cf. Eq. (5.15)) with the various parametrizations of the width.



(a)



(b)

Figure 5.3: Influence of the parametrization of the width on the total cross section for  $\nu_\mu p \rightarrow \mu^- \Delta^{++}$ : (a) without cut, (b) with cut at  $W = 1.6 \text{ GeV}$ .

## 5.4 Results

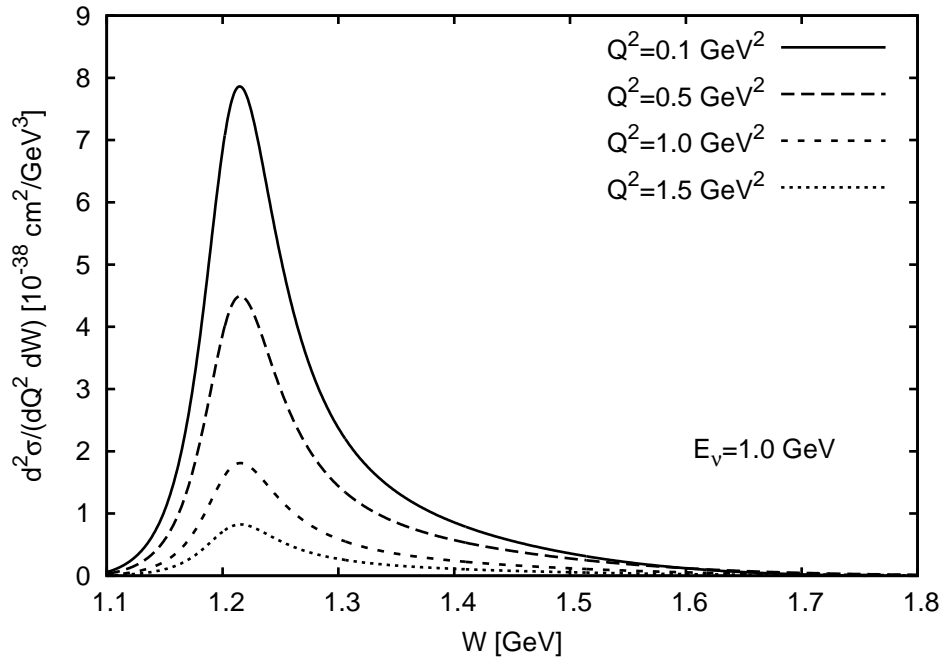
Having presented the full set of formulas required for our calculation we can now analyze the weak production of the  $\Delta$ . As an example, the results for the process  $\nu_\mu p \rightarrow \mu^- \Delta^{++}$  are discussed. In Fig. 5.4 we show the double differential cross section as a function of the invariant mass of the  $\Delta$  for different values of the momentum transfer. Panels (a) and (b) differ in the neutrino energy (1 GeV or 2 GeV, respectively). One clearly sees that the cross section peaks at the  $\Delta$  pole mass and that it decreases with increasing momentum transfer.

In Fig. 5.5 we plot the double differential cross section as a function of the momentum transfer for various invariant masses; (a) and (b) are as above. Also here the cross section becomes maximal if  $W$  equals the  $\Delta$  pole mass. The dip at very low  $Q^2$  is a threshold effect mainly due to the non-zero muon mass and is therefore bigger at smaller neutrino energies. We note that our results agree very nicely with the ones obtained by Sato et al. [SUL03] who used a different model. As in the quasielastic scattering case, the differential cross section is not very sensitive to the neutrino energy between 1 and 2 GeV and this also will yield a saturation in the total cross section as can be seen in Fig. 5.6.

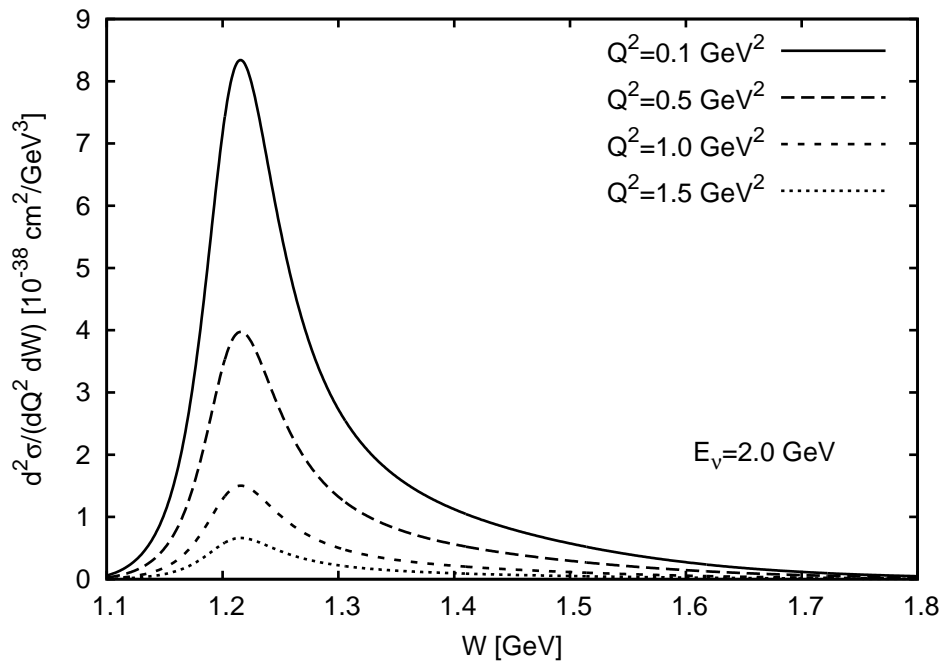
In this plot the solid line is the total integrated cross section (cf. Appendix B.3 for integration limits). The strong increase for low energies is, as in QE, an effect due to the opening phase space. Also here we are in agreement with the dynamical calculation of Sato et al.

In Fig. 5.6 we also study the contribution of the vector and axial vector form factors. While the dashed curve is obtained by setting all vector form factors to zero, i. e. only the axial ones contribute, it is done vice versa for the dotted curve. The axial current is clearly larger than the vector current but also interference terms between vector and axial vector form factors are important to obtain the full cross section.

We compare our model to experimental data (Fig. 5.7) obtained from Deuterium bubble chamber experiments. It can be seen that at low energies both agree well but the uncertainty of the data increases for higher energies. This again stresses the necessity of better quality data in order to learn more about the form factors, in particular about the axial form factors.

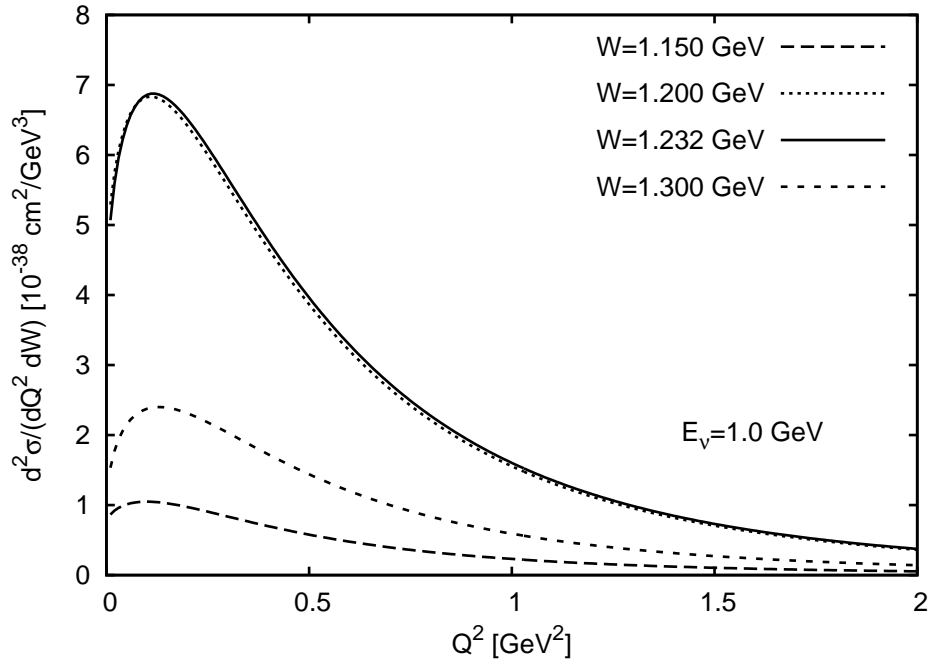


(a)

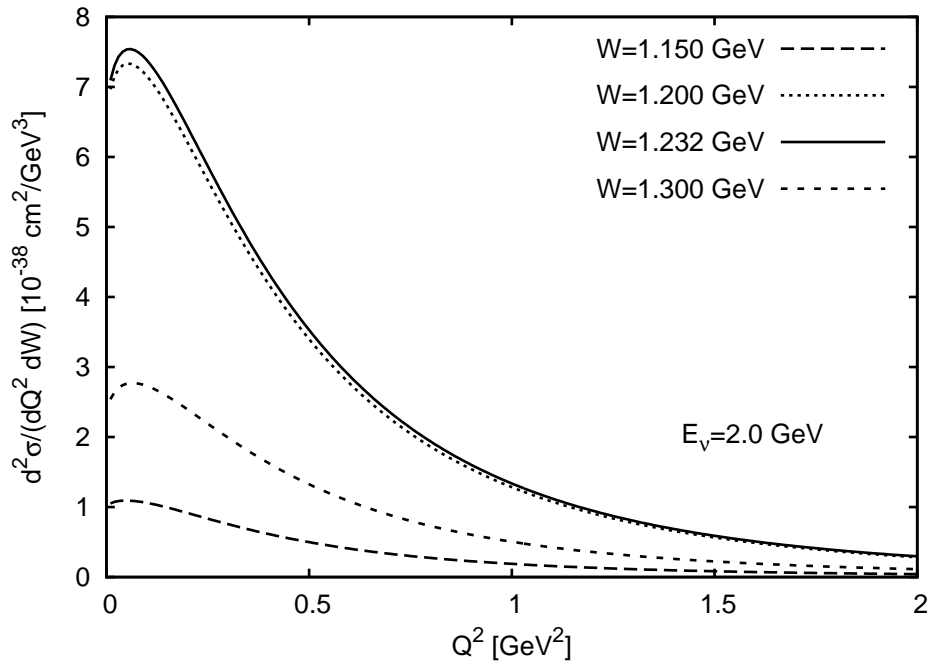


(b)

Figure 5.4: Double differential cross sections for  $\nu_\mu p \rightarrow \mu^- \Delta^{++}$  as function of the invariant mass  $W$  for various momentum transfers. (a)  $E_\nu = 1 \text{ GeV}$ , (b)  $E_\nu = 2 \text{ GeV}$ .



(a)



(b)

Figure 5.5: Double differential cross sections for  $\nu_\mu p \rightarrow \mu^- \Delta^{++}$  as function of the momentum transfer  $Q^2$  for various invariant masses. (a)  $E_\nu = 1$  GeV, (b)  $E_\nu = 2$  GeV.



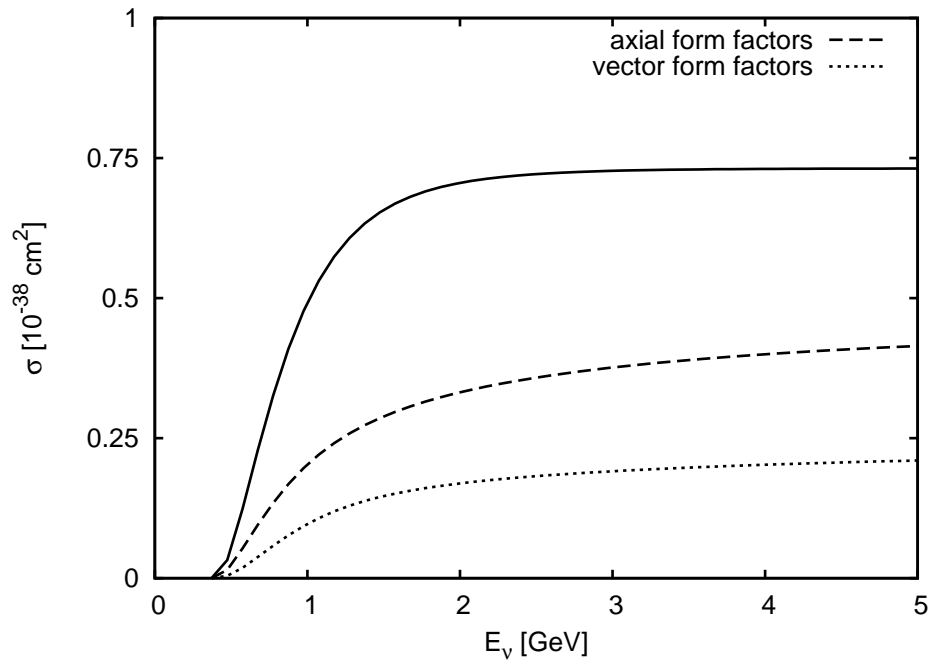


Figure 5.6: Formfactor contribution to the total cross section for  $\nu_{\mu}p \rightarrow \mu^{-}\Delta^{++}$ ; the solid line represents the total cross section.

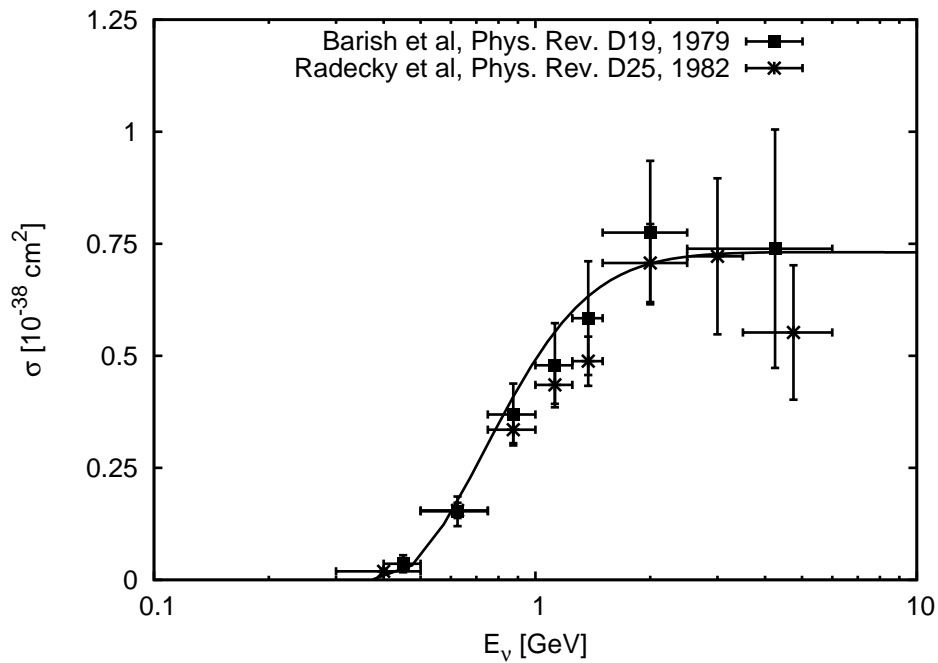


Figure 5.7: Total cross section for  $\nu_{\mu}p \rightarrow \mu^{-}\Delta^{++} \rightarrow \mu^{-}p\pi^{+}$ .



## 6 Remaining Contributions to Neutrino Nucleon Scattering

We want to close our discussions of neutrino nucleon scattering with a summary of processes not included in our model and an examination of their relative importance. It turns out that including quasielastic scattering and  $\Delta$  production is sufficient for studying weak pion production from nuclei at intermediate energies up to about 2 GeV. However, since we plan to scatter off nuclei we shall at least mention that scattering off electrons is negligible, simply because  $\sigma_{\nu e}/\sigma_{\nu N} \sim m_e/M$ . An important source of additional contributions comes from the production of higher-mass resonances. Further we consider the non-resonant background and higher energy processes as deep-inelastic scattering. Finally, we look at exotic channels containing strangeness production.

### 6.1 Higher-Mass Resonances

For charged current neutrino and antineutrino scattering we obtain the possible one pion production reactions:

$$\nu p \rightarrow l^- p \pi^+ \qquad \bar{\nu} p \rightarrow l^+ p \pi^- \qquad (6.1)$$

$$\nu n \rightarrow l^- n \pi^+ \qquad \bar{\nu} p \rightarrow l^+ n \pi^0 \qquad (6.2)$$

$$\nu n \rightarrow l^- p \pi^0 \qquad \bar{\nu} n \rightarrow l^+ n \pi^- \qquad (6.3)$$

whereas for neutral current scattering we have:

$$\nu p \rightarrow \nu p \pi^0 \qquad \bar{\nu} p \rightarrow \bar{\nu} p \pi^0 \qquad (6.4)$$

$$\nu p \rightarrow \nu n \pi^+ \qquad \bar{\nu} p \rightarrow \bar{\nu} n \pi^+ \qquad (6.5)$$

$$\nu n \rightarrow \nu n \pi^0 \qquad \bar{\nu} n \rightarrow \bar{\nu} n \pi^0 \qquad (6.6)$$

$$\nu n \rightarrow \nu p \pi^- \qquad \bar{\nu} n \rightarrow \bar{\nu} p \pi^- \qquad (6.7)$$

Using Clebsch-Gordon coefficients those reactions can be classified by isospin, e. g. for

the amplitudes  $\mathcal{A}$  of the first three reactions one gets:

$$\mathcal{A}(l^- p \pi^+) = \mathcal{A}_3, \quad (6.8)$$

$$\mathcal{A}(l^- n \pi^+) = \frac{1}{3}\mathcal{A}_3 + \frac{2\sqrt{2}}{3}\mathcal{A}_1, \quad (6.9)$$

$$\mathcal{A}(l^- p \pi^0) = -\frac{\sqrt{2}}{3}\mathcal{A}_3 + \frac{2}{3}\mathcal{A}_1, \quad (6.10)$$

with  $\mathcal{A}_3$  being the amplitude for isospin 3/2 resonances and  $\mathcal{A}_1$  corresponds to the sum of isospin 1/2 resonances. Thus, except for the very first reaction (and its antineutrino counterpart) all channels receive contributions from isospin 1/2 resonances. Interference effects can play a non-negligible role.

The production of higher-mass resonances is not covered too extensively in the literature. However, we shall mention Paschos et al. [PYS04] who extended the model of Ref. [FN79] and included, besides the  $\Delta$ , the resonances  $N(1440)$  and  $N(1535)$ . Second, there is the model of Rein and Sehgal [RS81] which includes all resonances up to an invariant mass of 2 GeV using old quark model calculations. Finally, the  $N(1440)$  was studied by Alvarez-Ruso et al. [ARSVV98]. They all agree that at medium energies, the  $\Delta$  is far more important than any other resonance with the  $\Delta$  being well separated from the others. This is nicely displayed in Fig. 3 of Ref. [PYS04]. In addition, the theoretical description and the form factors for higher resonances contain much more uncertainties than for the  $\Delta$ .

This encouraged us among others (cf. e. g. Refs. [SAA05, SVVO98] and references therein) to assume  $\Delta$  dominance for the energies of our interest. Nevertheless, we stress that in a full model those higher-mass resonances have to be included.

## 6.2 Non-Resonant Background

Not only resonances contribute to one pion production but also non-resonant background processes. They equally influence all the reactions mentioned above and, in addition, could also lead to interferences. A recent calculation obtains a small non-resonant one pion background [SUL03] but points out the importance of possible interference with the resonant amplitude. Also, two pion background is a possible contribution, but its discussion in the literature is very scarce [ADT81b, ADT81a]. However, non-resonant background is not considered in our model and we stress that for intermediate energies quasielastic scattering and  $\Delta$  production are clearly dominant.

## 6.3 Deep Inelastic Scattering

In contrast to the low energy processes like quasielastic scattering and resonance production or even non-resonant reactions, high energy deep inelastic scattering is well known and understood. So we refer the reader to one of the standard textbooks on High Energy Physics. Here we shall point out only two things: One redefines the structure functions to dimensionless structure functions depending on Bjorken- $x$  and  $Q^2$ , which can be related at high energies to quark distribution functions. Therefore, one has not to deal with phenomenological form factors as at low energies. Second, the DIS contribution gets more important for higher energies since it rises proportional to the energy as shown in Fig. 3.2. This can also be seen from Fig. 6.1 where a collection of data is plotted. For energies less than 10 GeV, quasielastic and resonance contributions are still visible in the data as bumps but disappear quickly when going further in energy.

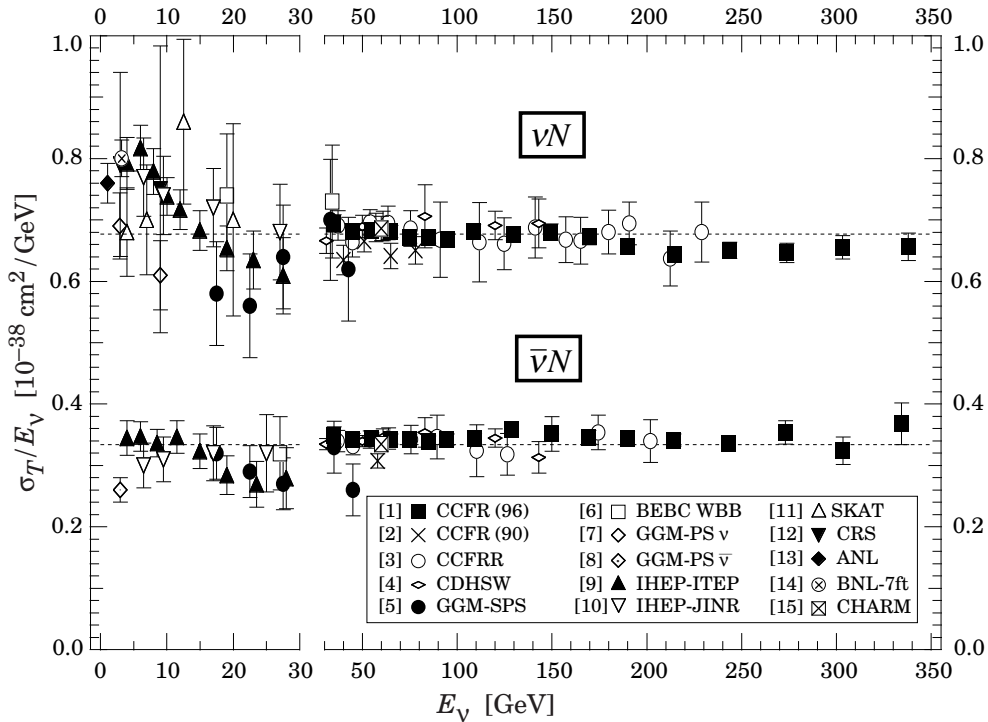


Figure 6.1: Measurements of the total neutrino and antineutrino cross section. Note the change of scale at 30 GeV (from Ref. [H<sup>+</sup>02], see references therein).

There are ongoing discussions on how to combine the resonance and deep inelastic regions [BPY05] but this is beyond the scope of this thesis.

## 6.4 Strangeness Production

Finally, to round off the picture of the variety of neutrino interactions we shall mention more exotic processes. Even at energies below deep inelastic scattering net strangeness can be produced due to the strangeness non-conserving weak current (cf. chapter 2 and in particular Eq. (2.12)). However, the selection rule  $\Delta S = \Delta Q$  restricts  $\Delta S = 1$  single hyperon production to antineutrinos rather than to neutrinos:

$$\bar{\nu}N \rightarrow l^+ + (\Lambda, \Sigma, Y^*). \quad (6.11)$$

From Eq. (2.12) we see that changing an up quark to a strange quark includes a factor of  $\sin \theta_C$ , therefore, those reactions are suppressed by the Cabbibo mixing angle and we can safely neglect them.

We conclude that our model contains the most important ingredients for neutrino scattering at medium energies and can be reliably applied to quasielastic reactions and one pion production from nuclei.

## **Part III**

# **Neutrino Nucleus Scattering**





# 7 Neutrino Nucleus Scattering within a BUU Transport Model

Having discussed neutrino scattering off nucleons we now turn to scattering off nuclei. In this chapter we will introduce our model for neutrino nucleus interactions. Some details of the numerical implementation will be given. We close this chapter with a review of other available models and a comparison.

## 7.1 BUU Transport Model

Any model aiming at the description of the interaction of neutrinos with nuclei should be first tested against the existing data of the interaction of photons and electrons with nuclei - this has been done for the Boltzmann-Uehling-Uhlenbeck (BUU) transport model which will be applied in the following. Originally developed to study heavy-ion collisions, this model has been extended to describe interactions of photons, electrons and pions with nuclei. The BUU model itself and its numerical implementation is covered extensively in Refs. [Leh03, Eff99].

We have extended the BUU model to describe neutrino nuclear reactions with particular emphasis on including both quasielastic and  $\Delta$  production as the most important processes into one model. In the simulation the interactions are factorized: After the nucleus is initialized, the neutrino scattering occurs and then the hadronic output undergoes final state interactions.

We shall briefly review the initialization and the transport part of the BUU model and its underlying physics before we discuss its extension to neutrino nucleus reactions.

### 7.1.1 Theoretical Background

#### Transport Theory

The space-time evolution of a many-body system under the influence of a mean-field potential and a collision term can be described by the BUU equation. The BUU equation is based on the classical Boltzmann equation and was modified by Nordheim, Uehling

and Uhlenbeck to incorporate the description of fermionic systems. For its derivation we refer the reader to Refs. [Leh03, Eff99].

For the one-particle distribution function  $f_1(\vec{r}, \vec{p}, t)$  one obtains for the BUU equation [Eff99]:

$$\frac{df_1(\vec{r}, \vec{p}, t)}{dt} = \left( \frac{\partial}{\partial t} + \frac{\partial H}{\partial \vec{p}} \frac{\partial}{\partial \vec{r}} - \frac{\partial H}{\partial \vec{r}} \frac{\partial}{\partial \vec{p}} \right) f_1(\vec{r}, \vec{p}, t) = I_{coll}(f_1(\vec{r}, \vec{p}, t)) \quad (7.1)$$

with the relativistic one-body Hamilton function

$$H = \sqrt{(M_0 + U_S)^2 + \vec{p}^2}. \quad (7.2)$$

Here  $U_S$  denotes the scalar mean field potential. The sum defines an effective mass

$$M_{eff} = M_0 + U_S. \quad (7.3)$$

In the case of a vanishing collision term  $I_{coll}$ , this equation is known as Vlasov equation.

The collision term describes the possibility of scattering of one particle out of its phase-space cell into another one. Therefore the collision term includes both gain and loss terms. Considering e. g. particle 1 in the two body process

$$1 + 2 \rightarrow 3 + 4, \quad (7.4)$$

then the loss term describes the possibility to scatter out from the phase-space cell. To take into account all collision partners, an integral over the momentum  $p_2$  of the scattering partner has to be included as well as over all possible final states with momenta  $p_3$  and  $p_4$ . Pauli blocking forbids scattering of fermions into occupied states, leading to factors of  $(1 - f_1^3)$  and  $(1 - f_1^4)$ , where the upper index in the one-particle distribution function denotes the particle under consideration. In the case of bosons, scattering into occupied states is possible, leading to factors of  $(1 + f_1^3)$  and  $(1 + f_1^4)$ . For the gain term describing the scattering into a phase-space cell, a similar argumentation holds and we arrive at

$$I_{coll}(f_1(\vec{r}, \vec{p}, t)) = \int dp_2 dp_3 dp_4 \left[ -T(\vec{p}_1 \vec{p}_2 \rightarrow \vec{p}_3 \vec{p}_4) f_1^1 f_1^2 (1 \pm f_1^3)(1 \pm f_1^4) \right. \\ \left. + T(\vec{p}_3 \vec{p}_4 \rightarrow \vec{p}_1 \vec{p}_2) f_1^3 f_1^4 (1 \pm f_1^1)(1 \pm f_1^2) \right]. \quad (7.5)$$

The probability of scattering  $T$  is related to the cross section.

The BUU simulation contains not only nucleons but many other hadrons and mesons (for a list of all considered particles see Ref. [Eff99]). Each particle species fulfills a separate transport equation. These distinct equations are coupled through the collision term

including all possible channels of scattering and through the potentials which might depend on the density distribution. This so-called coupled channel method yields to coupled integral-differential equations:

$$\frac{df_1^N(\vec{r}, \vec{p}, t)}{dt} = I_{coll}(f_1^N, f_1^\Delta, f_1^\pi, \dots) \quad (7.6)$$

$$\frac{df_1^\Delta(\vec{r}, \vec{p}, t)}{dt} = I_{coll}(f_1^N, f_1^\Delta, f_1^\pi, \dots) \quad (7.7)$$

...

For simplicity, we presented the formalism for on-shell particles. We want to emphasize that in our model resonances are propagated off-shell. For a detailed treatment we refer to Ref. [Leh03].

## Initialization

For the density distribution of the nucleus we assume a Woods-Saxon distribution:

$$\rho(r) = \rho_0 \left( 1 + \exp \frac{r - r_0}{\alpha} \right)^{-1}. \quad (7.8)$$

The parameters are listed in Ref. [Eff99] for different nuclei. In momentum space the nucleons are initialized within a local Thomas-Fermi approach with a density dependent Fermi momentum

$$p_F(\vec{r}) = \left( \frac{3}{2} \pi^2 \rho(\vec{r}) \right)^{\frac{1}{3}}. \quad (7.9)$$

## Potentials

For the nucleon mean field potential we take a parametrization of Welke [WPK<sup>+</sup>88],

$$V(\vec{r}, \vec{p}) = A \frac{\rho(\vec{r})}{\rho_0} + B \left( \frac{\rho(\vec{r})}{\rho_0} \right)^\tau + \frac{2C}{\rho_0} g \int \frac{dp'}{(2\pi)^3} \frac{f(\vec{r}, \vec{p}')}{1 + \left( \frac{\vec{p} - \vec{p}'}{\Lambda} \right)^2}, \quad (7.10)$$

in a local Fermi approach. For the parameters we use the so-called "medium momentum dependent" set of Ref. [Eff99]. This potential is used not only for the nucleons but for all baryons except for the  $\Delta$  resonances (isospin 3/2). Motivated by the phenomenological value of their potential, we use [Eff99]

$$V_\Delta = \frac{2}{3} V. \quad (7.11)$$

In this work we do not include potentials for mesons.

We now shall consider how this non-relativistic parametrization  $V$  is related to the relativistic Hamiltonian from Eq. (7.2). The general expression for the relativistic one-particle Hamiltonian is given as

$$H = \sqrt{(M_0 + S)^2 + (\vec{p} - \vec{U}_V)^2} + U_V^0, \quad (7.12)$$

where  $S$  is a scalar potential and  $(U_V^0, \vec{U}_V)$  a vector potential. Going into the local rest frame of the nuclear matter, i. e. the frame where the spatial components of the baryon current vanish, simplifies this expression, since in that particular frame the spatial components of the potential  $\vec{U}_V$  vanish [Leh03]. We can identify

$$U_V^0 = V \quad (7.13)$$

and

$$S = 0, \quad (7.14)$$

and obtain for the Hamiltonian

$$H_{LRF} = \sqrt{M_0^2 + \vec{p}_{LRF}^2} + V. \quad (7.15)$$

The scalar potential, which enters Eq. (7.2), is now defined as:

$$U_S = \sqrt{\left(\sqrt{M_0^2 + \vec{p}_{LRF}^2} + V\right)^2 - \vec{p}_{LRF}^2} - M_0. \quad (7.16)$$

## Collision Term

Scattering of various particles enters our model through the collision term. A complete description of all possible reactions and its cross sections can be found in Refs. [Leh03, Eff99]. The most important channels are ( $B$  denotes a baryon,  $m$  a meson and  $R$  a resonance)

$$\begin{aligned} NN &\leftrightarrow NN \\ NN\pi &\leftrightarrow NN \\ NN &\leftrightarrow NR \\ NN &\leftrightarrow \Delta\Delta \\ NR &\leftrightarrow NR' \\ mB &\leftrightarrow R, \text{ in particular } \pi N \leftrightarrow \Delta \\ \pi N &\leftrightarrow \pi N \\ \pi N &\leftrightarrow \pi\pi N \\ \pi N &\leftrightarrow \eta N. \end{aligned}$$

Note that there is no spin dependence included - all cross sections are spin averaged.

Usually vacuum cross section are used, parametrized as functions of the invariant mass  $\sqrt{s}$  of the two incoming particles 1 and 2. If one particle feels the attractive mean field potential, then the invariant mass is smaller than in the vacuum, leading to an error in the calculation of the cross section. Therefore, we introduce a "free" invariant mass  $\sqrt{s_{free}}$ :

$$\sqrt{s_{free}} = \sqrt{M_1^2 + p_{CM}^2} + \sqrt{M_2^2 + p_{CM}^2}, \quad (7.17)$$

with the vacuum masses  $M_1$  and  $M_2$  and their center of mass momentum  $p_{CM}$ .

We account for modified widths of resonances inside the nucleus. While the nucleons inside the nucleus are constrained to have momenta below the Fermi momentum, there is no such constraint for the production of the resonances. Their decay, however, is influenced by Pauli blocking, e. g. a resonance decaying into a pion nucleon pair is Pauli blocked if the nucleon's momentum is below the Fermi momentum. Therefore the width of the resonance inside the nuclear medium is modified.

For the  $\Delta$  resonance, as the most important one in our model, we also include modifications due to collisions inside the medium. For the total in-medium width we obtain

$$\Gamma_{tot}^{med} = \tilde{\Gamma} + \Gamma_{coll}, \quad (7.18)$$

where  $\tilde{\Gamma}$  is the Pauli blocked decay width. The collisional width  $\Gamma_{coll}$  accounts for additional decay channels of the  $\Delta$  inside the nucleus. Through two-body and three-body absorption processes like  $\Delta N \rightarrow NN$  or  $\Delta NN \rightarrow NNN$ , the  $\Delta$  can disappear without producing a pion, while via  $\Delta N \rightarrow \pi NN$  additional pions can be produced. Also elastic scattering  $\Delta N \rightarrow \Delta N$  contributes to  $\Gamma_{coll}$ .

One way of realization is the explicit inclusion of those processes into our simulation (cf. the list of the most important channels above. Note that three-body processes are not considered.). In this thesis, we use a different way: We "switch off" those explicit collisions and use a parametrization of  $\Gamma_{coll}$  by Oset and Salcedo [OS87] instead. For a comparison of both methods and more details we refer to Effenberger [Eff99].

## 7.1.2 Numerical Implementation

Finally, we want to consider the numerical implementation of the BUU transport code. The coupled BUU equations are solved with the so-called test particle ansatz. We replace the distribution function  $f_1$  of a nucleon through an ensemble of test particles:

$$f_1 = \frac{(2\pi)^3}{4} \frac{1}{N} \sum_i \delta(\vec{r} - \vec{r}_i(t)) \delta(\vec{p} - \vec{p}_i(t)) \quad (7.19)$$

where  $\vec{r}_i(t)$  and  $\vec{p}_i(t)$  are the position and the momentum of test particle  $i$  at time  $t$ .  $N$  denotes the number of test particles. In the parallel ensemble method, we split all test particles into  $N$  ensembles which do not influence each other. Furthermore, we use the concept of real and perturbative particles. Real particles are test particles representing the nucleons in the nucleus. Perturbative particles are test particles produced either in the initial neutrino nucleon reaction or in final state interactions. They are influenced in their propagation and in their interactions via collisions by the real particles, but the perturbative particles cannot influence the real particles in any way [Leh03].

With the test particle ansatz we can now solve the BUU equations. We distinguish between propagation and collisions. In between the collisions the particles are propagated according to the Vlasov equation where  $I_{coll} = 0$ . The test particle ansatz leads to the classical Hamilton equations of motion

$$\frac{d\vec{r}_i}{dt} = \frac{\partial H}{\partial \vec{p}_i}, \quad (7.20)$$

$$\frac{d\vec{p}_i}{dt} = -\frac{\partial H}{\partial \vec{r}_i}. \quad (7.21)$$

For the numerical treatment we refer to Refs. [Eff99, Leh03].

We divide the duration of the reaction in time intervals  $\Delta t$ . In every time step, we check whether a collision or a resonance decay takes place. The decision whether two particles 1 and 2 interact depends on their impact parameter  $b$ . A first criterion for scattering is based on the simple classical total cross section  $\sigma_{12}$ :

$$b \leq \sqrt{\frac{\sigma_{12}}{\pi}}. \quad (7.22)$$

Additionally, we define a cut-off for the cross sections to account for shadowing effects inside the medium [Eff99],

$$p(b) = \Theta(b_{max} - b) \Theta\left(\sqrt{\frac{\sigma_{12}}{\pi}} - b\right), \quad (7.23)$$

with the maximum impact parameter

$$b_{max} = \sqrt{\frac{\sigma_{12}^{max}}{\pi}}, \quad (7.24)$$

which is given in Ref. [Leh03] for various collision types. The actual time point for the scattering is determined following an algorithm due to Kodama et al. [KDC<sup>+</sup>84]. The final state particles and their kinematics are chosen via Monte Carlo decisions. If the final state particles are fermions we also check for Pauli blocking. The numerical implementation of Pauli blocking is described in Ref. [Eff99].

We check not only for collisions in a given time step, but also for resonance decays. A resonance decays with the probability

$$p = 1 - \exp\left(-\frac{\Delta t}{\gamma\tau}\right), \quad (7.25)$$

where  $\gamma$  is the Lorentz factor of the boost from the lab frame to the resonance rest frame and  $\tau$  is the lifetime.

Having outlined the main aspects of the BUU transport model in this chapter, this model now serves as a framework for our study of neutrino nucleus scattering and we shall proceed with the discussion of in-medium modifications of the neutrino nucleon cross sections and their implementation into the BUU transport code.

## 7.2 Numerical Implementation of Neutrino Cross Sections

In order to use the vacuum cross sections derived in Part II, we assume the validity of the so-called impulse approximation. Impulse approximation implies that the incoming particle interacts only with a single nucleon of the nucleus, an assumption adopted already for photo- and electroproduction. Due to the even smaller weak coupling constant, impulse approximation is also applicable for neutrino nucleus scattering.

Aiming at a model which incorporates both quasielastic scattering and  $\Delta$  production we need to find a way of implementing those processes simultaneously. For that, we first need to discuss the kinematics. In the nucleon rest frame the following condition has to be fulfilled:

$$s = (p + q)^2 = M^2 - Q^2 + 2E_q M \equiv M'^2, \quad (7.26)$$

where  $M'$  is either the nucleon mass  $M$  or the  $\Delta$  mass  $W$ . If we assume that  $M'$  is fixed, the kinematics of the process is completely determined by two quantities, e. g. the neutrino energy  $E_\nu$  and the four-momentum transfer squared  $Q^2$ . The energy of the outgoing lepton  $E_l$  is then simply given by

$$E_l = E_\nu - E_q, \quad (7.27)$$

with  $E_q$  from Eq. (7.26). Then all four-vectors of the system are known: Assuming the momentum of the incoming neutrino in  $z$ -direction gives

$$k_\alpha = (E_\nu, 0, 0, E_\nu). \quad (7.28)$$

From the energy of the outgoing lepton we know its momentum

$$|\vec{k}'| = \sqrt{E_l^2 - m_l^2} \quad (7.29)$$

and from the four-momentum transfer also the angle between  $\vec{k}$  and  $\vec{k}'$ ,

$$\cos \theta_{lab} = -\frac{Q^2 + m_l^2 - 2E_\nu E_l}{2E_\nu |\vec{k}'|}. \quad (7.30)$$

The angle  $\phi$  of the outgoing lepton is chosen randomly for a given event which then defines the direction of the lepton

$$\vec{e}_l = (\sin \theta \cos \phi, \sin \theta \sin \phi, \cos \theta). \quad (7.31)$$

This yields the four-momentum of the outgoing lepton

$$k'_\alpha = (E_l, |\vec{k}'| \vec{e}_l) \quad (7.32)$$

and further, the four-momentum of the exchanged vector boson

$$\begin{aligned} q_\alpha &= k_\alpha - k'_\alpha \\ &= (E_\nu - E_l, \vec{k} - \vec{k}'). \end{aligned} \quad (7.33)$$

Knowing  $E_\nu$ ,  $Q^2$  and the mass of the outgoing hadron thus results directly in  $k$ ,  $k'$  and  $q$ . The four-momenta of the nucleons  $p$  are determined from their initialization within the code. Then the hadronic final state is fully defined: Energy and momentum conservation yields:

$$p' = p + q. \quad (7.34)$$

Inside the nuclear medium, Eq. (7.26) has to be changed. We obtain in the nucleus rest frame

$$s = M_{eff}^2 - Q^2 + 2E_q E - 2\vec{p} \cdot \vec{q} \equiv M_{eff}'^2. \quad (7.35)$$

$\vec{p}$  is the Fermi momentum of the nucleon and  $\vec{q}$  is the momentum of the exchanged vector boson. This equation further takes into account that the nucleon and the  $\Delta$  are bound in a mean field potential with

$$M_{eff} = M + U_S \quad (7.36)$$

and

$$M_{eff}' = M' + U_S'. \quad (7.37)$$



$M'$  again denotes either the nucleon mass  $M$  or the  $\Delta$  mass  $W$ . We emphasize that the potential is momentum dependent. Since the momenta of the initial nucleons are known,  $U_S$  is fully determined. But  $U'_S$  depends on  $p'$ . And, as just shown,  $p'$  depends on  $E_q$ . This makes this equation non-trivial.

A possible solution is to assume three independent kinematical quantities to be known. In addition to  $E_\nu$  and  $Q^2$  we, require, for instance,  $E_l$  to be fixed. This allows us to go back to Eq. (7.27) without any assumption of the mass of the outgoing particle. The calculation yields again all four-vectors of the system. With  $p'$  we can obtain  $U'_S$  and the effective mass  $M'_{eff}$  and hence also  $M'$  by using

$$M' = \sqrt{E'^2 - \vec{p}'^2} - U'_S. \quad (7.38)$$

We conclude that for a correct treatment of the potentials three independent kinematical quantities have to be known. We choose  $E_\nu$ ,  $Q^2$  and  $E_l$ . Then we can calculate specific cross sections fixed by the neutrino energy and the properties of the outgoing lepton. It has to be noted that we pay for this with an increased numerical effort.

For the  $\Delta$  resonance, the implementation is straightforward assuming a given set of  $E_\nu$ ,  $Q^2$  and  $E_l$ . We have shown how then the mass  $M' = W$  is calculated. The cross section is given in the nucleon rest frame in Eq. (5.13) as a function of  $E_\nu$ ,  $Q^2$  and  $W$  and thus fully defined. In terms of  $E_l$  it is written as

$$\frac{d^2\sigma}{dQ^2 dE_l} = \frac{M}{W} \frac{d^2\sigma}{dQ^2 dW}. \quad (7.39)$$

Assuming  $\Delta$  dominance, we have so far implemented only the  $\Delta$  but in the future other resonances can be added easily provided the form factors are known (cf. discussion in chapter 6).

For quasielastic scattering we have an additional constraint. For the given set of  $E_\nu$ ,  $Q^2$  and  $E_l$ ,  $M'$  is calculated as outlined above. But only if  $M' = M$ , quasielastic scattering is possible:

$$\frac{d^2\sigma}{dQ^2 dM'^2} = \frac{d\sigma}{dQ^2} \delta(M'^2 - M^2). \quad (7.40)$$

$d\sigma/dQ^2$  is given in Eq. (4.12) in the nucleon rest frame as a function of  $Q^2$  and  $E_\nu$ . This constraint, of course, limits the number of possible combinations of  $E_\nu$ ,  $Q^2$  and  $E_l$  leading to quasielastic scattering and therefore causes problems in our numerical treatment for distinct values of  $E_\nu$ ,  $Q^2$  and  $E_l$ . To solve this issue, we allow events leading to values of  $M'$  not exactly equal the nucleon mass to be counted as quasielastic. To guarantee that

only values rather close to  $M$  can contribute, we introduce a weighting function  $\omega$  which has to fulfill

$$\frac{d\sigma}{dQ^2} = \int \frac{d\sigma}{dQ^2} \omega(M') dM'^2. \quad (7.41)$$

We choose for  $\omega(M')$

$$\omega(M') = \frac{1}{\pi} \frac{\epsilon M'}{(M'^2 - M^2)^2 + M'^2 \epsilon^2} \quad (7.42)$$

where  $\epsilon$  determines the range of possible  $M'$ . We choose  $\epsilon = 1$  MeV as a value which is sufficiently smaller than any other physical scale, and which is still numerically feasible. Note that this affects only the decision whether a quasielastic event is possible or not, the cross section  $d\sigma/dQ^2$  is calculated with the "real" nucleon mass. Finally, we obtain

$$\frac{d^2\sigma}{dQ^2 dE_l} = \frac{d\sigma}{dQ^2} 2M\omega(M'). \quad (7.43)$$

Due to the large variety of possible combinations of  $E_\nu$ ,  $E_l$  and  $Q^2$  the numerics is very time consuming. For every set allowed by kinematics a calculation could be done. We did the calculations on a grid with distinct steps for the three quantities. At each test particle in every ensemble a neutrino interaction is initialized and, according to the cross section, a final state is then chosen by Monte Carlo. This yields  $N \cdot A$  reactions with  $N$  being the number of testparticles and  $A$  being the mass number of the nucleus. If the produced particles are not Pauli blocked, they undergo final state interactions. While for pions absorption and charge exchange are most important, the main final state interaction process for nucleons is rescattering.

The cross section for the  $\nu A$  reaction is then given by a summation over the contributions of all nucleons. For a distinct channel, e. g.  $\pi^+$  production, all the contributions have to be weighted with the multiplicity of that final state [Leh03]:

$$\frac{d^2\sigma_{\nu A \rightarrow lFX}}{dQ^2 dE_l} = 4 \int_{\text{Nucleus}} d^3r \int^{p_F} \frac{d^3p}{(2\pi)^3} \frac{d^2\sigma_{\nu N \rightarrow lFX}}{dQ^2 dE_l} M_F, \quad (7.44)$$

where  $d^2\sigma_{\nu N \rightarrow lFX}/(dQ^2 dE_l)$  are the cross sections per nucleon in the nucleus rest frame (cf. Ref. [Eff96] for details on the Lorentz transformation). The multiplicity  $M_F$  is calculated in the BUU transport simulation and contains e. g. information about Pauli blocking, final state interactions and the momentum distributions.

Finally, we note that we do not include any corrections due to the Coulomb potential for the outgoing lepton. We expect the effect to be negligible for the lepton energies under consideration due to the smallness of the electromagnetic coupling constant.

## 7.3 Other Models and Comparison

Having now completely specified our model we shall briefly review other available approaches before presenting the results of our calculation of cross sections.

Many event generators for neutrino interactions exist, among them are NUANCE, NEUGEN, NEUT and NUX-FLUKA (cf. for detailed comparisons Refs. [GCHS05, Zel03]). Commonly they apply impulse approximation and use the Llewellyn-Smith formalism for quasielastic events [LS72] and the Rein-Sehgal model for the resonances [RS81]. Pros and cons of the Rein-Sehgal model were discussed recently in Ref. [NuI] with the conclusion that an improvement of this model is urgent. Problematic, in particular, are the form factors used and the fact that resonances in this model decay only in  $\pi N$ .

The generators differ substantially in how they implement in-medium effects and final state interactions. As an example, we briefly discuss NEUT [Hay02] and NUANCE [Cas02] used for the Super-Kamiokande analysis [Super-K05]. Both use the relativistic Fermi gas model of Smith and Moniz [SM72] assuming a flat momentum distribution for the nucleons up to fixed Fermi surface momentum. The nuclear binding energy is set to a fixed value. Pauli blocking and modifications of the  $\Delta$  width are taken into account only in the NEUT model. NUANCE, however, does not consider in-medium effects on the resonance widths. The final state interactions are treated by using a cascade model specific to Oxygen with inelastic scattering, charge exchange and absorption of pions included.

Another model available for pion production, also using a Monte-Carlo simulation for the reaction process, is from Paschos et al. (originally developed in Ref. [ANP74] and improved in Refs. [PPY00, PSY05]). As in our model, they use the Rarita-Schwinger formalism for the production of the  $\Delta$  with form factors of Alvarez-Ruso et al. [ARSVV98]. Higher resonances are also included following the formalism of Ref. [BP70]. The nuclear effects are modeled by a "random walk" of the pion through the nucleus undergoing multiple scattering, absorption and charge exchange. Also Pauli blocking is included in the pion production process. There are several simplifying assumptions made in this model, most important among them are the neglect of Fermi motion and nucleon recoil effects and the assumption that the cross sections are not modified inside the nucleus. Furthermore, in contrast to our model, excited resonances decay immediately or are absorbed, but not transported.

Even though the literature is rich on neutrino induced  $\Delta$  production on free nucleons, there is only very little discussion about the production on nuclei. We already mentioned works of Paschos et al., furthermore we shall add Oset and Singh [SVVO98, SAA05]. They modify the  $\Delta$  propagator to account for in-medium effects and also use a modified decay width due to Pauli blocking. The cross section is then calculated using a local

density approximation. For the nuclear density either a Gaussian or a Fermi distribution is applied. Absorption is included by using an eikonal approximation.

For inclusive neutrino quasielastic scattering on nuclei there are innumerable publications. We shall not review them here but refer the reader to an up-to-date overview in Ref. [M<sup>+</sup>05].

Our model, with a well tested transport approach, uses a more realistic initialization for the nucleus than the Monte Carlo generators mentioned above by applying a density dependent Woods-Saxon distribution and local Fermi momentum. We systematically take into account all hadronic potentials. Our treatment of resonances differs also from the above models: We not only use in-medium widths but also propagate resonances off-shell. This is an important feature of our approach missing in the other models. The inclusion of a large variety of possible final state interactions - we only mentioned the most important ones - is a noteworthy enhancement compared to other approaches. We emphasize that the BUU model has been extensively and successfully tested against experimental data for  $\gamma A$  and  $eA$  reactions which provided a check in particular for the final state interactions. This experimental cross-check has not been done for all of the mentioned Monte Carlo codes.

But not only the BUU part differs from the above approaches: We seamlessly included the two most important contributions at neutrinos energies of about 1 GeV, namely quasielastic scattering and  $\Delta$  production. For that we used, in contrast to the models applying the Rein-Sehgal model, a state-of-the-art formalism for the vacuum cross sections with more realistic form factors. Furthermore, our model is quite general. In contrast to the Monte Carlo codes above, we can do calculations for arbitrary nuclei apart from Oxygen. As well we included charged and neutral current interactions for all neutrino flavors.

Finally we note that other models calculate integrated cross sections while we calculate double differential cross sections. The latter are physically far more interesting, as they are more exclusive as we will see in the next chapter. We paid for those with a costly numerics. We did our time-consuming calculations on a grid with a fixed binning for the three kinematical quantities  $E_\nu$ ,  $E_l$  and  $Q^2$  not yet close enough for a numerical integration. To compare with the old bubble chamber experiments we use a simplified model for charged current quasielastic scattering which neglects the potentials (cf. chapter 9). This reduces the numerical complexity and therefore calculations of integrated cross sections can be done easily. However, we emphasize that the proposed experiments MINER $\nu$ A and FINeSSE plan to measure the double differential cross sections.

## 8 Results for Neutrino Nucleus Scattering

Motivated by the proposed experiments, we have studied, as representative examples the reaction  $\nu_\mu {}^{56}\text{Fe} \rightarrow \mu^- X$  for neutrino energies of 0.4 - 2.0 GeV and various values of  $Q^2$  and  $E_\mu$ . Iron is one of the first targets MINER $\nu$ A is going to use [MINER $\nu$ A04a].

For the measurement of the inclusive cross section only the final state lepton is detected. In neutrino experiments, the detection of the outgoing hadrons is crucial in order to discriminate quasielastic and inelastic events. Inelastic events as pion production through  $\Delta$  excitation are identified as quasielastic if the final state pion is absorbed in the nucleus. Within our transport model we can study those charge exchange and side-feeding effects.

In this chapter we discuss the inclusive cross section and its sensitivity to the in-medium modifications introduced in the previous chapter for quasielastic scattering and  $\Delta$  production. Then we investigate one pion production and nucleon knockout. Note that all cross sections presented in this chapter are per nucleon.

### 8.1 Inclusive Cross Section

#### 8.1.1 Quasielastic Contribution

In Fig. 8.1 we show the quasielastic inclusive cross section as a function of  $E_\nu$  for fixed values of  $Q^2$  and  $E_\mu$ . Neglecting the potentials, Fermi motion and Pauli blocking, the differential cross section is a  $\delta$  function in  $E_\nu$  (cf. chapter 7.2) whose position is marked by an arrow in Fig. 8.1. This position follows from Eq. (7.26) with  $M' = M$

$$s = (p + q)^2 = M^2 - Q^2 + 2E_q M \equiv M^2, \quad (8.1)$$

which yields

$$E_q = \frac{Q^2}{2M}. \quad (8.2)$$

Thus, quasielastic scattering is possible for the following neutrino energy:

$$E_\nu = \frac{Q^2}{2M} + E_\mu. \quad (8.3)$$

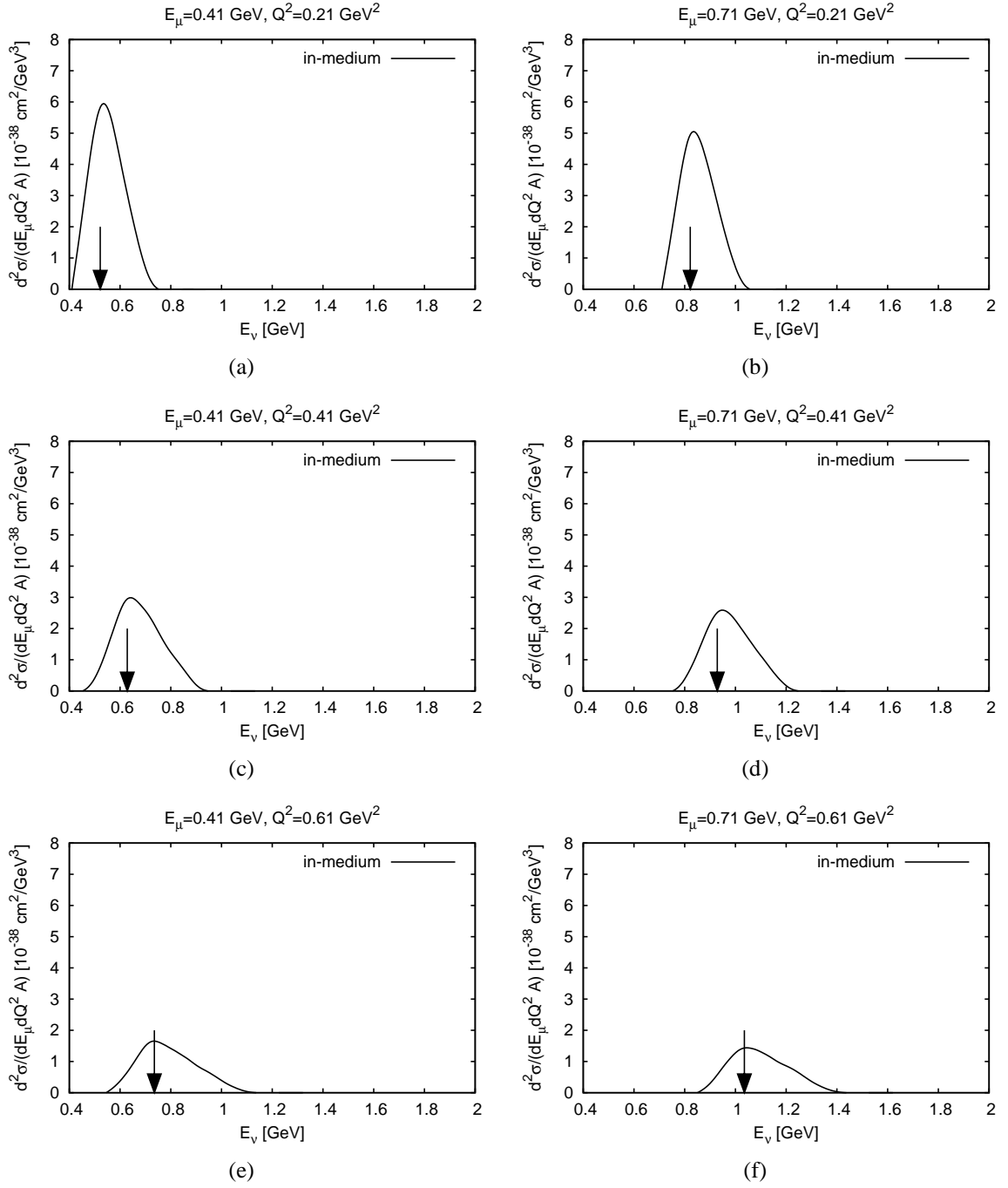


Figure 8.1: Quasielastic inclusive cross section for various muon energies and momentum transfers. The arrows denote the position of the  $\delta$ -like result in the case of the medium modifications "switched off", cf. text.

With increasing  $Q^2$  and  $E_\mu$ , also  $E_\nu$  increases simply due to this relation - because only for a certain combination, namely the one given in Eq. (8.3), quasielastic scattering can occur; all other combinations are forbidden according to Eq. (7.40).

Now we "switch on" the potentials, Fermi motion and Pauli blocking, denoted as "in-medium" in Fig. 8.1. It turns out that Pauli blocking is not important for  $Q^2 > 0.2 \text{ GeV}^2$  (cf. chapter 9). In all cases we find that quasielastic scattering is now possible for a range of values of  $E_\nu$  with  $Q^2$  and  $E_\mu$  fixed. Basically, the shape of the peak is determined by  $Q^2$ . This can be understood from Eq. (7.35):

$$s = M_{eff}^2 - Q^2 + 2E_q E - 2\vec{p} \cdot \vec{q} \equiv M_{eff}'^2, \quad (8.4)$$

with  $M_{eff}'^2 = M + U'_S$  and the Fermi momentum  $\vec{p}$ . For a given set of  $Q^2$  and  $E_\mu$  this equation can be fulfilled for a continuous set of values of  $E_q$  peaking around the on-shell position of Eq. (8.2). With increasing  $Q^2$  also the number of possible values of  $E_q$  increase. This yields via

$$E_\nu = E_q + E_\mu \quad (8.5)$$

to a broad range of possible  $E_\nu$ . Thus, increasing  $E_\mu$  leads to a peak movement to higher neutrino energies.

To conclude, the broadened peak is a direct consequence from the fact that the nucleons are not at rest in the nucleus but have a Fermi momentum.

### 8.1.2 $\Delta$ Resonance Contribution

In Fig. 8.2 we show the  $\Delta^{++}$  inclusive cross section for various muon energies and momentum transfers as a function of the neutrino energy. "Elementary" denotes the calculation without in-medium modifications, thus this reproduces the cross section on a free nucleon. The position of the peak is given by Eq. (7.26) with  $M' = M_\Delta$

$$s = (p + q)^2 = M^2 - Q^2 + 2E_q M \equiv M_\Delta^2, \quad (8.6)$$

where  $M_\Delta = 1.232 \text{ GeV}$  is the pole mass. This yields for the neutrino energy, using  $E_\nu = E_q + E_\mu$ ,

$$E_\nu = \frac{Q^2 - M^2 + M_\Delta^2 + 2ME_\mu}{2M}, \quad (8.7)$$

and, thus, explains the movement of the peak with increasing  $Q^2$  and  $E_\mu$  to higher values of  $E_\nu$ . The shape of the peak, in particular the decrease for increasing  $Q^2$ , reflects the behavior of the free nucleon cross section and we refer back to chapter 5.4.

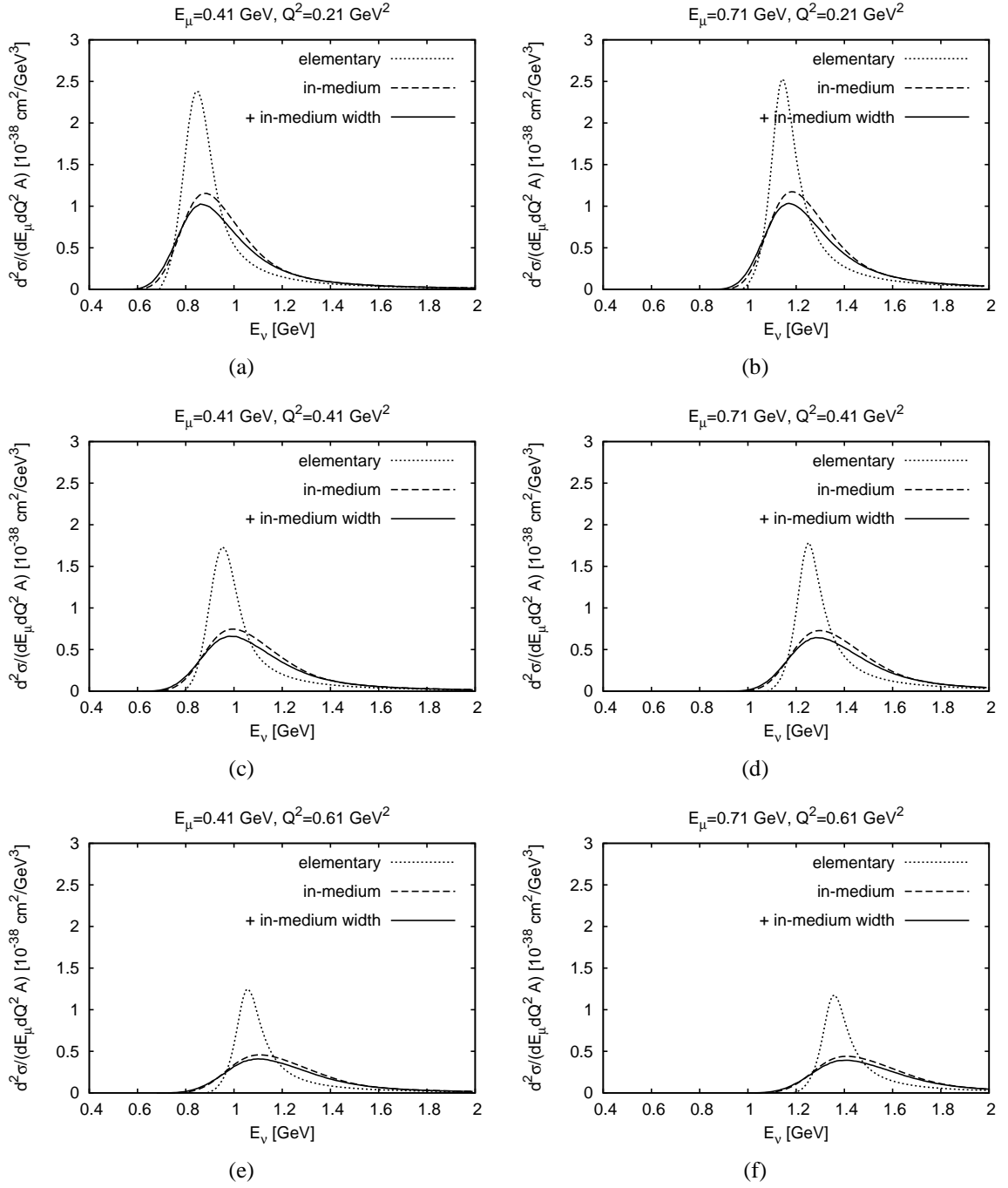


Figure 8.2: Medium modifications of the  $\Delta^{++}$  inclusive cross section for various muon energies and momentum transfers.



Next we consider the effects of Fermi motion, Pauli blocking and the hadronic potentials. The result is labeled in Fig. 8.2 as "in-medium". Fermi motion, the most dominant process among them, lowers and broadens the peak, for the same arguments as in the previous section. We conclude that with increasing  $Q^2$  the  $\Delta$  peak becomes less pronounced.

We further take into account the in-medium modification of the width of the  $\Delta$  resonance, labeled in Fig. 8.2 as "+ in-medium width". The vacuum width is replaced by a sum of the vacuum width modified due to Pauli blocking and a collisional width accounting for additional channels in the medium, as discussed in Eq. (7.18). For the collisional width we use the parametrization of Oset and Salcedo [OS87]. Since the cross section scales with the inverse of the width this lowers and broadens the peak slightly.

We infer that the in-medium modifications reduce the cross section in the peak region by more than a factor of two, mainly due to the Fermi motion; the effect of the in-medium width is less important.

### 8.1.3 Inclusive Double Differential Cross Section

In Fig. 8.3 we show the inclusive double differential cross section as a function of  $E_\nu$  and  $Q^2$  for two values of  $E_\mu$  as indicated in the figure. These plots combine the two contributions discussed in the previous sections.

For  $Q^2 < 0.4$  GeV two peaks can be distinguished. The one at lower  $E_\nu$  corresponds to quasielastic events, whereas the one at higher  $E_\nu$  results from  $\Delta$  production. For higher  $Q^2$  the structure of a well separated quasielastic and  $\Delta$  peak is smeared out totally. In the previous sections we discussed the broadening and the decrease of the single peaks with increasing  $Q^2$  for both quasielastic scattering and the  $\Delta$  production. Plotting both together shows, that the broadening leads to an overlap and that, with increasing  $Q^2$ , the distinct peak structure vanishes and the inclusive cross section tends to zero.

Comparing the upper and the lower plot reveals a shift of the curves, in the lower plot the minimal neutrino energy is higher than in the upper plot. This is simply due to energy conservation. Assuming  $Q^2 \rightarrow 0$ , a certain neutrino energy is already required only for the production of a massive muon with energy  $E_\mu$  (cf. chapter B.2). This minimal neutrino energy increases when energy is transferred to the hadronic system, i. e. with increasing momentum transfer  $Q^2$ .

Those cross sections can be obtained with an experiment which measures the energy and the scattering angle of the outgoing lepton. As of today, these measurements are not available, but the experiments are already proposed.

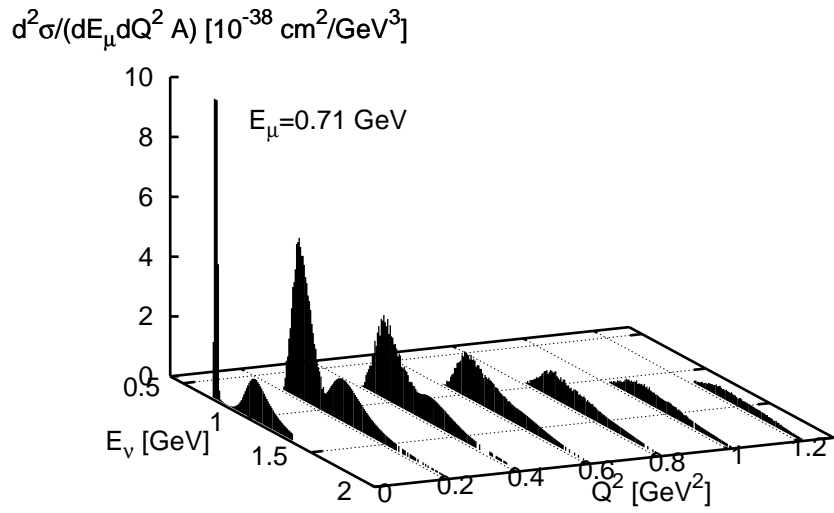
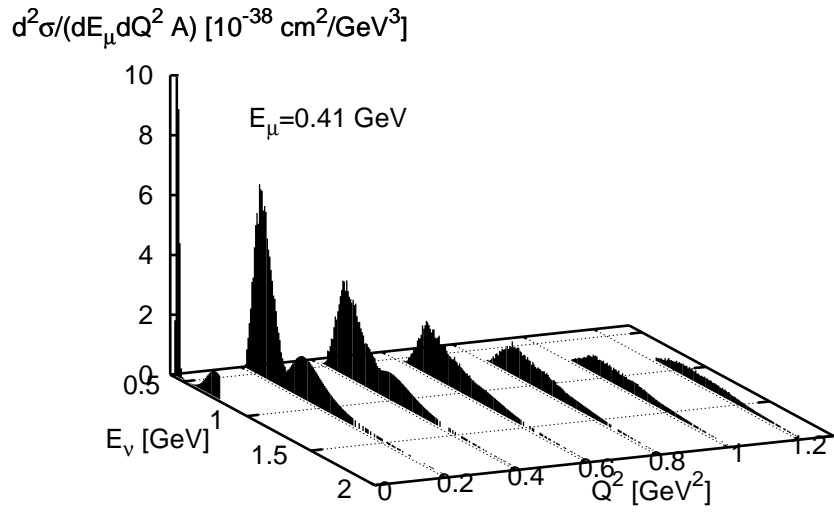


Figure 8.3:  $\nu_\mu A \rightarrow \mu^- X$  cross section on  $^{56}\text{Fe}$ .

## 8.2 Pion Production

### 8.2.1 One Pion Production Cross Section

We start our discussion of pion production with the double differential cross section for one pion production integrated over the pion momenta. In Fig. 8.4 we show the exclusive cross section for neutrino induced  $\pi^+$  production as a function of the neutrino energy for various values of  $E_\mu$  and  $Q^2$ . The dotted line represents a calculation where we included the potentials, Fermi motion and Pauli blocking, but used the vacuum width for the  $\Delta$  production. In this calculation all final state interactions are suppressed, except for resonance decay, which still might be Pauli blocked. For the calculation shown by the long-dashed line we used the in-medium modified width but still without final state interactions. Those are "switched on" in the calculation represented by the solid line.

A possible origin for pions is not only through the initial  $\Delta$ , but also through quasielastic scattering. In panel (e) and (f) also the origin of the pion is indicated - "Δ" denotes pions stemming from the initial  $\Delta$  production, "QE" labels the pions which are produced in final state interactions of the initially produced nucleon. There the nucleon rescatters in the nucleus, and can produce pions through  $NN \rightarrow N\Delta$  and  $NN \rightarrow NN\pi$ . However, we found that this effect, being only possible with high momentum transfer  $Q^2$ , is negligible.

The influence of final state interactions on the pion can be seen by comparing the long-dashed with the solid line. Roughly half of the originally produced pions do not survive the final state interactions depending on the given kinematics. This is due to absorption through  $\pi N \rightarrow \Delta$ ,  $NN\pi \rightarrow NN$  or charge exchange through  $\pi N \rightarrow \pi N$ .

In Fig. 8.5 we show the equivalent plot for  $\pi^0$  - the lines are as explained above. Notice that the cross sections for  $\pi^0$  is about a factor of five lower. This reduction is a consequence of the production process itself:

$$\nu p \rightarrow l^- \Delta^{++}, \quad (8.8)$$

$$\nu n \rightarrow l^- \Delta^+. \quad (8.9)$$

The first process is enhanced by an isopin factor of three. Those  $\Delta$  decay into pions via

$$\Delta^{++} \rightarrow p\pi^+, \quad (8.10)$$

$$\Delta^+ \rightarrow p\pi^0, \quad (8.11)$$

$$\Delta^+ \rightarrow n\pi^+. \quad (8.12)$$

In chapter 6.1 we discussed the isospin amplitudes of those processes. With them we obtain a ratio of  $\pi^+ : \pi^0 = 4.4 : 1$  for the cross sections without final state interactions. Taken into account are the proton and neutron numbers of Iron. Also for  $\pi^0$  production

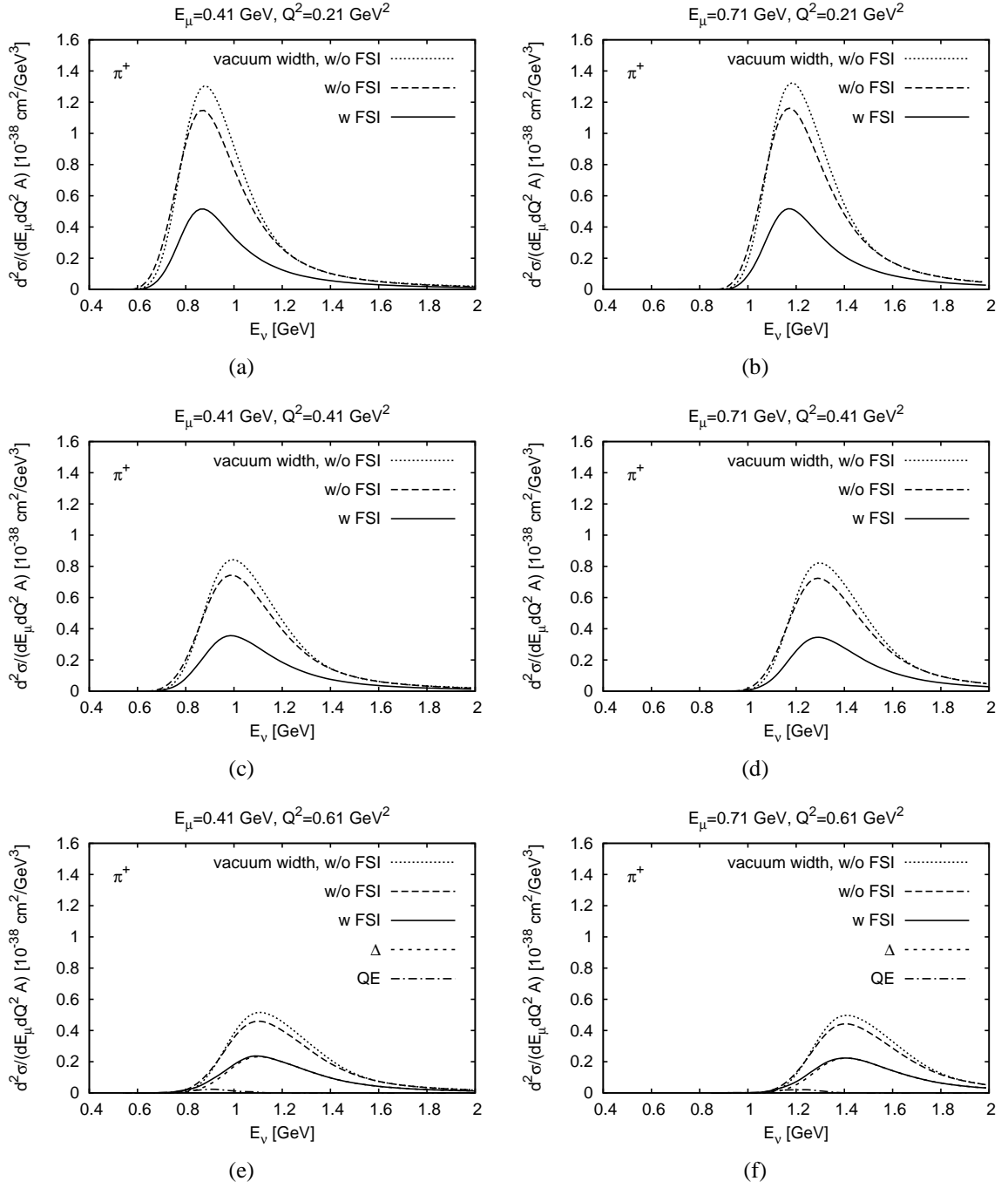


Figure 8.4: Influence of final state interactions on  $\nu_\mu {}^{56}\text{Fe} \rightarrow \mu^- \pi^+ X$ . The different lines are explained in the text.

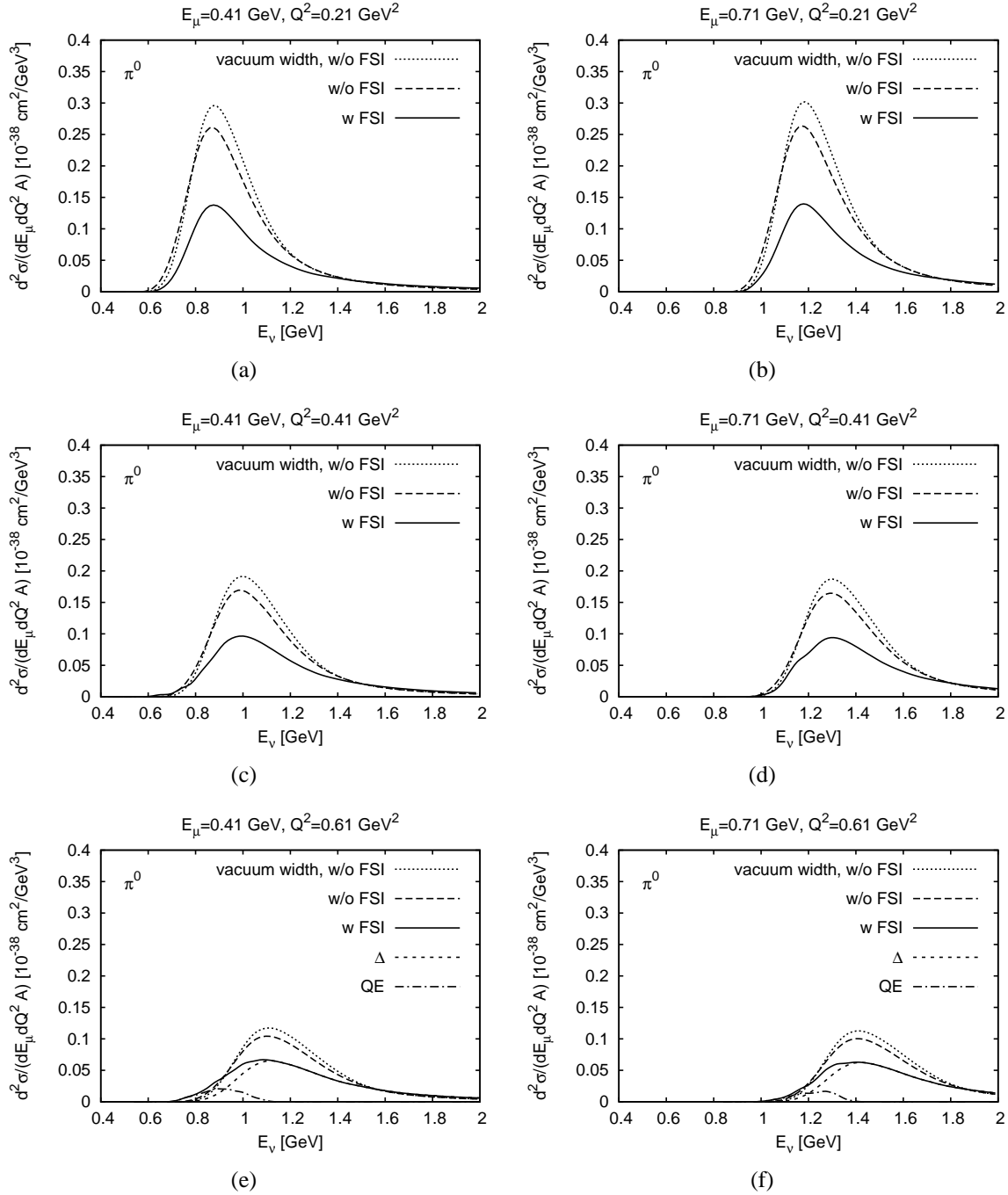


Figure 8.5: Influence of final state interactions on  $\nu_\mu {}^{56}\text{Fe} \rightarrow \mu^- \pi^0 X$ . The different lines are explained in the text.

we found that pion production through quasielastic scattering is negligible (cf. Fig. 8.5 (e) and (f)), even though more important than in the  $\pi^+$  channel. This follows from the fact that the production of both  $\pi^0$  and  $\pi^+$  from initial quasielastic scattering is basically the same while the ratio of the ones from initially produced  $\Delta$  resonances is about a factor of five as just outlined.

$\pi^-$  cannot be produced directly in the neutrino nucleon reactions, only via final state interactions. In Fig. 8.6 we show the exclusive cross section for neutrino induced  $\pi^+$ ,  $\pi^0$  and  $\pi^-$  production as a function of the neutrino energy for various values of  $E_\mu$  and  $Q^2$ . This plot was obtained with a full calculation including the in-medium modified width and final state interactions. We already commented on the strong difference between  $\pi^+$  and  $\pi^0$ .  $\pi^-$  plays only a minor role. Note that this situation is reversed in antineutrino reactions when only  $\Delta^-$  and  $\Delta^0$  can be produced in the initial interaction.

## 8.2.2 Pion Momentum Distribution

For a better understanding of the pion production cross sections in the medium we now study the pion momentum distributions. In Fig. 8.7 we show the momentum differential cross section for  $\pi^+$  and in Fig. 8.8 for  $\pi^0$  versus the pion momentum for different values of  $E_\mu$  and  $Q^2$ . The neutrino energy is fixed at 1.2 GeV. The dashed line shows the calculation without final state interactions, the solid line denotes the full calculation. Apparently, the spectra are very sensitive to the choice of  $E_\mu$  and  $Q^2$  and also of  $E_\nu$ .

The maximal value of the pion momentum  $p_\pi$  is determined by the muon energy  $E_\mu$  as a consequence of energy-momentum conservation. We shall now compare the momentum distributions of the  $\pi^+$  and  $\pi^0$ , where the momentum differential cross section is plotted for a choice of  $E_\mu$  leading to a relatively wide interval of allowed pion momenta (left plots). The right plots show the equivalent but with another choice of  $E_\mu$  leading to a rather narrow interval of allowed pion momenta.

The maximum of the solid curve (i. e. the calculation with final state interactions) peaks at 0.15 - 0.2 GeV in all plots shown in Fig. 8.7 and in Fig. 8.8. This is due to the energy dependence of the pion absorption: The absorption is small for those pions. Low momentum pions are mainly absorbed through  $\pi NN \rightarrow NN$ . The higher energetic pions (cf. the dashed curve in both figures) are mainly absorbed through the reaction  $\pi N \rightarrow \Delta$ , followed by  $\Delta N \rightarrow NN$ . This strong reduction for high momentum pions can be seen by comparing the dashed and the solid lines. Those absorption processes equally influence  $\pi^+$  and  $\pi^0$ .

But the pions do not only undergo absorption when propagating through the nucleus. Of particular importance is elastic scattering  $\pi N \rightarrow \pi N$  for pions of all energies. This leads to charge exchange and redistributes the momenta.

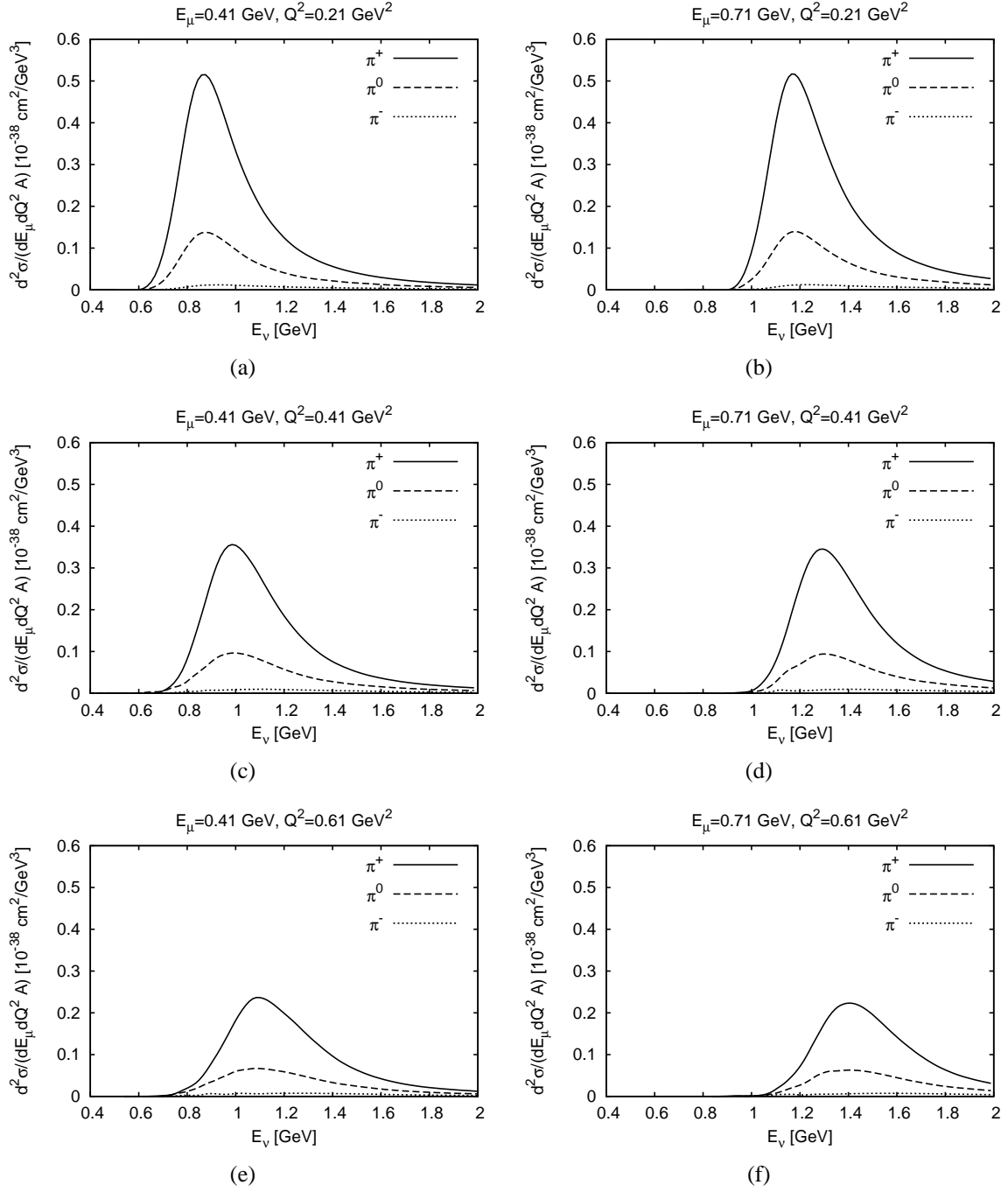


Figure 8.6: Exclusive cross section for neutrino induced  $\pi^+$ ,  $\pi^0$  and  $\pi^-$  production.

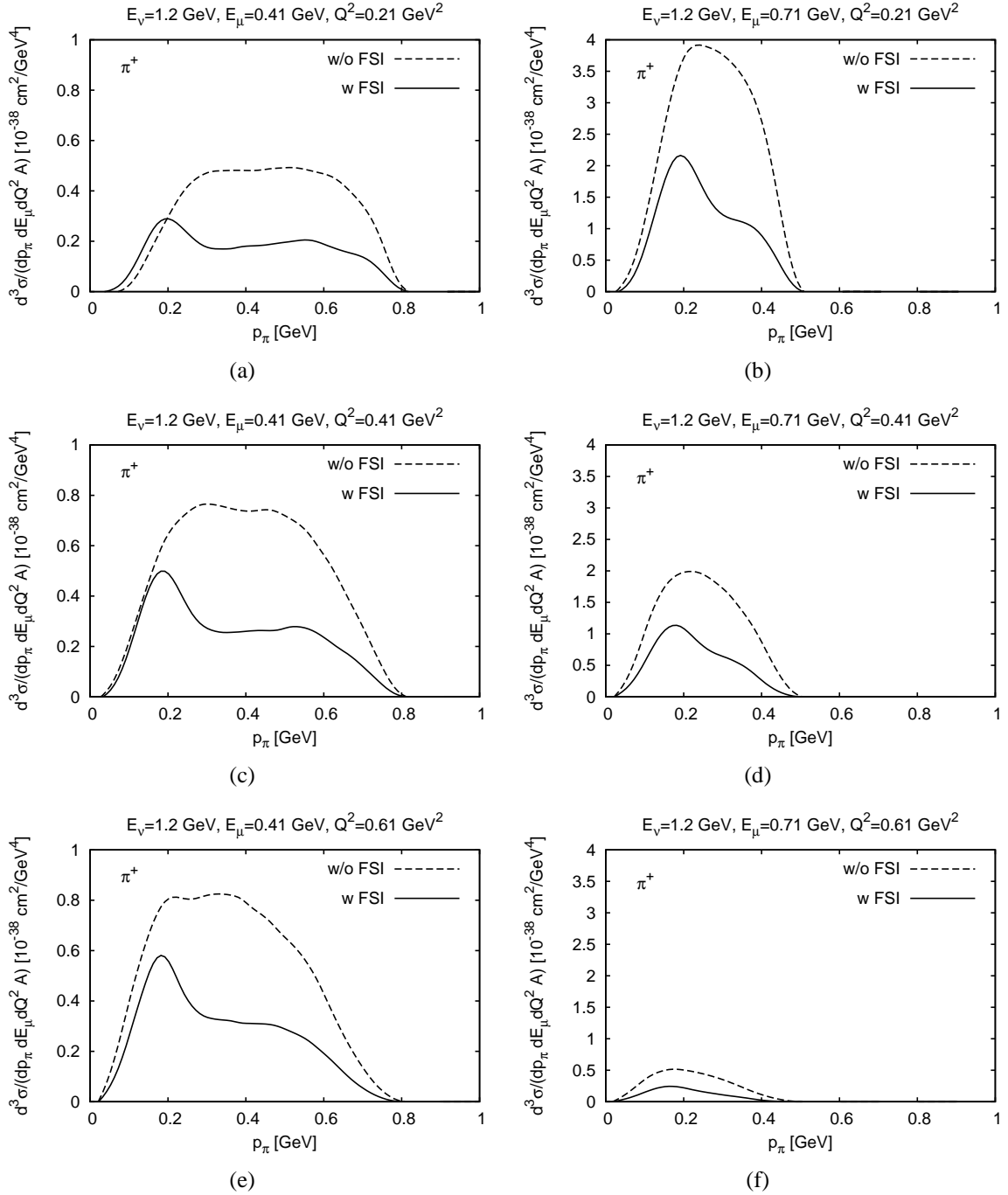


Figure 8.7: Momentum differential cross section for  $\pi^+$  at  $E_\nu = 1.2 \text{ GeV}$ . Note the different scales.



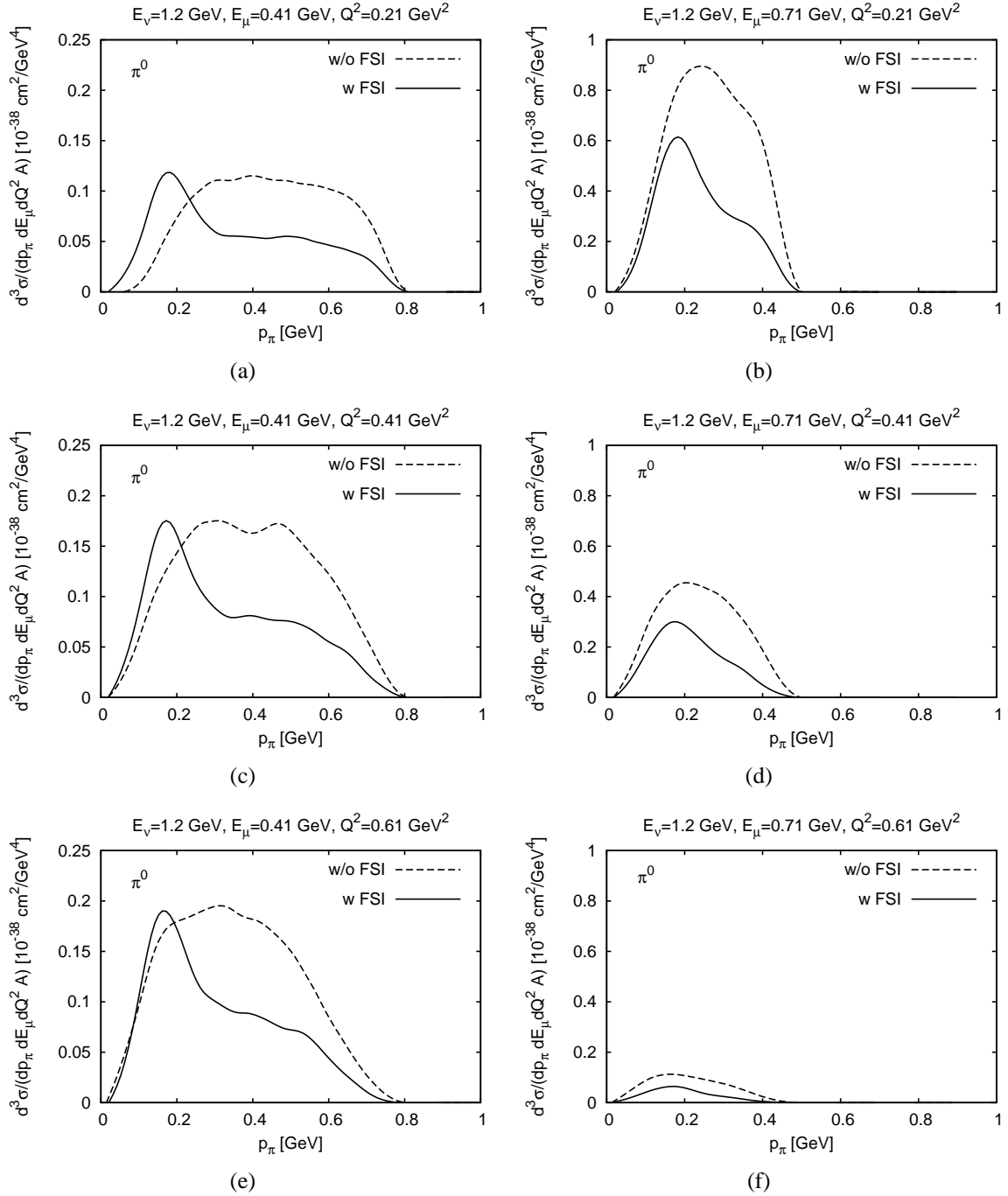


Figure 8.8: Momentum differential cross section for  $\pi^0$  at  $E_\nu = 1.2$  GeV. Note the different scales.

For  $\pi^+$  in Fig. 8.7 the discussed effects reduce the cross section significantly by about a factor of two compared to the calculation without final state interactions for both muon energies.

Considering the  $\pi^0$  channel in Fig. 8.8 reveals some differences to the  $\pi^+$  channel. The general reduction of a factor of 5 was discussed in the previous chapter. However, in the peak region, the deviation between the calculation including final state interactions and the one neglecting final state interactions differs from the  $\pi^+$  calculation. For  $E_\mu = 0.71$  GeV the reduction is less compared to Fig. 8.7, for  $E_\mu = 0.41$  GeV we even get an enhancement of  $\pi^0$  at low momentum compared to the calculation without final state interactions. Those additional contributions are a consequence of their "disappearance" in the  $\pi^+$  channel:  $\pi^+$  undergoing reactions like  $\pi N \rightarrow \pi N$  are likely to contribute to the  $\pi^0$  channel leading to the observed side-feeding. The effect is more significant for the kinematical choice which leads to a wide interval of pion momenta, since higher momentum  $\pi^+$  can also contribute to the  $\pi^0$  channel through  $\pi N \rightarrow \Delta$  followed by  $\Delta \rightarrow \pi N$ . Note that the other way round is strongly suppressed by the ratio of  $\pi^+$  to  $\pi^0$  production on the nucleon.

### 8.3 Nucleon Knockout

The channel under investigation now is nucleon knockout, i. e. nucleons leaving the nucleus due to the reaction. Note that we only include events where the nucleons' kinetic energy is larger than 0.1 GeV. In Fig. 8.9 we plot the exclusive proton cross section as a function of the neutrino energy for various values of  $Q^2$  and  $E_\mu$ . The dash-dotted line shows the calculation without final state interactions, the solid one the calculation with final state interactions. We see that the inclusion of final state interactions reduces the overall cross section. Especially rescattering distributes the kinetic energy among the nucleons, which then do not fulfill the above criterion any more.

For low  $Q^2$  two clearly separated peaks can be seen. The one at lower  $E_\nu$  corresponds to the protons produced in initial quasielastic events (indicated by the dashed line), whereas the one at higher  $E_\nu$  denotes protons from  $\Delta$  production (dotted line). Therefore also the protons are clearly allocatable. This clear separation is lost for higher momentum transfer: We have seen in chapter 8.1 that the inclusive cross section is smeared out with increasing  $Q^2$  due to Fermi motion. The shape of the inclusive cross section is reflected in the exclusive proton production cross section plotted here. As a consequence, the peaks in Fig. 8.9 overlap for higher  $Q^2$  and are not distinguishable any more.

In Fig. 8.10 we show the equivalent plots for neutrons - the different lines are as above. Note first the different scale of the neutron knockout cross section compared to the one for protons in Fig. 8.9. The significant differences in proton and neutron knockout is due

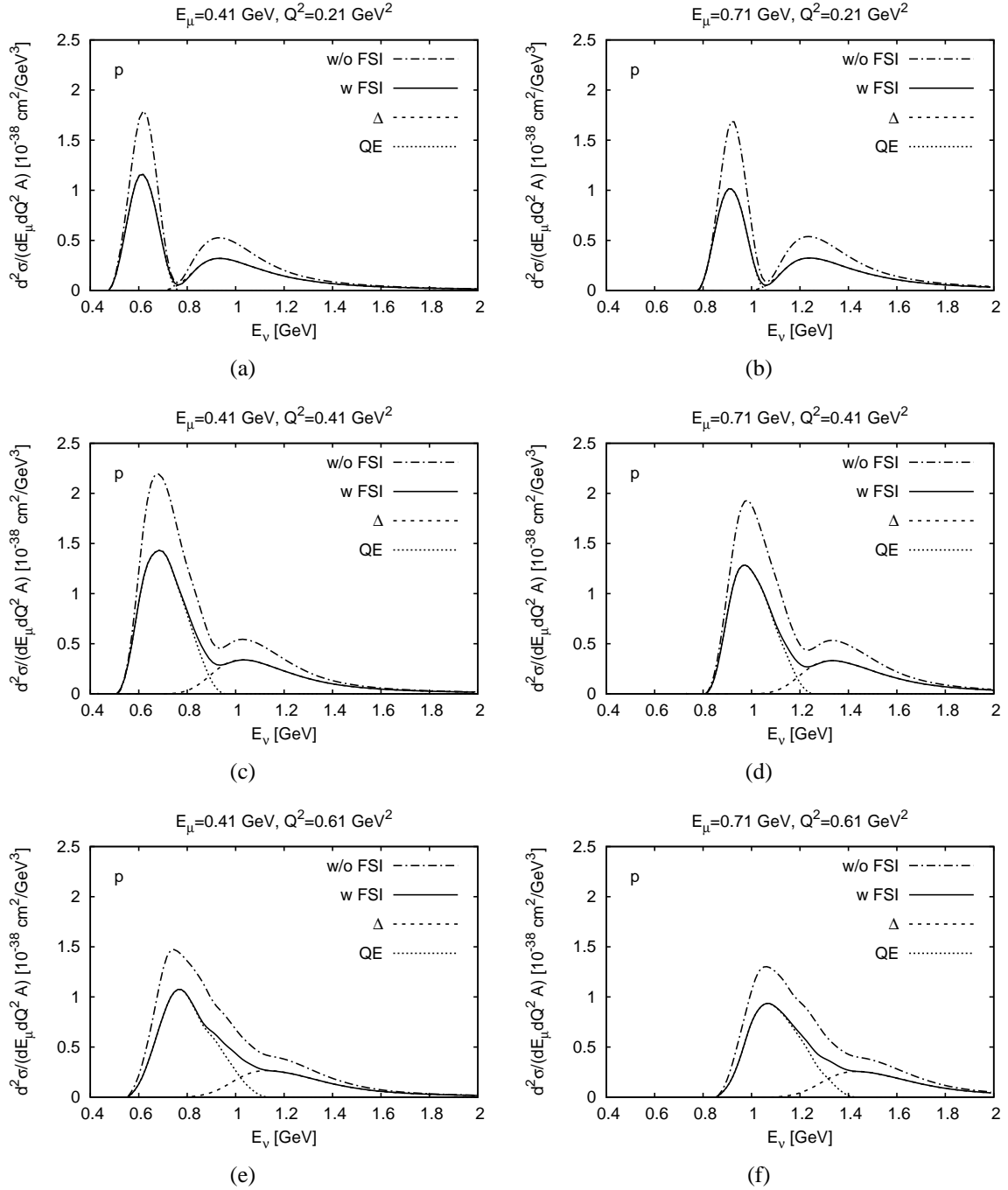


Figure 8.9: Influence of final state interactions on  $\nu_\mu {}^{56}\text{Fe} \rightarrow \mu^- p X$ . The different lines are explained in the text.

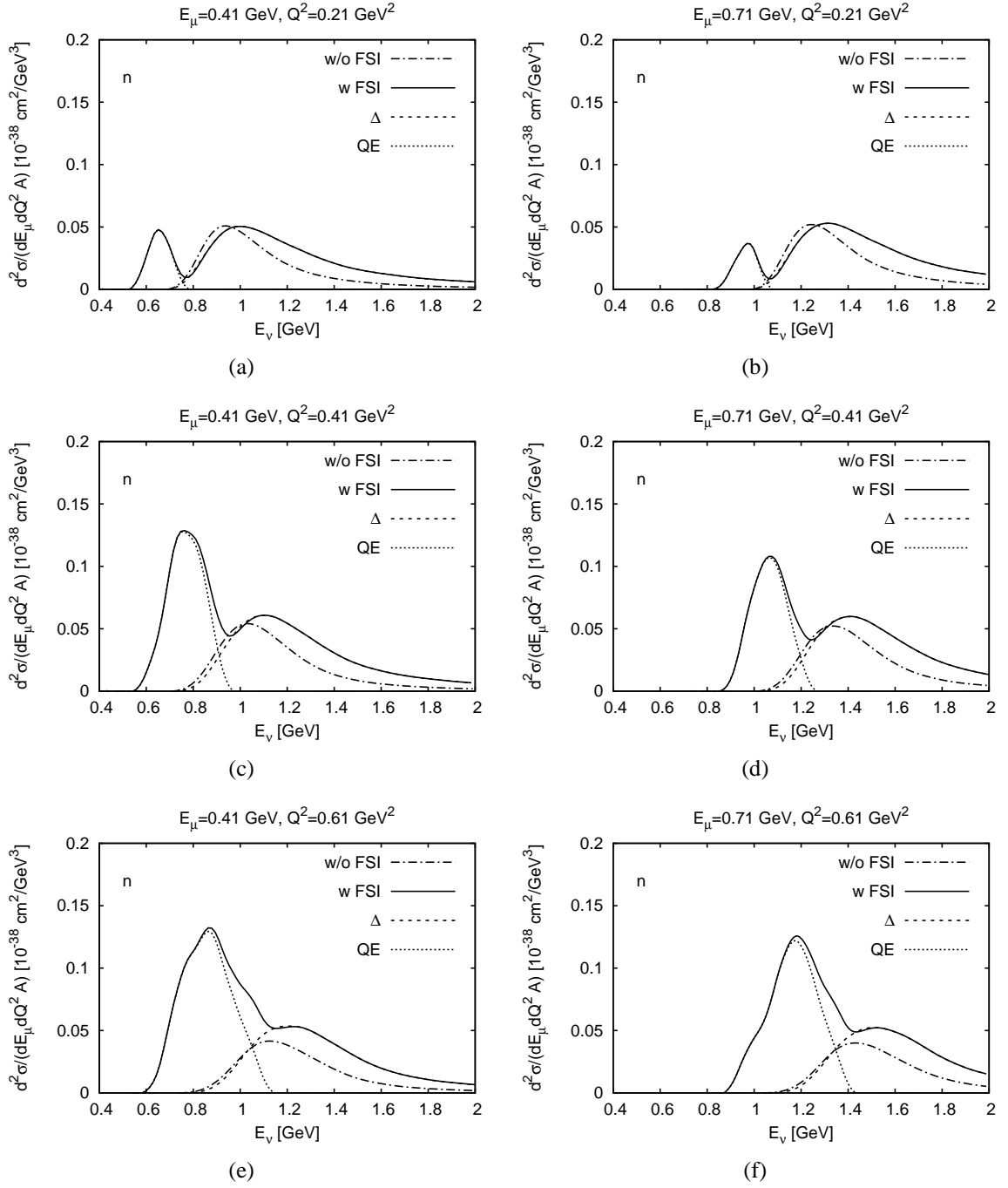


Figure 8.10: Influence of final state interactions on  $\nu_\mu {}^{56}\text{Fe} \rightarrow \mu^- n X$ . The different lines are explained in the text.

to the initial neutrino nucleon production process: Quasielastic scattering produces only protons via

$$\nu n \rightarrow l^- p. \quad (8.13)$$

Also the  $\Delta$  production mechanism favors protons

$$\nu p \rightarrow l^- \Delta^{++} \rightarrow l^- p \pi^+, \quad (8.14)$$

$$\nu n \rightarrow l^- \Delta^+ \rightarrow l^- p \pi^0, \quad (8.15)$$

$$\nu n \rightarrow l^- \Delta^+ \rightarrow l^- n \pi^+, \quad (8.16)$$

since the first process is enhanced by a factor of three. Using the isospin amplitudes of chapter 6.1 we obtain a ratio of  $p : n = 9.5 : 1$  in the  $\Delta$  region for Iron.

Therefore, in the calculation without final state interaction, proton and neutron knockout differ by roughly a factor of ten in the  $\Delta$  region. Note that no neutrons are produced in the initial quasielastic interactions.

If we now "switch on" the final state interactions, this scenario changes. Comparing the dash-dotted line (without FSI) in Fig. 8.10 with the solid line (with FSI) shows that additional neutrons are produced in the final state interactions. We first discuss the neutron production through FSI in the quasielastic peak region. The initial neutrino nucleon quasielastic reaction produces only protons. Those protons can undergo elastic and inelastic nucleon-nucleon collisions which lead to charge exchange, and thus, produce neutrons. In the region of the  $\Delta$  (this corresponds to the right peaks), we initially produce ten times more protons than neutrons. Through final state interactions these protons also yield a side-feeding of the neutron channel. Since this is more likely for higher energy protons, we find the enhancement of the neutron cross section in the higher energy tail.

We conclude that final state interactions reduce the number of protons, but enhance the neutron cross section.

In Fig. 8.11 proton and neutron cross sections are compared directly. Here all final state interactions are included. One again sees the strong difference of proton and neutrons coming from the initial neutrino neutron to proton production ratio, even though this difference is reduced through the inclusion of final state interactions.

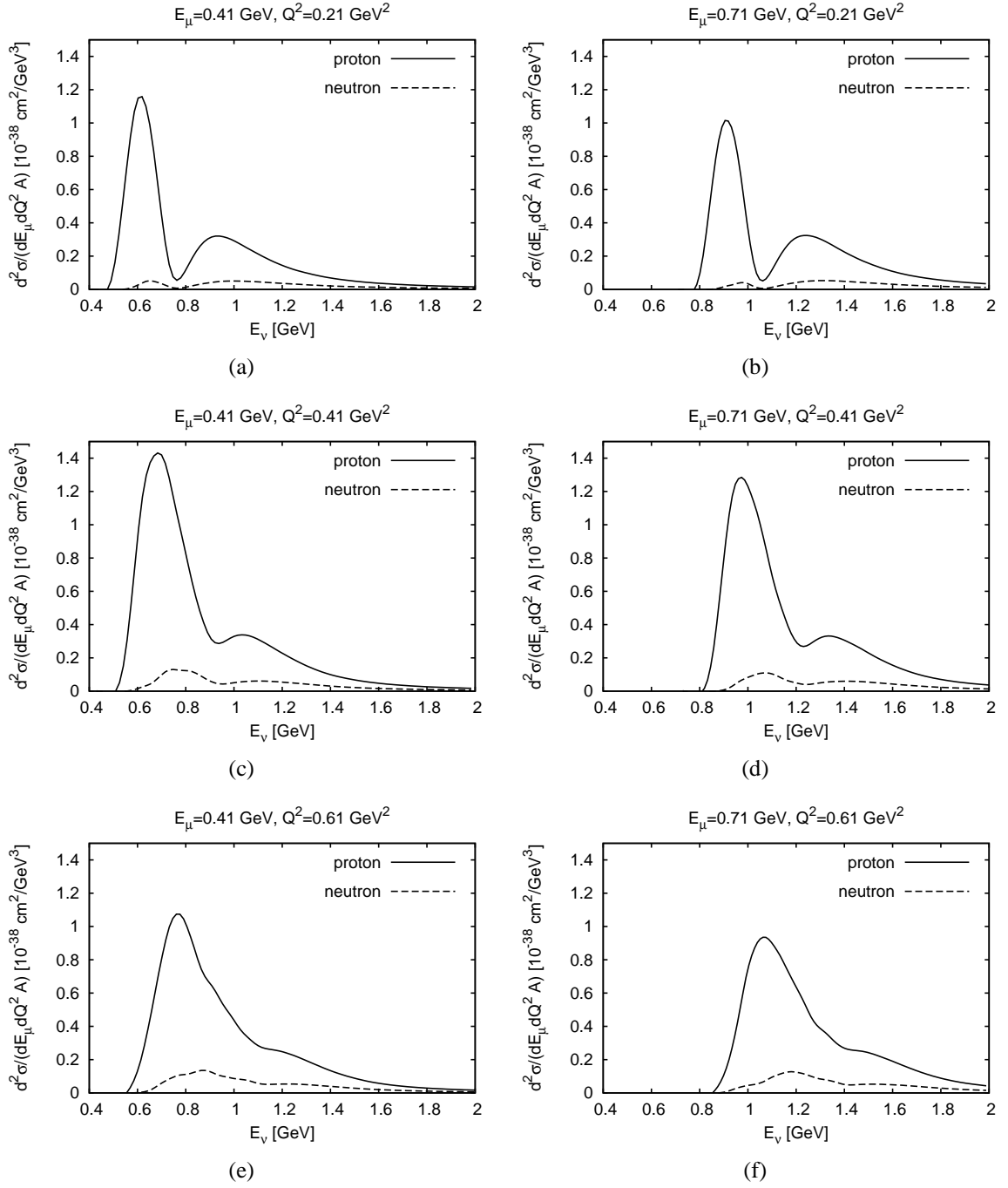


Figure 8.11: Exclusive cross section for  $\nu_\mu {}^{56}\text{Fe} \rightarrow \mu^- pX$  and  $\nu_\mu {}^{56}\text{Fe} \rightarrow \mu^- nX$ . The different lines are explained in the text.

## 9 Simplified Model for Quasielastic Neutrino Nucleus Scattering

Finally, in this chapter we calculate the differential and total inclusive cross section for charged current quasielastic scattering. To do so, we simplify our model in order to reduce the numerical effort. Then the numerical integration is doable. This allows the direct comparison with the old bubble chamber data. We shall first discuss the approximation applied here and then present the obtained results.

### 9.1 Implementation

Neglecting the hadronic potentials simplifies Eq. (7.35) to

$$s = M^2 - Q^2 + 2E_q E - 2\vec{p} \cdot \vec{q} \equiv M^2. \quad (9.1)$$

$\vec{p}$  is known from the initialization within the code (cf. chapter 7.1.1). Then only two independent quantities are sufficient to determine the full kinematics. We choose  $E_\nu$  and  $Q^2$ . Further we assume  $\vec{q} = |\vec{q}|\vec{e}_z$ . The above equation then yields  $E_q$  and therefore the four-vector  $q$ . With that, the system is completely determined: The scattering angle between the neutrino and the charged lepton follows from

$$\cos \theta = -\frac{m_l^2 + Q^2 - 2E_\nu E_l}{2E_\nu \sqrt{E_l^2 - m_l^2}}, \quad (9.2)$$

with  $E_l = E_\nu - E_q$ . This yields for the neutrino four-vector  $k$  [Leh99]

$$k_3 = \frac{\vec{k} \cdot \vec{q}}{|\vec{q}|} = \frac{E_\nu^2 - E_\nu \sqrt{E_l^2 - m_l^2} \cos \theta}{|\vec{q}|}, \quad (9.3)$$

$$k_2 = 0, \quad (9.4)$$

$$k_1 = \sqrt{|\vec{k}|^2 - k_3^2}. \quad (9.5)$$

Finally,  $p'$  simply follows from energy-momentum conservation.

We emphasize again that the third independent kinematical quantity was only required to account for the potentials. Having one degree of freedom less, the numerical effort is significantly reduced. No more simplifications are used compared to our "full" model.

Again, we initialize a neutrino event at every testparticle and after checking for Pauli blocking the cross section is calculated according to

$$\frac{d\sigma_{\nu A \rightarrow l^- X}}{dQ^2} = 4 \int_{\text{Nucleus}} d^3r \int^{p_F} \frac{d^3p}{(2\pi)^3} \frac{d\sigma_{\nu N \rightarrow l^- X}}{dQ^2}. \quad (9.6)$$

Those cross sections are Lorentz transformed from the nucleon rest frame to the rest frame of the nucleus [Eff96]. We multiply the cross section per nucleon with a factor of

$$\frac{A}{A - Z}, \quad (9.7)$$

with  $A$  being the mass number and  $Z$  being the charge of the nucleus, to obtain cross sections per neutron. This choice is motivated by the vacuum quasielastic scattering which is only possible on neutrons

$$\nu_{\mu} n \rightarrow \mu^{-} p, \quad (9.8)$$

and therefore allows a direct observation of in-medium effects since this cancels differences due to the proton-neutron number ratio in different nuclei.

## 9.2 Results

The in-medium charged current quasielastic differential cross section per neutron is plotted in Fig. 9.1 for a reaction of muon neutrinos on Calcium for different neutrino energies. "In-medium" denotes here the calculation including Pauli blocking and Fermi motion with the kinematics as outlined in the previous section. For comparison the vacuum calculation is shown by the dashed line. For low momentum transfers up to about 0.2 GeV the cross section is reduced significantly due to Pauli blocking. In contrast to the previous chapter the effect of Fermi motion is negligible here for the following reason: The observable is the cross section  $d\sigma_{\nu A \rightarrow l^- X}/dQ^2$  which is a function of  $Q^2$  and  $E_{\nu}$ . The expression used for the calculation is given in Eq. (4.12) in the nucleon rest frame. Therefore, we have to Lorentz transform  $E_{\nu}$  into the nucleon rest frame and the obtained result for  $d\sigma_{\nu N \rightarrow l^- X}/dQ^2$  has to be transformed back. Only this Lorentz transformation is influenced by the Fermi motion of the nucleons and not the observable itself as in the previous chapter. The cross section on the nucleus, which follows from Eq. (9.6), is integrated over all momenta, which averages those effects. We conclude that the reduction for low  $Q^2$  is a consequence of Pauli blocking.

Fig. 9.2 shows a comparison between different nuclei. The mass number dependence in the initialization through the density dependent Woods-Saxon distribution and the local Fermi momentum influences the Pauli blocking and thus, is reflected in minor differences



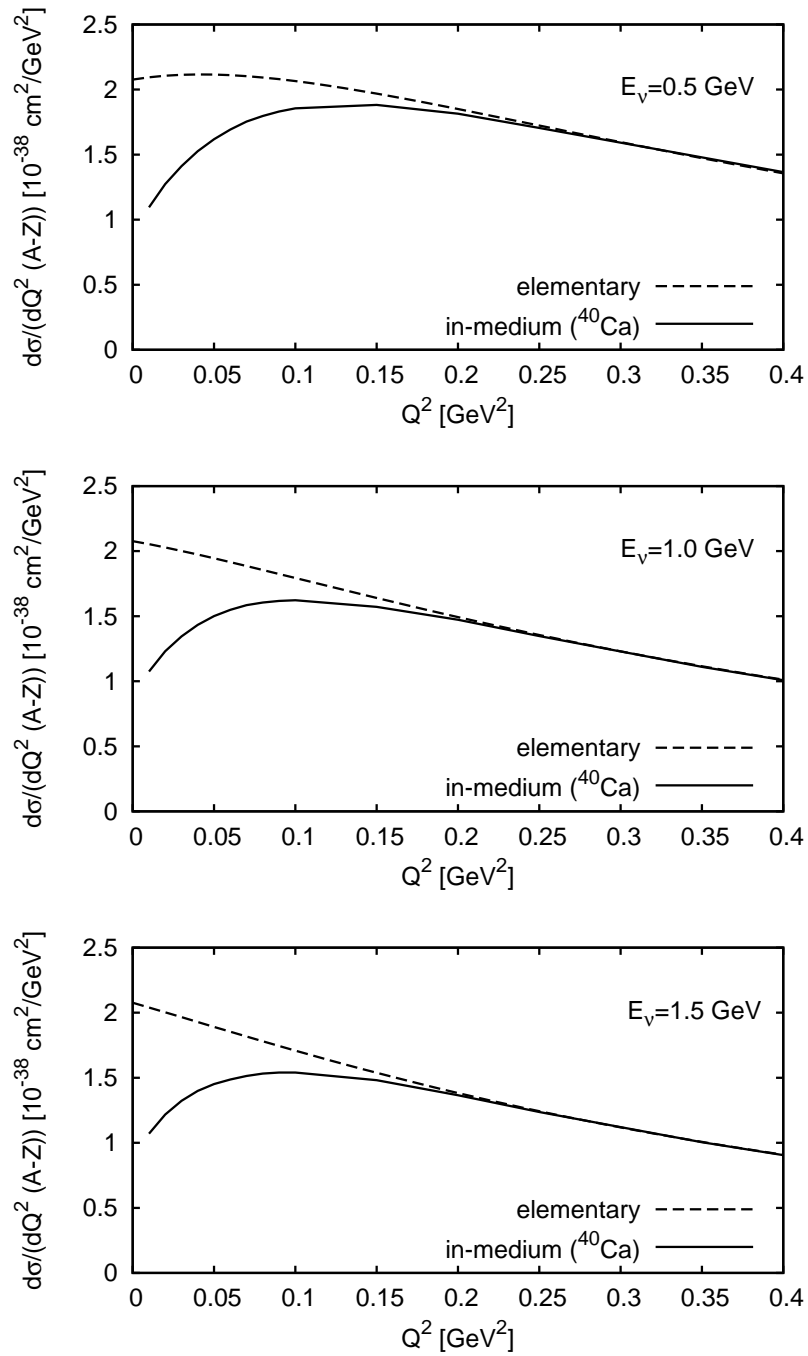


Figure 9.1: In-medium effects on the inclusive quasielastic differential cross section for  $\nu_\mu A \rightarrow \mu^- X$  per neutron.

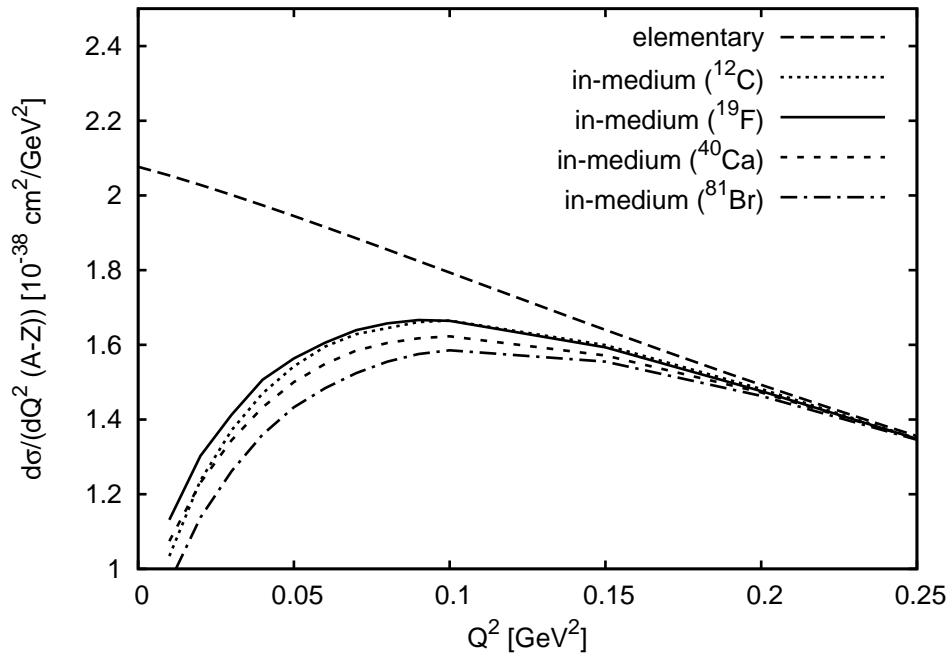


Figure 9.2: In-medium effects on the inclusive quasielastic differential cross section for different nuclei,  $E_\nu = 1.0 \text{ GeV}$ .

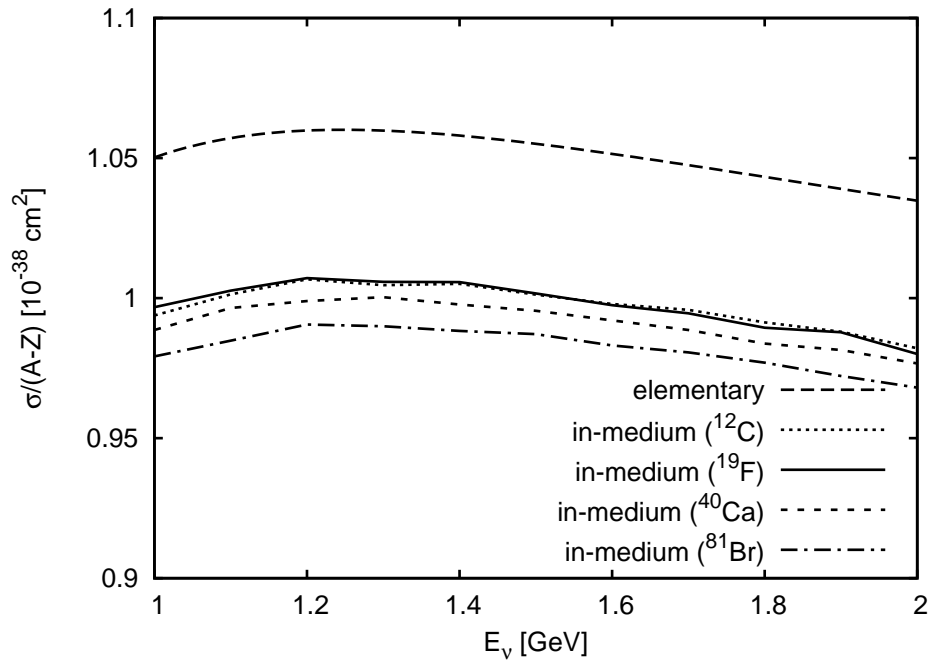


Figure 9.3: In-medium effects on the inclusive quasielastic total cross section for different nuclei.

in the in-medium cross sections. The equivalent plot for the total cross section is shown in Fig. 9.3. The total reduction of the cross section as an effect of Pauli blocking is of the order of about 6 - 7 % slightly depending on the nucleus. For comparison, the long-dashed line shows the elementary cross section.

Finally, in Fig. 9.4 we show the total cross sections for various nuclei together with available data from bubble chamber experiments.

In this simplified framework, our results agree nicely with the experimental data as well as with other calculations e. g. of Bodek et al. [BBA05], Paschos et al. [PY02] and Oset et al. [SO92].

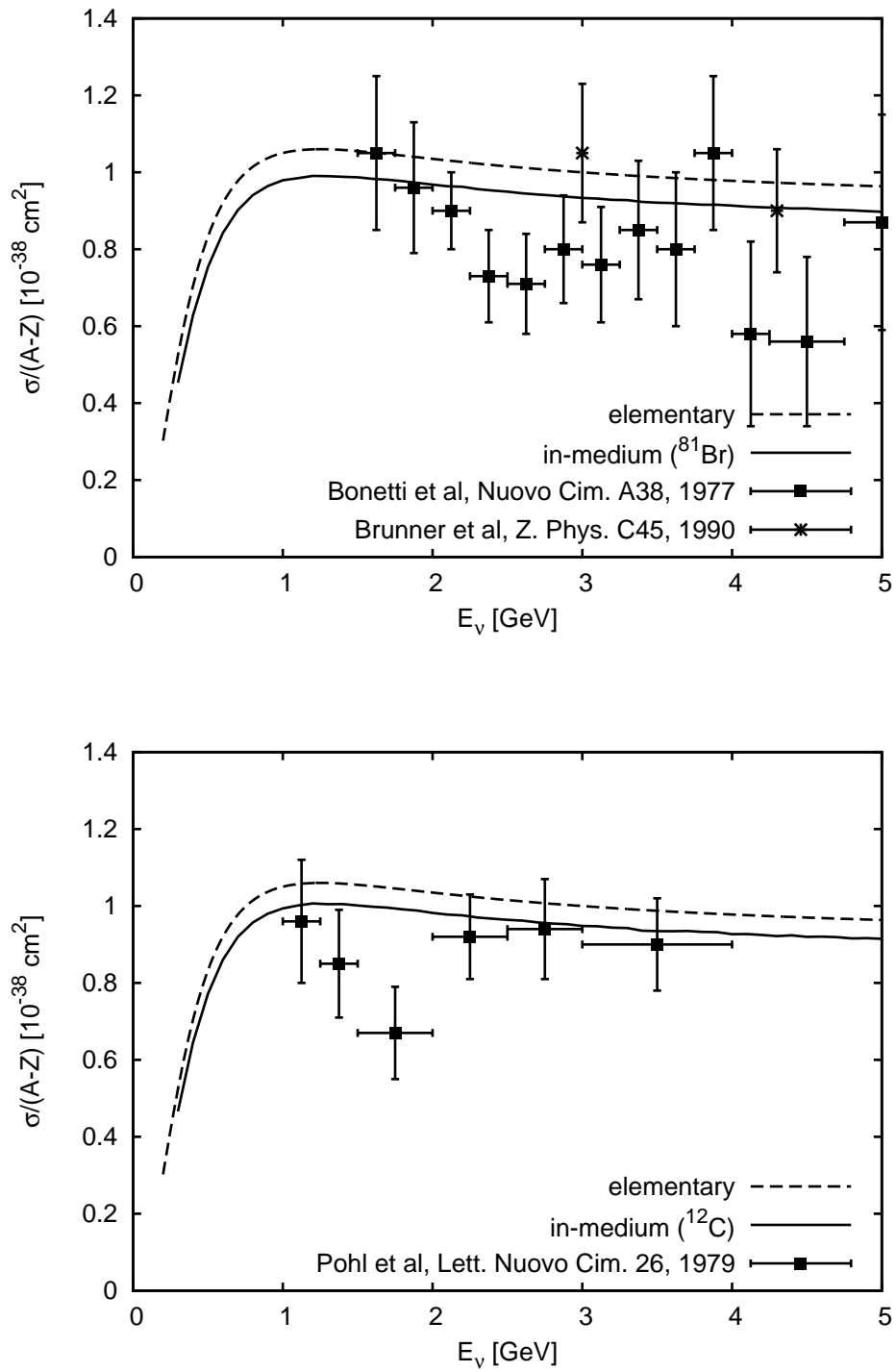


Figure 9.4: In-medium effects on the inclusive quasielastic total cross section.

## 10 Summary and Outlook

In this work we have investigated neutrino interactions with nucleons and nuclei. The model developed in the framework of this thesis should be able to describe neutrino reactions on both nucleons and nuclei at intermediate energies of interest for future neutrino experiments.

The first part of this thesis provided the preliminaries: After a brief review of neutrino physics and related experiments, we have started in chapter 2 with the Standard Model of Particle Physics. Within the Standard Model, neutrinos can interact only weakly by exchanging charged or neutral vector bosons. We discussed the charged and neutral weak currents in detail, pointing out important relations and symmetries needed for further calculations.

In Part II we have discussed neutrino nucleon scattering in detail. In chapter 3 we have calculated the inclusive cross section of neutrino nucleon scattering as a function of five unknown structure functions. This emphasized the need for more explicit models of the hadronic vertex. The decomposition of the neutrino cross section made clear that at intermediate energies mainly two processes contribute, namely quasielastic scattering and  $\Delta$  production. We have discussed the large variety of possible reactions, among them are higher-mass resonances and non-resonant background, and found them to be negligible compared to the two mentioned above.

Charged and neutral current (quasi)elastic scattering have been discussed in detail in chapter 4. We have developed a fully-relativistic formalism to calculate charged and neutral current cross sections in terms of vector and axial form factors. We applied general arguments as CVC to relate the neutrino vector form factors to those obtained from electron scattering and PCAC to relate the axial form factor to the pseudoscalar one, but also to relate the axial form factors of neutral current scattering to those of charged current scattering. We have shown how the form factors have been parametrized in the literature and summarized the current problems. We have found, assuming the strange quark content to be isoscalar, that the purely isovector charged current is insensitive to the strangeness in contrast to the neutral current reaction. Further, we have shown that the same three form factors enter the neutral and the charged current processes but with considerably different qualitative impact. We have seen that, for instance, the proton neutral current form factor  $\bar{F}_1^p$  is strongly suppressed compared to its charged current counterpart  $F_1^V$ . Hence, while the proton neutral current cross section is dominated by a single form factor, namely the

axial form factor, this is not the case for charged current reactions where all form factors contribute.

$\Delta$  production off nucleons has been discussed in chapter 5. We have developed a general formalism for the production of spin  $3/2$  resonances by neutrinos provided that the form factors are available. The calculational techniques were similar to those of quasielastic scattering, we have also applied CVC and PCAC. The vector form factors were taken from electron scattering, for the axial ones we used a parametrization available in the literature. We have found that the contributions of the axial form factors to the cross section are more important than of their vector counterparts. Further, the influence of the  $\Delta$  width on the cross section was studied by using different parametrizations; this changed the cross section by a few per cent. Finally, we have calculated explicit cross sections and found reasonable agreement with other calculations and experimental data.

In Part III of this thesis we have extended our model of neutrino interactions to scattering off nuclei. For a numerical realization we reverted to the BUU transport model, a working approach for electro- and photoproduction. We have extended the BUU model to describe neutrino nucleus interactions using the nucleon cross sections derived in Part II. Both quasielastic reactions and neutrino induced  $\Delta$  production are included.

The BUU model, the required modifications and the numerical implementation were discussed in chapter 7. For calculations on nuclei, the in-medium effects taken into account are Pauli blocking, Fermi motion (both within a local density approximation), hadronic potentials and final state interactions. The in-medium modification of the  $\Delta$  resonance due to Pauli blocking and collisional broadening has been included. The final state interactions are implemented by means of the BUU coupled channel semiclassical transport model.

Motivated by the advent of new experiments we have calculated inclusive double differential cross sections  $d^2\sigma/(dQ^2 dE_l)$  for  $\nu_\mu {}^{56}\text{Fe} \rightarrow \mu^- X$  at neutrino energies of 0.4 - 2 GeV. We have shown that the dominant in-medium effect is the Fermi motion of the nucleons which "smears out" the inclusive double differential cross sections with increasing  $Q^2$ . The effect of the in-medium  $\Delta$  width has been found to be rather small. Taking the in-medium modifications together, the inclusive cross section inside the nucleus in the  $\Delta$  region is only half of the vacuum value.

The in-medium effects and especially the final state interactions reduce the neutrino induced exclusive pion cross section significantly and also give rise to a small fraction of  $\pi^-$ , which can not be produced in the elementary interaction. The basic processes are absorption and charge exchange. Quasielastic scattering followed by  $\pi$  production in  $NN$  collisions does not contribute significantly to the pion production - in the kinematical region under investigation, the pions were mainly originating from the initial  $\Delta$  production. Furthermore, we have found an enhancement of the  $\pi^0$  channel through side-feeding from

---

the dominant  $\pi^+$  channel. Moreover, we have seen that the total as well as the momentum differential cross section strongly depend on the initial choice of kinematics.

The influence of the final state interactions on nucleon knockout is significant. While the elementary quasielastic reaction cannot produce neutrons, but only protons, we found as a consequence of the final state interaction a distinct fraction of neutrons while the proton cross section is reduced. Also in the  $\Delta$  region we found an enhancement of neutrons due to final state interactions. The nucleons produced in the elementary interaction rescatter in the nucleus, and starting with a strong dominance of protons, additional neutrons are produced due to rescattering and charge exchange. To conclude for nucleon knockout we have found a reduction of the cross section for protons and an enhancement for neutrons due to final state interactions.

Finally, we have presented a simplified model for quasielastic neutrino nucleus scattering, where we neglected the hadronic potentials. The calculated total cross section is reduced compared to the vacuum case by less than 10 % mainly due to Pauli blocking.

We emphasize that an unsatisfactory aspect of the present investigations is the lack of extensive and good quality data. Hopefully, the situation will be improved in the near future when new neutrino facilities will be built and start data taking.

In the future, we will further improve our model. The replacement of the old  $N - \Delta$  transition vector form factors has the first priority. For that, recent electron scattering data have to be included, which will also improve the quality of the fit of the axial form factors. The proposed experiments will measure those more precisely within the next few years. We found that quasielastic reactions and  $\Delta$  production are the most important processes. But nevertheless, for a full model we will include higher-mass resonances and non-resonant background as well as more exotic channels. When studying neutrino nucleus reactions, a next step might involve to consider also the modification, or so-called quenching, of the form factors inside the nuclear medium.





# Appendices



# A Reference Formulæ

## A.1 Abbreviations

CC	charged current
CVC	conserved vector current hypothesis
DIS	deep inelastic scattering
FSI	final state interaction
NC	neutral current
PCAC	partially conserved axial current hypothesis
QE	quasielastic
RES	resonance

## A.2 Conventions

### Natural Units

In this thesis we work in so-called natural units, with

$$\hbar = c = 1. \tag{A.1}$$

This avoids dealing with factors of  $\hbar$  and  $c$  throughout the calculation and has the following implications for the dimension of mass, length and time:

$$[M] = [L]^{-1} = [T]^{-1}. \tag{A.2}$$

For all masses, energies and momenta we use GeV as a standard unit.

Cross sections are calculated in this units and have the dimension  $\text{GeV}^{-2}$ . Neutrino cross sections are usually given in the SI-system in units of  $10^{-38} \text{ cm}^2$ . To convert to an area, one uses Eq. (A.2)

$$[\sigma] = [L]^2 = [M]^{-2} \tag{A.3}$$

and the conversion formula

$$\hbar c = 0.197 \text{ GeV fm} \tag{A.4}$$

and ends up with

$$1 \text{ GeV}^{-2} = 3.8939 \cdot 10^{10} \cdot 10^{-38} \text{ cm}^2 = 0.38939 \text{ mb} \quad (\text{A.5})$$

where a millibarn, mb, is  $1 \text{ mb} = 10^{-31} \text{ m}^2$ . Thus, a typical neutrino cross sections of  $10^{-38} \text{ cm}^2$  corresponds to  $10^{-11} \text{ mb}$  or  $0.1 \text{ fb}$ .

## Dirac Matrices

To avoid notational confusion with neutrinos  $\nu$  and muons  $\mu$ , Dirac indices are usually denoted as  $\alpha$  and  $\beta$ . Throughout this thesis the conventions of Ref. [BD67] are used: The metric tensor is given as

$$g^{\alpha\beta} = \begin{pmatrix} 1 & 0 & 0 & 0 \\ 0 & -1 & 0 & 0 \\ 0 & 0 & -1 & 0 \\ 0 & 0 & 0 & -1 \end{pmatrix}. \quad (\text{A.6})$$

For the the Dirac matrices the following representation is used:

$$\gamma^\alpha = (\gamma^0, \vec{\gamma}), \quad (\text{A.7})$$

$$\gamma^0 = \gamma_0 = \begin{pmatrix} \mathbb{1} & 0 \\ 0 & -\mathbb{1} \end{pmatrix}, \quad \vec{\gamma} = \begin{pmatrix} 0 & \vec{\sigma} \\ -\vec{\sigma} & 0 \end{pmatrix} \quad (\text{A.8})$$

with the  $2 \times 2$  unit matrix  $\mathbb{1}$  and the Pauli spin matrices

$$\vec{\sigma} = (\sigma_x, \sigma_y, \sigma_z), \quad (\text{A.9})$$

$$\sigma_x = \begin{pmatrix} 0 & 1 \\ 1 & 0 \end{pmatrix}, \quad \sigma_y = \begin{pmatrix} 0 & -i \\ i & 0 \end{pmatrix}, \quad \sigma_z = \begin{pmatrix} 1 & 0 \\ 0 & -1 \end{pmatrix}. \quad (\text{A.10})$$

Furthermore we need combinations of those matrices, namely

$$\gamma_5 = \gamma^5 = i\gamma^0\gamma^1\gamma^2\gamma^3 = \begin{pmatrix} 0 & \mathbb{1} \\ \mathbb{1} & 0 \end{pmatrix} \quad \text{and} \quad \sigma^{\alpha\beta} = \frac{i}{2}[\gamma^\alpha, \gamma^\beta]. \quad (\text{A.11})$$

Under Lorentz transformation the following bilinears transform as:

$\bar{\psi}\psi$	scalar
$\bar{\psi}\gamma^\alpha\psi$	vector
$\bar{\psi}\sigma^{\alpha\beta}\psi$	antisymmetric tensor
$\bar{\psi}\gamma^5\gamma^\alpha\psi$	pseudovector (axialvector)
$\bar{\psi}\gamma^5\psi$	pseudoscalar.

Finally, we use the totally antisymmetric tensor  $\epsilon_{\alpha\beta\rho\sigma}$  with the convention  $\epsilon_{0123} = 1$ .

### Isospin and Gell-Mann Matrices

We use the standard isospin matrices

$$\tau_1 = \begin{pmatrix} 0 & 1 \\ 1 & 0 \end{pmatrix}, \quad \tau_2 = \begin{pmatrix} 0 & -i \\ i & 0 \end{pmatrix}, \quad \tau_3 = \begin{pmatrix} 1 & 0 \\ 0 & -1 \end{pmatrix} \quad (\text{A.12})$$

with

$$\vec{\tau} = (\tau_1, \tau_2, \tau_3), \quad \tau_{\pm} = (\tau_1 \pm i\tau_2). \quad (\text{A.13})$$

For the  $SU(3)$  Gell-Mann matrices we use

$$\lambda_1 = \begin{pmatrix} 0 & 1 & 0 \\ 1 & 0 & 0 \\ 0 & 0 & 0 \end{pmatrix}, \quad \lambda_2 = \begin{pmatrix} 0 & -i & 0 \\ i & 0 & 0 \\ 0 & 0 & 0 \end{pmatrix}, \quad (\text{A.14})$$

$$\lambda_3 = \begin{pmatrix} 1 & 0 & 0 \\ 0 & -1 & 0 \\ 0 & 0 & 0 \end{pmatrix}, \quad \lambda_8 = \frac{1}{\sqrt{3}} \begin{pmatrix} 1 & 0 & 0 \\ 0 & 1 & 0 \\ 0 & 0 & -2 \end{pmatrix}, \quad (\text{A.15})$$

with

$$\lambda_{\pm} = (\lambda_1 \pm i\lambda_2). \quad (\text{A.16})$$

## A.3 Weak Interaction Constants

The physical constants used are [E<sup>+</sup>04]:

$$\text{Fermi coupling constant: } G_F = 1.16637(1)10^{-5} \text{ GeV}^{-2} \quad (\text{A.17})$$

$$\text{W boson mass: } M_W = 80.425(38) \text{ GeV}/c^2 \quad (\text{A.18})$$

$$\text{Z boson mass: } M_Z = 91.1876(21) \text{ GeV}/c^2 \quad (\text{A.19})$$

$$\text{Weinberg angle: } \sin^2 \theta_W = 0.23120(15) \quad (\text{A.20})$$

These constants are related by

$$e = g \sin \theta_W, \quad (\text{A.21})$$

$$\cos \theta_W = \frac{M_W}{M_Z}, \quad (\text{A.22})$$

$$\frac{G_F}{\sqrt{2}} = \frac{g^2}{8M_W^2}, \quad (\text{A.23})$$

where  $e$  is the positron electric charge.



# B Neutrino Kinematics

## B.1 Notation

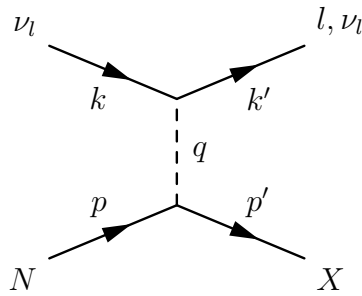


Figure B.1: Kinematic quantities in neutrino scattering

The notation used for the relativistic kinematics in this thesis is indicated in Fig. B.1.

- incoming neutrino  $\nu$ :
  - four-momentum:  $k_\alpha = (E_\nu, \vec{k})$
  - mass: 0
- outgoing lepton  $l$  or  $\nu_l$ :
  - four-momentum:  $k'_\alpha = (E_l, \vec{k}')$
  - mass:  $m_l$
- incoming nucleon  $N$ :
  - four-momentum:  $p_\alpha = (E, \vec{p})$
  - mass :  $M$
- outgoing hadrons  $X$ :
  - four-momentum:  $p'_\alpha = (E', \vec{p}')$
  - mass:  $W$
- exchanged vector boson  $W$  or  $Z$ :
  - four-momentum:  $q_\alpha = (E_q, \vec{q})$

CC	$E_\nu$ for QE	$E_\nu$ for $\Delta$
$\nu_e$	$\sim 0$ GeV	0.177 GeV
$\nu_\mu$	0.111 GeV	0.305 GeV
$\nu_\tau$	3.450 GeV	3.940 GeV
NC		
$\nu_x$	0 GeV	0.175 GeV

Table B.1: Threshold energies for QE and  $\Delta$  production

## B.2 Energy Thresholds for Neutrino Production

The thresholds for the incoming neutrino energy are given by simple relativistic kinematics. Assume we scatter on a nucleon of mass  $M$  and produce a particle of mass  $W$ . The total four-momentum of the incoming neutrino and the nucleon is in the lab frame

$$P^\alpha = (E_\nu + M, \vec{k}) \quad (\text{B.1})$$

and that of the outgoing system in the center of mass frame

$$P'^\alpha = (m_l + W, \vec{0}). \quad (\text{B.2})$$

This yields for the minimum neutrino energy in the lab frame

$$E_\nu = \frac{m_l^2 + W^2 + 2m_l W - M^2}{2M}. \quad (\text{B.3})$$

The numerical values for different processes are given in Table B.1 where for the  $\Delta$  resonance we assume for the threshold neutrino energy a minimal mass of  $W = M + m_\pi$ .

## B.3 Integration Limits for $\nu\text{N}$ (Quasi)Elastic Scattering and $\Delta$ Production

### B.3.1 (Quasi)Elastic Scattering

The total cross section is given by:

$$\sigma(E_\nu) = \int_{Q_{min}^2}^{Q_{max}^2} dQ^2 \frac{d^2\sigma}{dQ^2} \quad (\text{B.4})$$



with integration limits ( $s = M^2 + 2ME_\nu$ )

$$\begin{aligned} Q_{min}^2 &= -m_l^2 + 2E_\nu(E_l - |\vec{k}'|) \\ &= \frac{2E_\nu^2 M - Mm_l^2 - E_\nu m_l^2 - E_\nu \sqrt{(s - m_l^2)^2 - 2(s + m_l^2)M^2 + M^4}}{2E_\nu + M}, \end{aligned} \quad (\text{B.5})$$

$$\begin{aligned} Q_{max}^2 &= -m_l^2 + 2E_\nu(E_l + |\vec{k}'|) \\ &= \frac{2E_\nu^2 M - Mm_l^2 + E_\nu m_l^2 + E_\nu \sqrt{(s - m_l^2)^2 - 2(s + m_l^2)M^2 + M^4}}{2E_\nu + M}. \end{aligned} \quad (\text{B.6})$$

### B.3.2 $\Delta$ Production

Integration over the invariant mass yields:

$$\frac{d\sigma}{dQ^2} = \int_{W_{min}}^{W_{max}} dW \frac{d\sigma}{dQ^2 dW}. \quad (\text{B.7})$$

For each  $Q^2$  we have to integrate over  $W$ . The lower limit of  $W$  is fixed but the upper bound depends on  $Q^2$  and therefore changes continuously [LP05]:

$$\begin{aligned} W_{min} &= M + m_\pi, \quad (\text{B.8}) \\ W_{max} &= \left[ \frac{\frac{1}{4}s^2 a_-^2 \left( \frac{m_l^4}{s^2} - 2\frac{m_l^2}{s} \right) - \left( Q^2 + \frac{m_l^2}{2} a_+^2 \right)^2 + s a_- \left( Q^2 + \frac{m_l^2}{2} a_+ \right)}{[a_- (Q^2 + m_l^2)]} \right]^{-\frac{1}{2}}, \end{aligned} \quad (\text{B.9})$$

where  $s = M^2 + 2ME_\nu$  and  $a_\pm = 1 \pm M^2/s$ .

Also for the cross section integrated over  $Q^2$  the integration limits depend on the observable:

$$\frac{d\sigma}{dW} = \int_{Q_{min}^2}^{Q_{max}^2} dQ^2 \frac{d\sigma}{dQ^2 dW} \quad (\text{B.10})$$

where

$$Q_{min}^2 = \frac{1}{2E_\nu + M} \left( 2E_\nu^2 M - Mm_l^2 - E_\nu(W^2 - M^2 + m_l^2) - E_\nu \sqrt{(s - m_l^2)^2 - 2(s + m_l^2)W^2 + W^4} \right), \quad (\text{B.11})$$

$$Q_{max}^2 = \frac{1}{2E_\nu + M} \left( 2E_\nu^2 M - Mm_l^2 + E_\nu(-W^2 + M^2 - m_l^2) + E_\nu \sqrt{(s - m_l^2)^2 - 2(s + m_l^2)W^2 + W^4} \right). \quad (\text{B.12})$$

Combining both yields the total cross section:

$$\sigma(E_\nu) = \int_{W_{min}}^{W_{max}} dW \int_{Q_{min}^2}^{Q_{max}^2} dQ^2 \frac{d\sigma}{dQ^2 dW} \quad (\text{B.13})$$

with

$$W_{min} = M + m_\pi \quad \text{and} \quad W_{max} = \sqrt{s} - m_l \quad (\text{B.14})$$

and  $Q_{min}^2$  and  $Q_{max}^2$  as in Eq. (B.11) and Eq. (B.12).

# C Cross Sections and Feynman Rules for Weak Interaction

## C.1 General Expression for the Cross Section

The general expression of the differential cross section for the collision of two particles ( $i = 1, 2$ ) and  $N$  outgoing particles ( $f = 1, \dots, N$ ) is given as (see e. g. Ref. [MS93]):

$$d\sigma = (2\pi)^4 \delta^4 \left( \sum_f p'_f - \sum_i p_i \right) \frac{1}{4[(p_1 \cdot p_2)^2 - m_1^2 m_2^2]^{\frac{1}{2}}} \left( \prod_f \frac{d^3 p'_f}{(2\pi)^3 2E'_f} \right) |\mathcal{M}|^2. \quad (\text{C.1})$$

The amplitude  $\mathcal{M}$  is the invariant matrix element for the process under consideration. For particles with non-zero spin, unpolarized cross sections are calculated by averaging over initial spin components and summing over final. For the neutrinos there is no averaging over initial neutrino helicities since they occur only left-handed. However, for convenience of calculation, one can formally sum over both helicity states - the factor  $(1 - \gamma_5)$  guarantees that right-handed neutrinos do not contribute to the cross section.

## C.2 Feynman Rules

The amplitude can be calculated explicitly by using the Feynman rules of the weak interaction. Their derivation is given in any standard textbook on Quantum Field Theory - here we collect those needed for neutrino scattering as a reference.

The amplitude  $\mathcal{M}$  follows from a Feynman graph as a product of factors associated to different parts of the graph:

- **External particle:** An external line representing a lepton or a quark leads to a factor of  $u(k, s)$  or  $v(k, s)$  for incoming particles or  $\bar{u}(k', s')$  or  $\bar{v}(k', s')$  for outgoing particles, respectively.

- **Propagator:** A propagator represents the exchange of a gauge boson and gets a factor of

$$\frac{i}{q^2 - M_V^2} \left( -g^{\alpha\beta} + \frac{q^\alpha q^\beta}{M_V^2} \right), \quad (\text{C.2})$$

where  $M_V$  is either the mass of the  $W^\pm$  or of the  $Z$  boson.

- **Vertex:**

- Charged Current: For leptons we get a factor of

$$-i \frac{g}{\sqrt{2}} \gamma_\alpha \frac{1 - \gamma_5}{2} \quad (\text{C.3})$$

and for quarks a factor of

$$-i \frac{g}{\sqrt{2}} U_{qq'} \gamma_\alpha \frac{1 - \gamma_5}{2}, \quad (\text{C.4})$$

where  $U_{qq'}$  is the appropriate entry of the Cabbibo mixing matrix.

- Neutral Current: Here the vertex factor is given by

$$\frac{-ie}{\sin \theta_W \cos \theta_W} \gamma_\alpha \left( c_L \frac{1 - \gamma_5}{2} + c_R \frac{1 + \gamma_5}{2} \right), \quad (\text{C.5})$$

where  $c_L$  and  $c_R$  are as follows: For massless neutrinos we have

$$c_L = \frac{1}{2}, \quad c_R = 0, \quad (\text{C.6})$$

for up quarks

$$c_L = +\frac{1}{2} - \frac{2}{3} \sin^2 \theta_W, \quad c_R = -\frac{2}{3} \sin^2 \theta_W, \quad (\text{C.7})$$

and for down quarks

$$c_L = -\frac{1}{2} + \frac{2}{3} \sin^2 \theta_W, \quad c_R = \frac{1}{3} \sin^2 \theta_W. \quad (\text{C.8})$$

## Bibliography

- [A<sup>+</sup>87] L. A. Ahrens et al., *Measurement of Neutrino-Proton and Antineutrino-Proton Elastic Scattering*, Phys. Rev. **D35**, 785 (1987).
- [A<sup>+</sup>99] W. M. Alberico et al., *Strange Form Factors of the Proton: A New Analysis of the  $\nu$  ( $\bar{\nu}$ ) Data of the BNL-734 Experiment*, Nucl. Phys. **A651**, 277 (1999), hep-ph/9812388.
- [A00] M. K. Jones et al. [Jefferson Lab Hall A Collaboration],  *$G(E(p))/G(M(p))$  Ratio by Polarization Transfer in  $e(\text{pol.})p \rightarrow ep(\text{pol.})$* , Phys. Rev. Lett. **84**, 1398 (2000), nucl-ex/9910005.
- [A02] O. Gayou et al. [Jefferson Lab Hall A Collaboration], *Measurement of  $G(E(p))/G(M(p))$  in  $e(\text{pol.})p \rightarrow ep(\text{pol.})$  to  $Q^2 = 5.6 \text{ GeV}^2$* , Phys. Rev. Lett. **88**, 092301 (2002), nucl-ex/0111010.
- [A404] F. E. Maas et al. [A4 Collaboration], *Measurement of Strange Quark Contributions to the Nucleon's Form Factors at  $Q^2 = 0.230 \text{ (GeV/c)}^2$* , Phys. Rev. Lett. **93**, 022002 (2004), nucl-ex/0401019.
- [ABM02] W. M. Alberico, S. M. Bilenky and C. Maieron, *Strangeness in the Nucleon: Neutrino Nucleon and Polarized Electron Nucleon Scattering*, Phys. Rept. **358**, 227 (2002), hep-ph/0102269.
- [ADT81a] S. A. Adjei, D. A. Dicus and V. L. Teplitz, *Charged Current Two Pion Production from Nucleons*, Phys. Rev. **D24**, 623 (1981).
- [ADT81b] S. A. Adjei, D. A. Dicus and V. L. Teplitz, *Neutral Current Two Pion Production from Nucleons*, Phys. Rev. **D23**, 672 (1981).
- [AF03] G. Altarelli and F. Feruglio, *Theoretical Models of Neutrino Masses and Mixings*, in *Neutrino Mass*, edited by G. Altarelli and K. Winter, volume 190 of *Springer Tracts in Modern Physics*, page 169, Springer, Berlin, 2003.
- [AH96] I. J. R. Aitchison and A. J. G. Hey, *Gauge Theories in Particle Physics*, Institute of Physics Publishing, 1996.

- [ANP74] S. L. Adler, S. Nussinov and E. A. Paschos, *Nuclear Charge Exchange Corrections to Leptonic Pion Production in the (3,3) Resonance Region*, Phys. Rev. **D9**, 2125 (1974).
- [AR99] L. Alvarez-Ruso, *Excitation of Baryonic Resonances Induced by Nucleons and Leptons*, PhD thesis, Universidad de Valencia, 1999.
- [AR05] L. Alvarez-Ruso, private communication, 2005.
- [ARSVV98] L. Alvarez-Ruso, S. K. Singh and M. J. Vicente Vacas, *Charged Current Weak Electroproduction of Delta Resonance*, Phys. Rev. **C57**, 2693 (1998), nucl-th/9712058.
- [ARSVV99] L. Alvarez-Ruso, S. K. Singh and M. J. Vicente Vacas,  $\nu d \rightarrow \mu^- \Delta^{++} n$  *Reaction and Axial Vector  $N - \Delta$  Coupling*, Phys. Rev. **C59**, 3386 (1999), nucl-th/9804007.
- [B<sup>+</sup>79] S. J. Barish et al., *Study of Neutrino Interactions in Hydrogen and Deuterium: Inelastic Charged Current Reactions*, Phys. Rev. **D19**, 2521 (1979).
- [Bai77] D. Bailin, *Weak Interactions*, Sussex University Press, London, 1977.
- [BBA03] H. Budd, A. Bodek and J. Arrington, *Modeling Quasielastic Form Factors for Electron and Neutrino Scattering*, (2003), hep-ex/0308005.
- [BBA05] H. Budd, A. Bodek and J. Arrington, *Vector and Axial Form Factors Applied to Neutrino Quasielastic Scattering*, Nucl. Phys. Proc. Suppl. **139**, 90 (2005), hep-ex/0410055.
- [BD67] J. D. Bjorken and S. D. Drell, *Relativistische Quantenmechanik*, Bibliographisches Institut, Mannheim, 1967.
- [BEM02] V. Bernard, L. Elouadrhiri and U. G. Meissner, *Axial Structure of the Nucleon*, J. Phys. **G28**, R1 (2002), hep-ph/0107088.
- [Bil94] S. M. Bilenky, *Basics of Introduction to Feynman Diagrams and Electroweak Interactions Physics*, Editions Frontieres, Gif-sur-Yvette, 1994.
- [BL04] V. D. Burkert and T. S. H. Lee, *Electromagnetic Meson Production in the Nucleon Resonance Region*, Int. J. Mod. Phys. **E13**, 1035 (2004), nucl-ex/0407020.
- [BP70] J. D. Bjorken and E. A. Paschos, *High-Energy Inelastic Neutrino Nucleon Interactions*, Phys. Rev. **D1**, 3151 (1970).
- [BPY05] A. Bodek, I. Park and U.-k. Yang, *Improved Low  $Q^{*2}$  Model for Neutrino and Electron Nucleon Cross Sections in Few GeV Region*, Nucl. Phys. Proc. Suppl. **139**, 113 (2005), hep-ph/0411202.

- [Cas02] D. Casper, *The nuance Neutrino Physics Simulation, and the Future*, Nucl. Phys. Proc. Suppl. **112**, 161 (2002), hep-ph/0208030.
- [CNG] CNGS, <http://proj-cngs.web.cern.ch/proj-cngs/>.
- [DONUT01] K. Kodama et al. [DONUT Collaboration], *Observation of  $\tau$  Neutrino Interactions*, Phys. Lett. **B504**, 218 (2001), hep-ex/0012035.
- [Dre99] D. Drechsel, *The Structure of the Nucleon*, (1999), nucl-th/0003061.
- [E<sup>+</sup>04] S. Eidelman et al., *Review of Particle Physics*, Phys. Lett. **B592**, 1 (2004).
- [Eff96] M. Effenberger, *Gammaabsorption an Kernen*, Diplomarbeit, Justus-Liebig-Universität Gießen, 1996.
- [Eff99] M. Effenberger, *Eigenschaften von Hadronen in Kernmaterie in einem vereinheitlichten Transportmodell*, PhD thesis, Justus-Liebig-Universität Gießen, 1999.
- [EJ74] J. R. Ellis and R. L. Jaffe, *A Sum Rule for Deep Inelastic Electroproduction from Polarized Protons*, Phys. Rev. **D9**, 1444 (1974).
- [EMC89] J. Ashman et al. [EMC Collaboration], *An Investigation of the Spin Structure of the Proton in Deep Inelastic Scattering of Polarized Muons on Polarized Protons*, Nucl. Phys. **B328**, 1 (1989).
- [ERM05] J. Erler and M. J. Ramsey-Musolf, *Low Energy Tests of the Weak Interaction*, Prog. Part. Nucl. Phys. **54**, 351 (2005), hep-ph/0404291.
- [FGM58] R. P. Feynman and M. Gell-Mann, *Theory of the Fermi Interaction*, Phys. Rev. **109**, 193 (1958).
- [FINeSSE04] L. Bugel et al. [FINeSSE Collaboration], *A Proposal for a Near Detector Experiment on the Booster Neutrino Beamline: FINeSSE: Fermilab Intense Neutrino Scattering Scintillator Experiment*, (2004), hep-ex/0402007.
- [FKR71] R. P. Feynman, M. Kislinger and F. Ravndal, *Current Matrix Elements from a Relativistic Quark Model*, Phys. Rev. **D3**, 2706 (1971).
- [FN79] G. L. Fogli and G. Nardulli, *A New Approach to the Charged Current Induced Weak One Pion Production*, Nucl. Phys. **B160**, 116 (1979).
- [GCHS05] H. Gallagher, D. Casper, Y. Hayato and P. Sala, *Event Generator Comparisons*, Nucl. Phys. Proc. Suppl. **139**, 278 (2005).

- [Gei03] A. Geiser, *Experimental Results on Neutrino Oscillations*, in *Neutrino Mass*, edited by G. Altarelli and K. Winter, volume 190 of *Springer Tracts in Modern Physics*, page 75, Springer, Berlin, 2003.
- [GLW93] G. T. Garvey, W. C. Louis and D. H. White, *Determination of Proton Strange Form Factors from Neutrino  $p$  Elastic Scattering*, *Phys. Rev. C* **48**, 761 (1993).
- [H<sup>+</sup>02] K. Hagiwara et al., *Review of Particle Physics*, *Phys. Rev. D* **66**, 010001 (2002).
- [HAPPEX05] K. A. Aniol et al. [HAPPEX Collaboration], *Constraints on the Nucleon Strange Form Factors at  $Q^2 \approx 0.1 \text{ GeV}^2$* , (2005), nucl-ex/0506011.
- [Har] D. A. Harris, *Systematic Uncertainties on  $\Delta m^2$  from Neutrino Physics Using Calorimetric Energy Reconstruction*, To appear in the proceedings of 2nd International Workshop on Neutrino Nucleus Interactions in the Few GeV Region (NuInt02), Irvine, California, 12-15 Dec 2002.
- [Hay02] Y. Hayato, *NEUT*, *Nucl. Phys. Proc. Suppl.* **112**, 171 (2002).
- [HERMES04] A. Airapetian et al. [HERMES Collaboration], *Flavor Decomposition of the Sea Quark Helicity Distributions in the Nucleon from Semi-Inclusive Deep Inelastic Scattering*, *Phys. Rev. Lett.* **92**, 012005 (2004), hep-ex/0307064.
- [IZ80] C. Itzykson and J. B. Zuber, *Quantum Field Theory*, International Series in Pure and Applied Physics, McGraw-Hill Book Company, New York, 1980.
- [K<sup>+</sup>90] T. Kitagaki et al., *Study of  $\nu d \rightarrow \mu^- pp(s)$  and  $\nu d \rightarrow \mu^- \Delta^{++}(1232)n(s)$  Using the BNL 7-foot Deuterium Filled Bubble Chamber*, *Phys. Rev. D* **42**, 1331 (1990).
- [K2K] K2K, <http://neutrino.kek.jp/>.
- [K2K03] M. H. Ahn et al. [K2K Collaboration], *Indications of Neutrino Oscillation in a 250-km Long- Baseline Experiment*, *Phys. Rev. Lett.* **90**, 041801 (2003), hep-ex/0212007.
- [K2K05] R. Gran [K2K Collaboration], *Charged Current Events in the K2K Near Detectors*, *Nucl. Phys. Proc. Suppl.* **139**, 54 (2005).
- [KamLAND03] K. Eguchi et al. [KamLAND Collaboration], *First Results from KamLAND: Evidence for Reactor Antineutrino Disappearance*, *Phys. Rev. Lett.* **90**, 021802 (2003), hep-ex/0212021.



- [Kay05] B. Kayser, *Neutrino Physics*, (2005), hep-ph/0506165.
- [KDC<sup>+</sup>84] T. Kodama, S. B. Duarte, K. C. Chung, R. Donangelo and R. A. M. S. Nazareth, *Causality and Relativistic Effects in Intranuclear Cascade Calculations*, Phys. Rev. **C29**, 2146 (1984).
- [KKDHK01] H. V. Klapdor-Kleingrothaus, A. Dietz, H. L. Harney and I. V. Krivosheina, *Evidence for Neutrinoless Double Beta Decay*, Mod. Phys. Lett. **A16**, 2409 (2001), hep-ph/0201231.
- [KM88] D. B. Kaplan and A. Manohar, *Strange Matrix Elements in the Proton from Neutral Current Experiments*, Nucl. Phys. **B310**, 527 (1988).
- [KT03] A. F. Krutov and V. E. Troitsky, *Extraction of the Neutron Charge Form Factor from the Charge Form Factor of Deuteron*, Eur. Phys. J. **A16**, 285 (2003), hep-ph/0202183.
- [Leh99] J. Lehr, *Elektroproduktion von Mesonen an Kernen*, Diplomarbeit, Justus-Liebig-Universität Gießen, 1999.
- [Leh03] J. Lehr, *In-Medium-Eigenschaften von Nukleonen und Nukleonenresonanzen in einem semiklassischen Transportmodell*, PhD thesis, Justus-Liebig-Universität Gießen, 2003.
- [LEP05] P. Langacker, J. Erler and E. Peinado, *Neutrino Physics*, (2005), hep-ph/0506257.
- [Leu01] S. Leupold, *Life Time of Resonances in Transport Simulations*, Nucl. Phys. **A695**, 377 (2001), nucl-th/0008036.
- [Lip02] P. Lipari, *Neutrino Oscillation Studies and the Neutrino Cross Section*, Nucl. Phys. Proc. Suppl. **112**, 274 (2002), hep-ph/0207172.
- [Lip03] P. Lipari, *Introduction to Neutrino Physics*, CERN Yellow Report **2003-003** (2003).
- [LMZ95] J. Liu, N. C. Mukhopadhyay and L.-s. Zhang, *Nucleon to Delta Weak Excitation Amplitudes in the Nonrelativistic Quark Model*, Phys. Rev. **C52**, 1630 (1995), hep-ph/9506389.
- [LP05] O. Lalakulich and E. A. Paschos, *Resonance Production by Neutrinos.  $J = 3/2$  Resonances*, Phys. Rev. **D71**, 074003 (2005), hep-ph/0501109.
- [LS72] C. H. Llewellyn Smith, *Neutrino Reactions at Accelerator Energies*, Phys. Rept. **3**, 261 (1972).
- [LSND95] C. Athanassopoulos et al. [LSND Collaboration], *Candidate Events in a Search for Anti-Muon-Neutrino  $\rightarrow$  Anti-Electron-Neutrino Oscillations*, Phys. Rev. Lett. **75**, 2650 (1995), nucl-ex/9504002.

- [M<sup>+</sup>05] M. C. Martinez et al., *Relativistic Models for Quasielastic Neutrino Scattering*, (2005), nucl-th/0505008.
- [MIN] MINOS experiment, <http://www-numi.fnal.gov/>.
- [MINERvA04a] D. Drakoulakos et al. [MINERvA Collaboration], *Proposal to Perform a High-Statistics Neutrino Scattering Experiment Using a Fine-Grained Detector in the NuMI Beam*, (2004), hep-ex/0405002.
- [MINERvA04b] D. A. Harris et al. [MINERvA Collaboration], *Neutrino Scattering Uncertainties and their Role in Long-Baseline Oscillation Experiments*, (2004), hep-ex/0410005.
- [Mos99] U. Mosel, *Fields, Symmetries, and Quarks*, Texts and Monographs in Physics, Springer, Berlin, 1999.
- [MP04] R. N. Mohapatra and P. B. Pal, *Massive Neutrinos in Physics and Astrophysics*, volume 72 of *World Scientific Lecture Notes in Physics*, World Scientific, Singapore, 3rd edition, 2004.
- [MS93] F. Mandl and G. Shaw, *Quantenfeldtheorie*, AULA-Verlag, Wiesbaden, 1993.
- [NOI] Neutrino Oscillation Industry, <http://neutrinooscillation.org/>.
- [NPR05] M. Nowakowski, E. A. Paschos and J. M. Rodriguez, *All Electromagnetic Form Factors*, Eur. J. Phys. **26**, 545 (2005), physics/0402058.
- [NuI] *NuInt02: Proceedings*, Nuclear Physics B Proc. Suppl. (in press), Prepared for 2nd International Workshop on Neutrino Nucleus Interactions in the Few GeV Region (NuInt02), Irvine, California, 12-15 Dec 2002.
- [NuI02] *NuInt01: Proceedings*, Nuclear Physics B Proc. Suppl. **112** (2002), Prepared for 1st International Workshop on Neutrino Nucleus Interactions in the Few GeV Region (NuInt01), Tsukuba, Japan, 13-16 Dec 2001.
- [NuI05] *NuInt04: Proceedings*, Nuclear Physics B Proc. Suppl. **139** (2005), Prepared for 3rd International Workshop on Neutrino Nucleus Interactions in the Few GeV Region (NuInt04), Gran Sasso, Assergi, Italy, 17-21 Mar 2004.
- [NUn] Neutrino Unbound, <http://www.nu.to.infn.it/>.
- [OOM78] M. G. Olsson, E. T. Osypowski and E. H. Monsay, *Electroproduction of Low Hadronic Masses*, Phys. Rev. **D17**, 2938 (1978).

- [OS87] E. Oset and L. L. Salcedo, *Delta Selfenergy in Nuclear Matter*, Nucl. Phys. **A468**, 631 (1987).
- [Pon68] B. Pontecorvo, *Neutrino Experiments and the Question of Leptonic-Charge Conservation*, Sov. Phys. JETP **26**, 984 (1968).
- [Pos04] M. Post, *Hadronic Spectral Functions in Nuclear Matter*, PhD thesis, Universität Giessen, 2004.
- [PPY00] E. A. Paschos, L. Pasquali and J.-Y. Yu, *Single Pion Production in Neutrino Reactions and Estimates for Charge Exchange Effects*, Nucl. Phys. **B588**, 263 (2000), hep-ph/0005255.
- [PSY05] E. A. Paschos, I. Schienbein and J.-Y. Yu, *Pion Rescattering in Nuclei*, Nucl. Phys. Proc. Suppl. **139**, 119 (2005), hep-ph/0408148.
- [PY02] E. A. Paschos and J.-Y. Yu, *Neutrino Interactions in Oscillation Experiments*, Phys. Rev. **D65**, 033002 (2002), hep-ph/0107261.
- [PYS04] E. A. Paschos, J.-Y. Yu and M. Sakuda, *Neutrino Production of Resonances*, Phys. Rev. **D69**, 014013 (2004), hep-ph/0308130.
- [R<sup>+</sup>82] G. M. Radecky et al., *Study of Single Pion Production by Weak Charged Currents in Low-Energy Neutrino  $d$  Interactions*, Phys. Rev. **D25**, 1161 (1982).
- [RC53] F. Reines and C. L. Cowan, *Detection of the Free Neutrino*, Phys. Rev. **92**, 830 (1953).
- [Rol94] W. B. Rolnick, *The Fundamental Particles and Their Interactions*, Addison-Wesley, Reading, 1994.
- [RS81] D. Rein and L. M. Sehgal, *Neutrino Excitation of Baryon Resonances and Single Pion Production*, Ann. Phys. **133**, 79 (1981).
- [SAA05] S. K. Singh, M. S. Athar and S. Ahmad, *Weak Pion Production from Nuclei*, (2005), nucl-th/0507016.
- [Sak02] M. Sakuda, *Results from Low-Energy Neutrino Nucleus Scattering Experiments*, Nucl. Phys. Proc. Suppl. **112**, 109 (2002).
- [SAMPLE05] E. J. Beise et al. [SAMPLE Collaboration], *The SAMPLE Experiment and Weak Nucleon Structure*, Prog. Part. Nucl. Phys. **54**, 289 (2005), nucl-ex/0412054.
- [Sch97] N. Schmitz, *Neutrinophysik*, Teubner Studienbücher, Stuttgart, 1997.
- [SM72] R. A. Smith and E. J. Moniz, *Neutrino Reactions on Nuclear Targets*, Nucl. Phys. **B43**, 605 (1972).

- [SMC97] D. Adams et al. [SMC Collaboration], *Spin Structure of the Proton from Polarized Inclusive Deep Inelastic Muon Proton Scattering*, Phys. Rev. **D56**, 5330 (1997), hep-ex/9702005.
- [SNO01] Q. R. Ahmad et al. [SNO Collaboration], *Measurement of the Charged Current Interactions Produced by B-8 Solar Neutrinos at the Sudbury Neutrino Observatory*, Phys. Rev. Lett. **87**, 071301 (2001), nucl-ex/0106015.
- [SO92] S. K. Singh and E. Oset, *Quasielastic Neutrino (Antineutrino) Reactions in Nuclei and the Axial Vector Form Factor of the Nucleon*, Nucl. Phys. **A542**, 587 (1992).
- [Sto93] P. Stoler, *Baryon Form Factors at High  $Q^2$  and the Transition to Perturbative QCD*, Phys. Rept. **226**, 103 (1993).
- [SUL03] T. Sato, D. Uno and T. S. H. Lee, *Dynamical Model of Weak Pion Production Reactions*, Phys. Rev. **C67**, 065201 (2003), nucl-th/0303050.
- [Super-K98] Y. Fukuda et al. [Super-K Collaboration], *Evidence for Oscillation of Atmospheric Neutrinos*, Phys. Rev. Lett. **81**, 1562 (1998), hep-ex/9807003.
- [Super-K02] K. Kaneyuki [Super-K Collaboration], *Determination of Neutrino Oscillation Parameters with Atmospheric Neutrinos*, Nucl. Phys. Proc. Suppl. **112**, 24 (2002).
- [Super-K05] Y. Ashie et al. [Super-K Collaboration], *A Measurement of Atmospheric Neutrino Oscillation Parameters by Super-Kamiokande I*, Phys. Rev. **D71**, 112005 (2005), hep-ex/0501064.
- [SV03] A. Strumia and F. Vissani, *Precise Quasielastic Neutrino Nucleon Cross Section*, Phys. Lett. **B564**, 42 (2003), astro-ph/0302055.
- [SvH73] P. A. Schreiner and F. von Hippel, *Neutrino Production of the Delta (1236)*, Nucl. Phys. **B58**, 333 (1973).
- [SVVO98] S. K. Singh, M. J. Vicente-Vacas and E. Oset, *Nuclear Effects in Neutrino Production of Delta at Intermediate Energies*, Phys. Lett. **B416**, 23 (1998).
- [TH95] I. S. Towner and J. C. Hardy, *Currents and their Couplings in the Weak Sector of the Standard Model*, in *Symmetries and Fundamental Interactions in Nuclei*, edited by W. C. Haxton and E. M. Henley, page 183, World Scientific, Singapore, 1995.
- [TW01] A. W. Thomas and W. Weise, *The Structure of the Nucleon*, Wiley-VCH, Berlin, 2001.

- 
- [UNP] Ultimate Neutrino Page, <http://cupp.oulu.fi/neutrino/>.
- [vdVP05] B. I. S. van der Ventel and J. Piekarewicz, *Strange Quark Contribution to the Ratio of Neutral to Charged Current Cross Sections in Neutrino Nucleus scattering*, (2005), nucl-th/0506071.
- [vMWH85] K. von Meyenn, V. F. Weisskopf and A. Hermann, editors, *Wolfgang Pauli: Wissenschaftlicher Briefwechsel mit Bohr, Einstein, Heisenberg, u. a., Bd. 2: 1930-1939*, Springer, New York, 1985.
- [Wal95] J. D. Walecka, *Theoretical Nuclear and Subnuclear Physics*, Oxford University Press, New York, 1995.
- [Wei] W. Weise, *Quarks, Hadrons and Dense Nuclear Matter*, Given at Les Houches Summer School on Theoretical Physics, Session 66: Trends in Nuclear Physics, 100 Years Later, Les Houches, France, 30 Jul - 30 Aug 1996.
- [Wei58] S. Weinberg, *Charge Symmetry of Weak Interactions*, Phys. Rev. **112**, 1375 (1958).
- [Wei61] S. Weinberg, *Cross Sections at High Energies*, Phys. Rev. **124**, 2049 (1961).
- [Wha05] M. R. Whalley, *A New Neutrino Cross Section Database*, Nucl. Phys. Proc. Suppl. **139**, 241 (2005), hep-ph/0410399.
- [Wil00] D. H. Wilkinson, *Limits to Second-Class Nucleonic and Mesonic Currents*, Eur. Phys. J. **A7**, 307–315 (2000).
- [WPK<sup>+</sup>88] G. M. Welke, M. Prakash, T. T. S. Kuo, S. D. Gupta and C. Gale, *Azimuthal Distributions in Heavy Ion Collisions and the Nuclear Equation of State*, Phys. Rev. **C38**, 2101 (1988).
- [Zel03] G. P. Zeller, *Low Energy Neutrino Cross Sections: Comparison of Various Monte Carlo Predictions to Experimental Data*, (2003), hep-ex/0312061.



# Deutsche Zusammenfassung

Als Wolfgang Pauli im Jahre 1930 ein zusätzliches Teilchen - das Neutrino - postulierte, um so die Erhaltung von Energie und Impuls im  $\beta$ -Zerfall zu retten, befürchtete er, dass dieses neutrale und fast masselose Teilchen niemals gefunden werden könnte. Heute, 75 Jahre später, ist nicht nur der sichere Nachweis dreier Neutrinoarten erbracht, sondern ihre Wechselwirkungen bieten einzigartige Möglichkeiten, fundamentale Fragen in vielen Bereichen der Physik zu untersuchen.

Seit Neutrinoszillationen in unterschiedlichsten Experimenten bestätigt wurden, besteht kein Zweifel mehr, dass Neutrinos zwar eine kleine, aber doch von Null verschiedene Ruhemasse besitzen. Der absolute Wert dieser Masse ist jedoch noch immer unbekannt und bleibt somit eine der größten Herausforderungen in der heutigen Teilchenphysik. Aktuelle Experimente befassen sich zudem mit einer Reihe anderer ebenso wenig beantworteter Fragen, wie beispielsweise CP-Verletzung und der Existenz von sterilen Neutrinos.

Das Interesse an Neutrinos beschränkt sich allerdings nicht nur auf ihre Eigenschaften selbst, sondern erstreckt sich auf viele unterschiedliche Teilbereiche der Physik. So sind Neutrinos ein wertvolles Hilfsmittel, um nukleare und hadronische Fragestellungen zu untersuchen. Von aktuellem Interesse ist insbesondere das Verständnis hadronischer Strukturen im Rahmen der Quantenchromodynamik (QCD). Die Untersuchung von Nukleonen und Nukleonenresonanzen sowohl mit der elektromagnetischen als auch mit der schwachen Wechselwirkung ist dabei besonders wichtig, vor allem um hadronische Modelle zu überprüfen. Dabei ergänzen sich beide Methoden hervorragend: Durch die spezielle  $(V - A)$ -Struktur der schwachen Wechselwirkung können Eigenschaften der Hadronen untersucht werden, die in Elektronen- oder Photonenstreuung nicht direkt oder nur schwer zugänglich sind, und zwar vornehmlich die axiale Struktur der Hadronen. Die schwache Wechselwirkung mit geladenen Strömen ist zudem der einzig praktisch sinnvolle Weg, die axialen Formfaktoren des Nukleons zu untersuchen. Der Beitrag der See-Quarks zum Nukleonenspin dagegen ist mit neutralen Strömen sehr gut zugänglich. Unter den Nukleonenresonanzen ist die  $\Delta$ -Resonanz am wichtigsten und daher auf vielerlei Arten untersucht, u. a. auch mit Hilfe von Neutrinos. Besonders die axialen  $N - \Delta$ -Übergangsformfaktoren sind mit Neutrinostreuung direkt zugänglich.

Obwohl Neutrinos eine wichtige Rolle in vielen Bereichen der Physik spielen, bleibt ein wesentliches Problem: Sie unterliegen ausschließlich der schwachen Wechselwirkung

mit entsprechend kleinen Wirkungsquerschnitten und sind daher nur schwer zu detektieren. Einzig mit Hilfe der durch ihre Wechselwirkung mit Materie erzeugten Teilchen sind sie nachweisbar. Oft werden schwere Kerne als Targetmaterial benutzt, die relativ große Wirkungsquerschnitte bieten. Daher ist ein theoretisches Verständnis der Wechselwirkung von Neutrinos mit eben solchen Kernen unverzichtbar für die Auswertung von Neutrinoexperimenten.

In der Literatur gibt es zahlreiche Untersuchungen zur Neutrino-Kern-Wechselwirkung, die sich auf den quasielastischen Bereich konzentrieren. Systematische Studien von nuklearen Effekten und ihr Einfluss auf die Pion-Produktion gibt es dagegen kaum, obwohl genau diese Ungenauigkeit in der Kenntnis der Wirkungsquerschnitte die größte Unsicherheit der meisten Neutrinoexperimente darstellt.

Die beschriebene Situation lieferte die Motivation für die vorliegende Arbeit. Untersucht wurden Neutrino-Nukleon-Streuung und Neutrino-Kern-Wechselwirkungen für Neutrinoenergien bis 2 GeV. Bei der Neutrino-Nukleon-Streuung wurde besonderer Wert auf die systematische Untersuchung der Formfaktoren gelegt. Bei der Neutrino-Kern-Wechselwirkung wurde vorrangig der Einfluss von nuklearen Effekten auf den Pion-Produktionsquerschnitt und auf Nukleon-Knockout-Reaktionen untersucht. Letztere sind Reaktionen, bei denen ein Nukleon aus dem Kern freigesetzt wird.

Um Neutrino-Nukleon- bzw. Neutrino-Kern-Wirkungsquerschnitte zu berechnen, muss zunächst die zugrunde liegende Theorie behandelt werden. Neutrinoereaktionen werden im Rahmen des Standard-Modells der Teilchenphysik beschrieben. Sie wechselwirken ausschließlich schwach durch den Austausch geladener  $W$ -Bosonen oder neutraler  $Z$ -Bosonen. Besonders hervorzuheben ist die  $(V - A)$ -Struktur der schwachen Wechselwirkung, d. h. die explizite Unterscheidung rechts- und linkshändiger Felder. Für Leptonen und Quarks sind sowohl die geladenen als auch die ungeladenen Ströme wohldefiniert. Das ändert sich beim Übergang von Quarks zu Hadronen, also zusammengesetzten Systemen. Relevante Zusammenhänge und Symmetrien bleiben jedoch unverändert und erlauben damit das Aufstellen allgemeiner Aussagen für hadronische Ströme. Besonders wichtig für explizite Rechnungen sind die Hypothese vom erhaltenen Vektorstrom (CVC) und die Hypothese vom teilweise erhaltenen Axialstrom (PCAC).

Damit kann nun die Neutrino-Nukleon-Wechselwirkung berechnet werden. Im allgemeinsten Fall ist der inklusive  $\nu N$ -Wirkungsquerschnitt als Funktion von fünf unbekanntem Strukturfunktionen gegeben. Benötigt werden jedoch exklusive Querschnitte. Dazu ist zunächst der Wirkungsquerschnitt in seine Beiträge aufzuspalten. Man findet, dass der Wirkungsquerschnitt bei Energien bis etwa 2 GeV hauptsächlich durch zwei Beiträge dominiert wird, nämlich durch (quasi)elastische Prozesse  $\nu N \rightarrow lN'$  und inelastische  $\Delta$ -Produktion  $\nu N \rightarrow l\Delta$ . Höhere Resonanzen und nichtresonanter Untergrund sind in diesem Energiebereich von geringerer Bedeutung.



---

Bei (quasi)elastischen Reaktionen müssen zwei Möglichkeiten unterschieden werden. Die Reaktion kann entweder durch den Austausch eines geladenen (CC) oder eines neutralen (NC) Vektorbosons stattfinden. Erstere wird mit quasielastisch bezeichnet, letztere mit elastisch.

Der quasielastische differentielle Wirkungsquerschnitt der Reaktion  $\nu n \rightarrow l^- p$  ist eine Funktion von zwei Vektorformfaktoren und zwei Axialformfaktoren. Mittels CVC können die Vektorformfaktoren mit den Formfaktoren aus der Elektronenstreuung in Verbindung gebracht werden; PCAC setzt die Axialformfaktoren miteinander in Beziehung, d. h. CC-Reaktionen werden nur noch durch einen unabhängiger Axialformfaktor beschrieben. Da quasielastische Reaktionen nur noch von diesem einen Axialformfaktor abhängen, erlaubt diese Art von Reaktionen das direkte Studium der axialen Struktur des Nukleons.

Während die geladenen Ströme reinen Isektor-Charakter haben, gilt das nicht mehr für die neutralen Ströme. Diese haben sowohl isovektorielle als auch isoskalare Anteile. Letztere führen zu einer Sensitivität der neutralen Ströme darauf, welchen Beitrag die seltsamen See-Quarks am Nukleonspin haben. Der Wirkungsquerschnitt der Reaktion  $\nu N \rightarrow \nu N$  ist hier gegeben als Funktion von zwei Vektorformfaktoren und einem Axialformfaktor. Diese wiederum bestehen aus zwei Teilen: Der erste hängt direkt mit der oben genannten Sensitivität auf den Strange-Beitrag zusammen. Der zweite ergibt sich mittels CVC und PCAC direkt aus den quasielastischen Formfaktoren. Die Formfaktoren für Proton und Neutron unterscheiden sich signifikant. So ist der Vektorformfaktor für Protonen durch den schwachen Mischungswinkel stark unterdrückt. Es zeigte sich, dass die Reaktion  $\nu p \rightarrow \nu p$  stark von dem Axialformfaktor dominiert wird und daher sehr sensitiv auf den Strange-Beitrag zum Nukleonspin ist.

Neben (quasi)elastischer Streuung ist die Produktion der  $\Delta$ -Resonanz von besonderer Bedeutung. Für die Berechnung des Wirkungsquerschnitts wird wie bei den (quasi)elastischen Prozessen ein voll-relativistischer Formalismus verwendet. Nutzt man auch hier CVC und PCAC, bleibt je ein unabhängiger Vektor- und Axialformfaktor. Für ihre Parametrisierung wird in der Literatur üblicherweise eine nicht korrekte  $\Delta$ -Breite verwendet. Daher wurde der Untersuchung des Einflusses der  $\Delta$ -Breite auf den Wirkungsquerschnitt besondere Bedeutung beigemessen. Es zeigte sich, dass diese Unterschiede den Wirkungsquerschnitt um einige Prozent verändern.

Dieses Modell wurde erweitert, um Neutrino-Kern-Reaktionen zu beschreiben und berücksichtigt nukleare Effekte, wie die Fermibewegung der Nukleonen, das Pauli-Prinzip, Bindungsenergien und Endzustandswechselwirkungen. Die Modifikation der  $\Delta$ -Breite durch Kollisionsverbreiterung und Pauli-Prinzip im Medium ist ebenfalls berücksichtigt, ebenso wie eine veränderte Bindungsenergie. Für die Simulation der Endzustandswechselwirkungen wurde das BUU-Modell, ein semiklassisches Transportmodell, verwendet. Pionen und Nukleonen unterliegen Endzustandswechselwirkungen wie Ladungstransfer und elastischer Streuung mit den Nukleonen im Medium.

Motiviert durch zukünftige Experimente wie MINER $\nu$ A wurden zweifach differentielle Wirkungsquerschnitte  $d^2\sigma/(dQ^2 dE_l)$  exemplarisch für die Reaktion  $\nu_\mu \text{}^{56}\text{Fe} \rightarrow \mu^- X$  bei Neutrinoenergien von 0.4 - 2 GeV berechnet. Bei den inklusiven Wirkungsquerschnitten zeigte sich, dass die Fermibewegung der dominante Effekt ist und den Wirkungsquerschnitt mit zunehmendem Impulsübertrag  $Q^2$  vollkommen ausschmiert. Der Einfluss der In-Medium-Breite des  $\Delta$  ist dagegen gering.

Desweiteren wurden exklusive Wirkungsquerschnitte betrachtet, nämlich Pionproduktion und Nukleon-Knockout. Besonders der Einfluss der Endzustandswechselwirkungen wurde hier untersucht. Durch Absorption der Pionen im Kern reduziert sich der Produktionsquerschnitt um etwa einen Faktor zwei. Es zeigte sich, dass die produzierten Pionen fast völlig von ursprünglich angeregten  $\Delta$ -Resonanzen stammen. Pionproduktion als Folge von quasielastischer Streuung, gefolgt von Pionerzeugung durch  $NN$ -Kollisionen, ist vernachlässigbar für kleine  $Q^2$ . Da  $\pi^+$  und  $\pi^0$  in der elementaren Reaktion mit einem sehr großen Ungleichgewicht erzeugt werden ( $\pi^+ : \pi^0 \approx 5$ ), führt der Ladungstransfer in den Endzustandswechselwirkungen zu einer Umverteilung zu Gunsten der  $\pi^0$ .  $\pi^-$  können in der elementaren Reaktion nicht erzeugt werden, wohl aber durch Endzustandswechselwirkungen.

Der Einfluss der Endzustandswechselwirkung auf die Nukleonen, die den Kern verlassen, ist ebenfalls signifikant. Während quasielastische Prozesse in der elementaren Reaktion keine Neutronen, sondern nur Protonen erzeugen, findet man als Folge der Endzustandswechselwirkungen der Nukleonen einen deutlichen Anteil an Neutronen. Ähnliches beobachtet man auch für  $\Delta$ -Anregungen. Hier ist die Produktion von Neutronen im Vergleich zu Protonen in der elementaren Reaktion um einen Faktor zehn kleiner. Die Endzustandswechselwirkungen führen letztlich zu einem Verlust an Protonen und zu einer Zunahme an Neutronen.

Leider ist der direkte Vergleich dieser Rechnungen mit experimentellen Daten noch nicht möglich - entsprechende Experimente sind aber bereits in Planung.

Schließlich wurde, unter Vernachlässigung der hadronischen Potentiale, der totale inklusive quasielastische Querschnitt berechnet und mit Blasenkammerdaten verglichen. Es zeigte sich, dass im Vergleich zum Vakuumquerschnitt hauptsächlich das Pauli-Prinzip zu einer Reduktion von etwas weniger als 10 % führt.

Zusammenfassend lässt sich sagen, dass die In-Medium-Effekte und vor allem die Endzustandswechselwirkungen erheblichen Einfluss auf den gemessenen Wirkungsquerschnitt haben und daher nicht vernachlässigt werden können.

# Acknowledgments

First and foremost, I would like to thank Prof. Dr. Ulrich Mosel for giving me the opportunity of both joining his institute and working on a fascinating topic of great current interest. I am thankful for his advice and for the dedicated support. I am also grateful for the possibilities to attend international workshops, conferences and lecture weeks.

I am no less grateful to Dr. Luis Alvarez-Ruso for his instructive scientific guidance and valuable advice. His knowledge and steady interest influenced this work a lot and I want to acknowledge numerous fruitful discussions. I am in particular thankful for the careful proofreading of this thesis.

I thank Dr. André Peshier for very helpful and constructive discussions about physics and I am especially grateful for the painstaking and fast proofreading of this work.

Further, I would like to thank all my BUU colleagues, Oliver Buß, Dr. Thomas Falter, Pascal Mühlich, Dr. Jürgen Lehr and Dr. Alexei Larionov, for helping me in revealing the secrets of the BUU transport code.

As "Wasti power user" I want to thank the computer crew, Frank Frömel and Dr. Christoph Keil, for the perfectly working computer system.

I am grateful to Dr. Stefan Leupold not only for helping me with the  $\Delta$  resonance width, but also for answering any kind of question.

A special thanks goes to Lukas Jahnke for the excellent atmosphere in our office and for discussions on physics and clearly beyond. Not only, but in particular in times of exams, we spent a lot of both entertaining and productive time together. I appreciated it very much.

Thanks to Elke Jung for her help with any kind of paperwork and her administrative support.

Further, I would like to thank all members of the institute for the nice working atmosphere and the numerous visits to the "Partyzimmer".

Ganz besonders danke ich meinen Eltern. Ohne ihre - nicht nur finanzielle - Unterstützung wäre diese Arbeit nicht entstanden.